USING DISCRETE ELEMENT MODELING TO EVALUATE MATERIAL DISTRIBUTION USING SPINNER-DISC SPREADERS

by

Jonathan Bradford Hall

A thesis submitted to the Graduate Faculty of
Auburn University
in partial fulfillment of the
requirements for the Degree of
Master of Science

Auburn, Alabama
December 8, 2012

Keywords: discrete element modeling, 3D simulations, broiler litter, fertilizer, litter spreader

Approved by

John Fulton, Co-Chair, Associate Professor of Biosystems Engineering
Wesley Zech, Co-Chair, Associate Professor of Civil Engineering
Timothy McDonald, Associate Professor of Biosystems Engineering
Oladiran Fasina, Associate Professor of Biosystems Engineering
Larry Crowley, Associate Professor of Civil Engineering

ABSTRACT

Due to rising costs of inorganic fertilizers, more crop producers are turning to organic fertilizers as a soil amendment and fertilizer source. The inherent physical variability of litter makes it difficult to achieve uniform distribution across the swath of application. A new model approach, known as discrete element modeling (DEM), has been developed and used to simulate bulk material conveyance. Therefore, research was conducted to evaluate the ability of a DEM to simulate the conveyance and distribution of broiler litter from a commercially available spinner-disc spreader. The objectives were to: 1) Utilize discrete element modeling software to establish a working 3-D simulation for a typical litter spreader and establish assumed and measured properties of uniform, plastic BB's and broiler litter. 2) Calibrate the simulation model through comparisons of simulated particle trajectory to experimental field tests. 3) Validate the simulation model for a litter spreader by comparing the DEM results to empirical testing of conveyance and distribution.

Results for classifying broiler litter properties indicated that the bulk density increased as moisture content increased. The median particle size distribution (d_{50}) ranged from 0.8-mm at 18% MC to 7.2-mm at 24% MC. Model setup and calibration indicated that the coefficient of static friction, energy density coefficient (cohesion), and the coefficient of restitution impacted the simulated spread pattern by controlling the transverse landing location, longitudinal landing location, and concentration of the spread pattern, respectively. While calibrating the DEM model, limitations were discovered. The minimum particle size in which the model could

successfully simulate was 6-mm diameter, mostly attributed to computational power, number of particles, and the size of the domain in which the simulation took place. This discovery limited the model's ability to simulate litter particles and spread patterns that reflected experimental results (R^2= -0.41) since the range of particle sizes for litter was predominately less than 6-mm. The DEM model performed well simulating patterns for plastic BBs (R^2=0.85). Model validation for plastic BBs demonstrated that the DEM model lost its predictive ability to estimate the spread pattern when changing spinner-disc speed or drop location and the simulated spread patterns did not reflect those achieved from field experiments. When the disc speed was increased from 400 to 600-rpm, the coefficient of determination decreased to 0.30 from 0.85. Therefore, the model would require calibration for a new spreader hardware setup. It is hopeful that DEM modeling can be used in to support spinner-disc spreader design in the future.

ACKNOWLEDGEMENTS

First, I have to thank God for walking with me daily from beginning to end. Through all of the difficult times, He was there to guide me. I have to express my sincere gratitude to all of those in the Biosystems Engineering Department that, in so many ways, helped me finish my research and attain this degree. If not for those that helped me in running experiments and field tests, Daniel Mullenix, Ajay Sharda, Simerjeet Virk, Christian Brodbeck, Ravinder Thaper, David Herriot, Trey Tidmore, Tyler Phillips, Daniel Rogers, Jarrod Litton, John Lancaster, Aurelie Poncet, and Will Graham, I would not have completed my research and this thesis. A special thank you goes to Greg Pate and his staff at E.V. Smith Research Center, for allowing me to conduct my research on the premises and for going out of their way to assist me in any way possible. Thank you to those that served on my committee, Dr. Tim McDonald, Dr. Oladiran Fasina, Dr. Wesley Zech, and Dr. Larry Crowley. I want to especially thank Dr. John Fulton for serving as the co-chair on my committee and for advising me over the past three years. His leadership, knowledge, and wisdom that he shared with me will go with me into my career. Lastly, I must thank my parents (Terry and Susan), my sister (Anne-Marie) and the rest of my family and friends who prayed and supported me throughout my academic endeavors.

TABLE OF CONTENTS

LIST OF TABLES

LIST OF FIGURES

CHAPTER ONE

Introduction

1.1 Preface

Across the United States, the use of organic fertilizers in crop production has increased due to the escalating costs of inorganic fertilizers. Figure 1 illustrates the cost of the three most common types of fertilizers used in the U.S. from 1960 to 2011 for producing crops. Since 2006, the price for ammonium nitrate has increased by 31%, super phosphate by 95%, and potassium chloride by 120% (ERS-USDA, 2011). These trends indicate that fertilizer costs will continue to increase over time. Thereby, crop producers are considering the use of organic fertilizers since they usually provide a cheaper and readily available source of fertilizer.

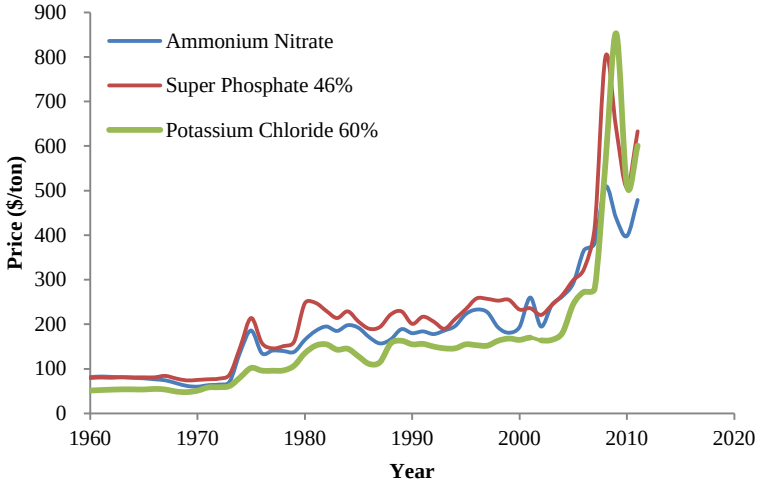

Figure 1. U.S. fertilizer pricing from 1960 to 2011 (ERS-USDA, 2011).

In Alabama, broiler litter represents the primary organic fertilizer generated due to the state's poultry industry. In 2006, approximately 1.7 million tons of poultry litter was produced in Alabama (Mitchell et al., 2006) with over 90% applied to pastureland and row crops (Dillard et al., 2012). Unfortunately, the majority of this litter application has occurred repeatedly over the same areas in the northern half of the state with 29% of the broiler production taking place in three neighboring counties: Cullman, Dekalb, and Marshall (NASS-USDA, 2011). This practice of repeated application over time has led to increasing environmental concerns when using organic fertilizers, especially litter, due to potential off-site movement of phosphorus (P) and nitrogen (N) into water bodies.

New technologies such as GPS-based guidance and variable-rate technology (VRT) are being implemented to apply litter only where it is needed, thereby reducing or eliminating the amount of over-application of nutrients. Unfortunately, the uniformity of spread when using litter can be poor, even with the latest technology. Poor uniformity can be attributed to the mechanical conveyance and distribution systems of a litter spreader. The most common type of applicator used to apply litter is the spinner-disc spreader since it is economical, simple mechanically, and easy to use.

The basic design of the spinner-disc spreader has remained the same over the years. Past research efforts have been conducted to optimize hardware design and settings. However, limited research has addressed using discrete element modeling (DEM) to evaluate the conveyance and distribution of litter. The concept of using DEM to evaluate and design spreader hardware is a new method that has not been thoroughly investigated. This research makes a step toward testing the hypothesis that simulations based on the DEM can aid in the development of

spinner-disc spreaders. Implementing DEM could reduce time spent designing and conducting experimental pan testing of different spreader hardware configurations and rate controller setups.

1.2 Justification

Limited spinner-disc spreader research has been conducted focusing on the application of poultry litter. Most research has addressed the application of inorganic fertilizers, such as urea, potash, ammonium nitrate, etc. With the increasing use of poultry litter for crop production and the potential negative environmental effects that are related with the over-application of litter, it is believed that measures are needed to improve metering accuracy and distribution uniformity of poultry litter during field application. These measures need to ensure that over-application or application in unwanted areas does not occur thereby reducing environmental risks. An effort by the fertilizer industry and the USDA-NRCS focuses on nutrient stewardship. This approach entails managing fertilizer, both organic and inorganic, in an environmentally sound manner and has been termed as the "4R's to Nutrition Stewardship." The 4R concept represents the: Right Source, Right Rate, Right Time, and Right Place. The importance of the 4R's was demonstrated through incorporation of this concept into the recent update of the NRCS Code 590 (USDA-NRCS, 2011).

Maintaining acceptable distribution and accurate metering of litter is essential to reduce over-application of litter in environmentally sensitive areas. The foremost environmental concern with litter is phosphorus (P) concentration. On average, litter has a fertilizer rating of 3-3-2 (N-P_2O_5-K_2O; Wood, 1992) indicating that it contains as much P_2O_5 as nitrogen (N). This concentration becomes a problem when farmers apply litter to meet N requirements which is typically much higher than P requirements. This type of action over the years leads to a buildup of P in the soil potentially causing harmful amounts of P to be deposited into surface waters via

runoff. This concern is particularly an issue in Alabama where approximately 90% of the litter generated is used to fertilize crop and pasture lands (Dillard et al., 2012). More recently, states are basing litter application on soil P levels to meet environmental regulations. If excessive P reaches surface water bodies, the process of eutrophication can occur, negatively impacting aquatic life.

Litter spreader designs are most likely based on research conducted using fertilizer spreaders. In previous research, spread pattern distribution tests were conducted to determine the effects of spreader hardware design and setup on the application of granular fertilizer. Research results have been applied to litter spreaders. Limited, scientific based, research and development has been conducted on litter spreaders due to litter having a small economic value relative to other dry materials (e.g. inorganic fertilizer). Effort related to litter spreader design by manufacturers has been based on experience or trial-and-error. DEM could provide a research and development tool for litter spreaders to aid in improving the mechanical design and suggesting hardware setups for field usage. DEM modeling also has the capability of predicting bottlenecks and obstructions in material flow, reducing the amount of empirical testing, thereby improving metering and application uniformity while proving to be an essential engineering tool for spinner-disc spreader manufacturers.

1.3 Objectives

The overall goal of this research is to evaluate a modeling approach to improve litter application by reducing time commitment of equipment manufacturers in research and development of spinner-disc spreaders along with setup recommendations to end-users. The objectives of this research were to:

1. Utilize discrete element modeling (DEM) software to establish a working 3-D simulation for a typical litter spreader and establish assumed and measured properties of uniform, plastic BB's and broiler litter.
2. Calibrate the simulation model through comparisons of particle trajectory simulations to experimental field tests.
3. Validate the simulation model for a litter spreader by comparing the DEM results to empirical testing of conveyance and distribution.

1.4 Thesis Organization

The *Introduction* chapter overviews the justification and emphasis of this research, including the overall research objectives. Chapter 2 provides a *Review of Literature* outlining the characteristics of poultry litter, poultry litter application, and the concept of discrete element modeling. The *Materials and Methods* chapter describes the experimental tests and related analysis. Chapter 4 presents the *Results and Discussion* reporting summarized data, statistical analyses, and corresponding discussion about the research findings. The *Conclusions* chapter outlines the research conclusions and suggestions for future research. A reference list and supporting appendices are presented.

CHAPTER TWO

LITERATURE REVIEW

As prices of inorganic fertilizers continue to increase, the use of organic fertilizers, such as poultry litter, has increased in crop production. Since organic fertilizers contain a significant source of nutrients and are inexpensive to attain compared to inorganic fertilizers, this trend is expected to continue. In recent years, the over-application of nutrients has generated environmental concerns due to potential off-site transport of P and N into water bodies. Therefore, uniform and accurate application of poultry litter is essential to limit over-application of nutrients while meeting target rates established through nutrient management planning. Research studies have been performed in order to gain a better understanding of the different variables associated with using poultry litter as a fertilizer or soil amendment along with possible environmental impacts. Prior literature was reviewed to assemble physical and chemical characteristics of both organic and inorganic fertilizers. However, limited research has been performed to fully understand the conveyance and distribution of litter and the ability to apply consistently in a uniform manner on crop- or pasture-lands using available spreaders. Literature was also reviewed to understand the concept of discrete element modeling (DEM) and its ability as a method to more efficiently design spinner-disc spreaders. With DEM in mind, the impact of spreader hardware components and litter properties on spread pattern uniformity were reviewed.

2.1 Poultry Litter

The use of poultry litter as a land-applied fertilizer or soil amendment is common in the state of Alabama due to its large poultry industry. According to the USDA-NASS (2010), Alabama ranks third in the US for poultry production; mainly broilers. As a result, about two million tons of poultry litter is generated annually (Mitchell and Tyson, 2001) with 90% of it land applied (Dillard et al., 2012). Poultry litter is recognized as an alternative fertilizer to synthetic fertilizers due to its high nutrient content and its comparable yields at lower costs (Wood, 1992). Most of Alabama's poultry production is located in the northern half of the state with production facilities centralized within a few counties. Land around these facilities is limited for litter application. Due to the high cost of fuel, it is not economical to transport litter over large distances. This situation has resulted in multiple applications within the same field or pasture over the years. Thereby, the continual application on the same field over the years has led to environmental concerns with the potential of excess phosphorus (P) levels to leach or runoff into water bodies.

2.1.1 Physical Properties and Impact on Distribution

Knowledge of the physical and flow properties of poultry litter are fundamental to designing and operating efficient conveyance and distribution systems. However, there is a lack of published research that targets the physical and flow properties of manure products. This limited information is partly due to the variability in material properties of poultry litter. Thirion et al. (1998) stated that the variability of animal manure characteristics is due to the large diversity of livestock, storage type, and handling equipment and that the performance of a spreader is directly related to the physical properties of the material being applied.

2.1.1.1 Particle Size and Distribution

Several publications have documented that particle size and distribution have an effect on spread pattern uniformity. Wilhoit et al. (1993) reported observations on the effect that particle size had on spreading distance. They concluded that small particles tended to land directly behind the spreader and large particles were distributed more evenly with a larger swath width. Glancey and Adams (1996) identified maximum lump size and moisture content as the physical properties presenting potential problems in manure conveyance.

Landry et al. (2004) used a soil sieve shaker to evaluate the particle size distribution of different manures, including poultry litter, and calculated the modified geometric mean lengths. They stated that large lumps that were retained on the top screen (25.4-mm openings) yielded an overestimation of the particles' geometric mean length. The calculations were then adapted to using 16.4-mm as the largest size opening to obtain a modified geometric mean length. Particles on the top screen were between 30 and 50-mm, but large lumps of 100 to 150-mm were measured as well. Landry et al. (2004) noted that the large lumps would affect the conveying behavior of manure products. Fasina (2006) determined the particle size distribution of poultry litter by placing 100-g of material on a set of sieves (3.2-mm, 1.6-mm, and 0.8-mm) and shaking them for 15 minutes. He reported the geometric mean diameter of the particles captured on each sieve as being 0.356-mm, 0.191-mm, and 0.143-mm, respectively.

Hofstee and Huisman (1990) stated that the importance of a material property for granular fertilizers depends on the process (e.g. conveyance, distribution, etc.) the fertilizer is in at any moment. They reported that particle size and distribution had an effect on production, storage, transportation, blending, and distributing. Reumers et al. (2003) investigated the effect of particle size and shape on the tangential and cylindrical distribution patterns. They concluded

that larger particle diameters cause the particles to achieve higher speeds on the disc causing them to leave the disc earlier. It was also reported that irregularly shaped particles will most likely result in wider distributions patterns. In their study of pattern sensitivity to location of fertilizer drop location, Parish and Chaney (1986) noted that the segregation of particle sizes at the center and overlap points within the spread pattern was obvious after performing a sieve analysis on the fertilizer captured at these locations. From this observation, Parish and Chaney (1986) noted that segregation of a fertilizer material could lead to uneven application of fertilizer. Pezzi and Rondelli (2002) studied four types of poultry litter differing in storage time. They indicated that particle size distribution is affected by storage time. The litter with the shortest amount of storage time had the greatest amount of large particles. Pezzi and Rondellie (2002) also noted that large particles impacted the drop location of litter onto the discs.

2.1.1.2 Bulk Density

Glancey and Hoffman (1996) investigated the physical properties of poultry manure and compost to determine bulk mechanical properties and their effect on material handling systems. They concluded that wet bulk density was dependent on the moisture content of the solid wastes and that knowledge of moisture content was more important than the type or source of material. In their development of a drop applicator, Wilhoit et al. (1994) noted that bulk density can vary considerably depending on moisture content. An average bulk density value was calculated to be 480-kg/m^3. Hofstee and Huisman (1990) reported that bulk density has an effect on the storage and transporting processes of granular fertilizers. Parish and Chaney (1986) observed that a lower density fertilizer has less pattern variability among replications. Reed and Wacker (1970) reported that bulk density has a significant effect on the distribution pattern in both width and

shape. Thirion et al. (1998) observed that bulk density varies greatly within the same batch of manure. It was suggested that the movement of livestock, which compacts the manure, attributes to the variability. Landry et al. (2003) quantified the bulk density of poultry litter at different levels of total solids concentration (TS) ranging from 20% to 50%. The bulk densities at 20%, 30%, 40%, and 50% were 1091.8-kg/m^3, 1028.2-kg/m^3, 884.7-kg/m^3, and 607.5-kg/m^3, respectively. Pezzi and Rondelli (2002) reported that the bulk density of the poultry litter in their study ranged from 220-kg/m^3 to 404-kg/m^3 and litter with the shortest storage time had the lowest density.

Glancey and Hoffman (1996) investigated the effects of grower practices on poultry manure physical properties. Samples were taken under the following conditions: fresh poultry manure total cleanout, fresh poultry manure crust out, poultry manure crust out stored outside for 5 weeks, and poultry manure crust out stored outside for 14 weeks. The crusted manure piles tested were all removed from a house after one flock. The total cleanout manure piles tested each had at least 12 flocks on the litter since the last cleanout and each of the houses were crusted out after each of the flocks. It was concluded that outside storage and an exposure to rainfall significantly increased the wet bulk density of poultry manure. The majority of the density increased within the first 5 weeks of outside storage. There was a dependency of bulk density on moisture content across all of the solid wastes evaluated. Glancey and Hoffman (1996) also reported that moisture content was increased due to outside storage and exposure to rainfall. They concluded that moisture content was more important than knowing the source of the waste material.

The American Society of Agricultural and Biological Engineers (ASABE) Standard, D384.2, Manure Production and Characteristics (ASABE Standards, 2005), provides

characteristics of different manures. Broiler litter was reported to have a moisture content of 31%. Tasistro et al. (2004) sampled poultry litter from truck loads and different areas of a commercial chicken house. The average moisture content of the truck loads was 34%. Samples collected from the center of the house, around the feeder, and vicinity of the central waterer averaged 29.7%, 17.4%, and 54.6%, respectively. Mitchell and Donald (1995) reported that poultry litter moisture content will average 70% to 77% when excreted, but average 20% after drying under normal house conditions. They also indicated that composted litter moisture content will be around 40%.

Pezzi and Rondelli (2002) reported moisture contents of poultry litter that was stored for different time periods. Moisture contents ranged from 28.8% to 39.6%. They concluded that the level of moisture content is important for the mechanical distribution of the material and that poor manure protection during storage can deteriorate the physical properties of the litter. Consequently, this deterioration would compromise the conveyance performance of a spreader. Landry et al. (2004) noted that as the total solids concentration of manure products decreased, the aggregation ability would increase.

2.1.1.3 Coefficient of Friction

Duhovnik et al. (2004) studied the material transport of cattle manure along the spinner disc to improve the working principles of spreading it. It was reported that manure with moisture contents of 79% and 70% had a coefficient of friction equal to 0.67 and 0.77, respectively. This variation indicated that manure with lower moisture contents had higher coefficient of friction values. Thirion et al. (1998) tested manure on an inclined plane to evaluate

friction. When the inclined plane was at approximately 40°, the manure began to slip. The friction coefficient was calculated as f = tan(40°) = 0.84.

Landry et al. (2003) calculated the amount of friction between different manures (pig, poultry, cattle, and sheep) and different surface materials (bare steel, painted steel, plastic, and plywood). The inclined plane method was used to measure the amount of friction. Results indicated that there was a fair amount of variability observed. However, similar values of friction coefficient were also present. When all coefficient of friction values were analyzed together, no significant differences were found between materials except for plywood. The resulting linear regression equation based on total solids concentration was:

$$\text{Static friction coeff.} = 1.34 - 0.11TS;\ R^2 = 0.71 \quad (1)$$

where TS is the total solids concentration. While no values for the static friction coefficient were reported, Landrey et al. (2003) used equation (1) to predict the static friction coefficient of the tested manure products over the selected surface materials.

Duhovnik et al. (2004) also reported that the coefficient of friction has an impact on both the length of the path traveled on the disc and the magnitude of radial speed. Higher coefficients of friction yield lower radial speeds. An increase in the coefficient of friction from 0.35 to 0.95 resulted in a 33% longer path and 40% decrease of the radial speed. Brinsfield and Hummel (1975) also reported the same conclusions. Hofstee and Huisman (1990) indicated that the coefficient of friction has an impact on discharge velocity of the particles, discharge angle, and discharge position on the spinning disc. Hofstee (1995) studied the influence of the coefficient of friction on the motion of particles on a disc and along a vane. A simulation model was utilized to help predict the impact of friction. Results showed that it was difficult to demonstrate the effect of friction on the motion of the particles. Glancey and Hoffman (1996) found little

practical difference of the static coefficients of friction for poultry manure with high (66.4%) or low (24.3%) moisture contents with regard to designing material handling systems.

2.1.1.4 Coefficient of Restitution

Little information has been published regarding the coefficient of restitution and how it affects the conveyance and distribution of fertilizers. The coefficient of restitution expresses the relative amount of energy a particle retains or its bounce once dropped from a known height and impacts a surface. Inns and Reece (1962) studied the motion of spherical particles on a disc when the feed of particles onto the disc was off-center. The effect of restitution becomes important when the off-centre distance increases. The dropped particle will make contact with a vane and will either leave the disc after the first or subsequent impacts with a gain in velocity or leave the disc after the impacts have subsided and it moves radially along the vane. Hofstee and Huisman (1990) reported that the coefficient of restitution has an effect on the distribution of fertilizer particles and that it is important when mass flows are considered instead of the case of a single particle. It was concluded that even though the bouncing of particles is limited due to particle-to-particle interaction, it is expected that the bouncing will result in a lower coefficient of friction than measured in friction studies. Hofstee and Huisman (1990) reported coefficient of restitution values ranging from 0.20 to 0.50 with some lower and higher extremes.

2.1.2 Nutrient Content and Value

Poultry litter is used primarily for its nitrogen (N) value when used in crop and pasture production. However, N availability from broiler litter is the most difficult of the three primary nutrients to predict according to Mitchell and Donald (1995). Approximately one-third of the total N present in broiler litter is in the form of ammonium (NH_4-N) and the rest is in an organic

form. The amount of N available for plant uptake is ammonium nitrogen plus the organic nitrogen that mineralizes during the growing season. The average nutrient grade of broiler litter is 3-3-2 (N-P_2O_5-K_2O) according to Mitchell and Donald (1995). Mitchell and Donald (1995) stated that the ammonium N fraction is subject to conversion to ammonia gas (NH_3) and atmospheric loss. Reported losses due to volatilization are typically 15% to 50% of the ammonium fraction when the broiler litter is surface applied. However, organic N becomes available for crop uptake as litter decomposes. Mitchell and Donald (1995) also indicated that for Alabama, 60% of the organic N may be released during the first year after application. Phosphorus (P) and Potassium (K) fractions are considered to be around 75% as effective as commercial fertilizers during the first year of application. If litter is applied at rates which supply the entire required N by the crop, there is a risk of over-application of P and K. When litter is applied frequently, P can buildup in the soil over time to high levels potentially generating environmental risks. Potassium may also buildup unless large quantities of hay or forage are removed during harvest periods.

With rising costs of commercial fertilizers, poultry litter is becoming more valuable. Farmers and landowners are finding that they can save money by substituting litter for commercial fertilizer. Ritz (2006) reported that the economic value of litter based on the commercial nitrogen, phosphate and potash costs at the time and the first year efficiency factors of 70%, 80%, and 100% for N, P, and K, respectively, was $47.20 per ton. Ritz (2006) further stated that litter was sold at $10 per ton. Three tons of litter per acre purchased for $30, supplies the same amount of nutrients in an equivalent commercial fertilizer application costing $179; a savings of $149 per acre.

2.1.3 Environmental Issues

In the past, fertility recommendations for litter were based on N requirements which could result in over-application of P. Over-application of P can produce water quality concerns since P requirements relative to plant needs are generally less than N requirements (Sharpley et al., 1993; Wood, 1998). A water quality issue associated with P is eutrophication, which can impair water bodies. Eutrophication is a process in which excess nutrient levels exist within the body of water. This excess of nutrients increases plant growth (e.g. algal bloom) decreasing the amount of dissolved oxygen available for aquatic life (Campbell et al., 2010b).

2.1.3.1 NRCS Code 590

The NRCS Code 590 (USDA-NRCS, 2011) was created to manage all aspects of nutrient application to the soil by setting regulations on amount, timing, source, and placement of nutrients, whether the sources be inorganic or organic. NRCS Code 590 (USDA-NRCS, 2002) provides rules that pertain to the application of poultry litter in Alabama are: application shall be 15.24-m from surface waters of the state, 30.48-m from the nearest occupied dwelling, church, school, hospital, park, or non-potable water wells, 61-m from Outstanding National Resources Water, Outstanding Alabama Water, potable water wells, or public water supply, and it is not to be applied across property boundaries unless the adjoining property owner consents in writing. Precautions should be taken to eliminate or minimize nonpoint source pollution to the ground and surface waters. Conservation plans developed to minimize agricultural nonpoint source pollution of surface or groundwater resources will include practices and/or management activities that will reduce the movement of nutrients from the site. Under a conservation plan, each site, farm, or field shall be evaluated using the P index and the Leaching Index to assess the

movement of applied nutrients in the soil to protect the quality of the water resources in the state. For those fields located in environmentally high risk areas, erosion, runoff, and water management controls shall be installed.

For Alabama, a soil test must be conducted using either the Auburn University Soils Testing Laboratory or an acceptable laboratory to determine the allowable amount of nutrients that can be applied (USDA-NRCS, 2011). Soil tests older than three years cannot be used within nutrient planning. It is recommended that soil amendments, such as lime, should be used to adjust soil pH prior to nutrient application. When it comes to nutrient application, NRCS 590 states that the application of nutrients needs to be based on current soil tests reports and that the application shall not exceed 10% of the intended rates of the field. When applying organic by-products, such as poultry litter, the acceptable rate is generally based on the amount of P that can be applied to the soil based on the P index rating for the field.

2.1.3.2 Phosphorus Index (P Index)

Recently, Alabama, along with most states, has started basing litter application recommendations on crop P requirements or on qualitative indices such as the phosphorus (P) index (P index; Sharply et al., 2003). The P index represents a tool used to assess P movement across the landscape and to make better P application decisions (USDA-NRCS, 2011). When the P index rating is low/low, litter can be applied to meet the N requirement of the crop being grown even if it means the P rating exceeds 10% of the established application rate. However, once the rating exceeds the medium rating, litter should be applied in accordance to the intended P rate. In this case, an additional source of N can be used to meet the N requirement. Organic fertilizers, such as litter, cannot be applied in Alabama during the fall and winter seasons unless

on an actively growing crop. However, for north Alabama, no application can occur between November 15 and February 15 due to crop inactivity (USDA-NRCS, 2011) through these winter months.

2.2 Overview of Spinner-Disc Spreaders

The spinner-disc spreader has been a popular choice for distributing organic and inorganic fertilizers for decades. Spinner-disc spreaders provide an economical application solution due to its simple design, ease of handling, and ease of cleaning (Brinsfield and Hummel, 1975). This type of applicator, shown in Figure 2, uses a chain to convey the material out of the hopper onto dual spinning discs which distribute the litter across some fixed width behind the spreader. A flow divider is used to divide the flow of material evenly to both discs as it drops off the conveyor chain.

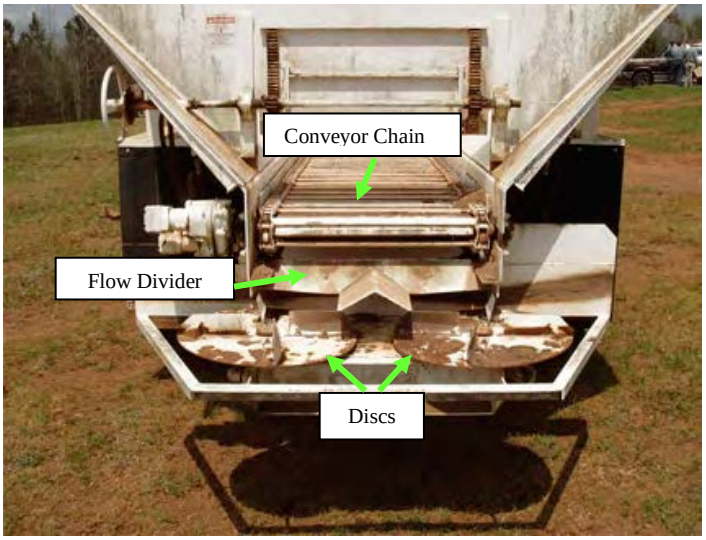

Figure 2. Conveyance and distribution hardware for a traditional spinner-disc spreader.

The application rate at any distance from the spreader centerline of travel varies, with the highest application rate at the center with decreasing amounts moving away from the center (Figure 3). The desirable pattern must be symmetric to the left and right of the center in order to

achieve a uniform distribution of material. Grift (2000) investigated the quality of spread patterns using a Spread Pattern Analysis tool (SPAT). He concluded that the best spread pattern had a Gaussian shape (bell curve). Desirable shapes were triangular or trapezoidal and undesirable shapes were skewed trapezoidal, M-shape (without skewness), and a crown shape.

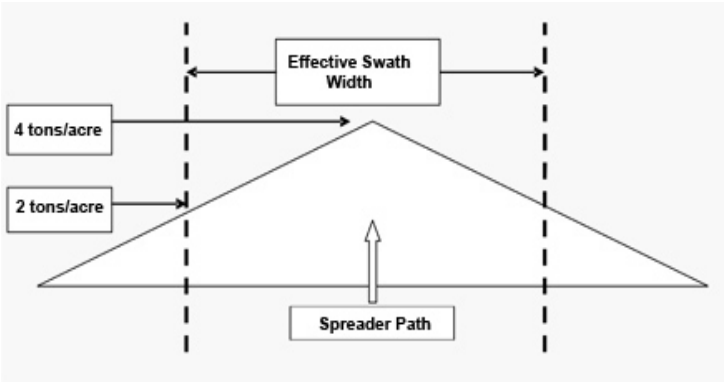

Figure 3. Desirable single-pass pattern and effective swath width (Worley et al., 2010).

Spinner spreaders rely on overlap from adjacent passes to achieve uniform distribution (Figure 4). The mean overall application rate and application uniformity depends on the overlap pattern of litter. The amount of overlap depends on how far the spinner discs throw material and on the swath width, which is the distance from the centerline of travel of one pass of the spreader to the centerline of travel of the adjacent pass. The overlap affects the two main objectives for poultry litter spreader operations; applying the litter at the desired application rate and as uniformly as possible (Wilhoit and Ling, 1999b).

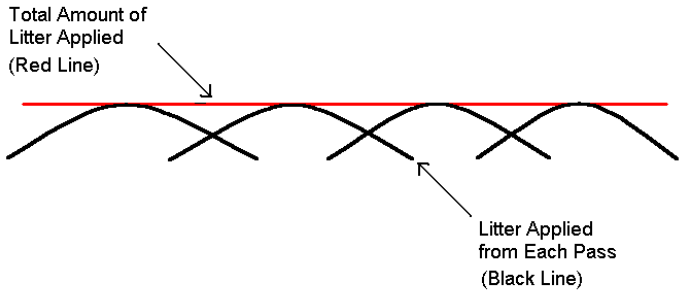

Figure 4. Multiple-pass spread pattern (Henshaw, 2005).

Spinner-disc spreaders have a disadvantage of producing an uneven (poor) distribution of material on a per pass basis (Figure 5 showing typical single-pass pattern). Pattern uniformity for dry spreaders, measured on a mass basis, is evaluated using the coefficient of variation (CV; ASABE Standard S341.3, 2009). An uneven distribution pattern can result in yield variations and losses. Hepherd and Pascal (1958) and Hawkins (1971) showed that any deviation from a uniform distribution pattern resulted in decreased crop yield.

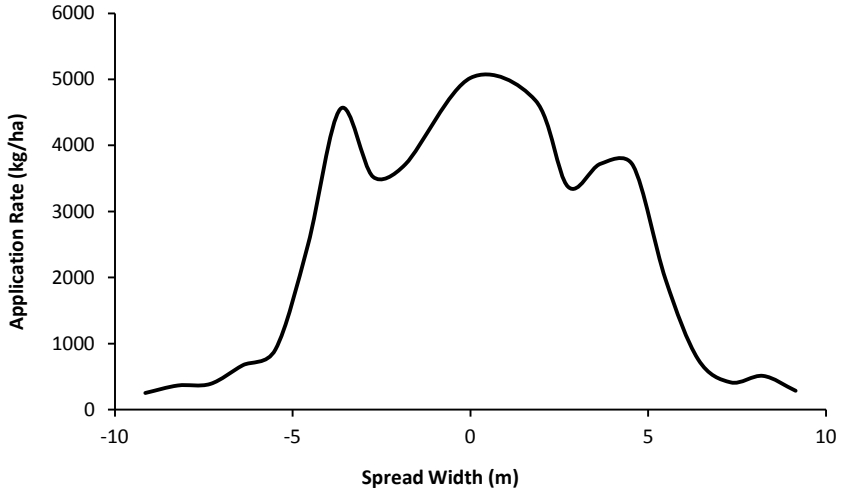

Figure 5. Typical single-pass spread pattern from a litter spreader.

Sogaard and Kierkegaard (1994) found that values for CV are higher during field application than in controlled laboratory settings. CVs for the best spreaders corresponding to

the transverse spreading pattern are between 15% and 20%. Fulton et al. (2005a) considered CVs less than or equal to 20% acceptable for spinner spreaders when using inorganic fertilizers and suggested that most managers of granular applicators commonly accept CVs less than 20%. However, Campbell et al. (2010) suggested that when using poultry litter, a CV of 25% or less might be acceptable due to the inherent variability of litter compared to inorganic fertilizers.

2.2.1 Calibration of Spinner Spreaders

Calibration is an important procedure to ensure spreaders are applying the proper target rate uniformly for a particular setup. The procedure of calibration is normally performed on an annual basis or when a new product is being applied for the first time. When using animal or poultry manure, the spreader cannot be utilized effectively unless the user knows how much is being applied to a given area. Ogburn and Donald (1990) stated that only by knowing the application rate of a spreader can one correctly apply manure in a corresponding manner to crop needs. Over-application of fertilizers can increase the chance of ground water contamination (Hammond et al., 1997) by providing excess nutrients not used by the growing crop. Fulton et al. (2005b) found that simulated overlap graphs could be used to make pattern adjustments generating a more uniform distribution patterns for all applicators. They also stated that overlap patterns should be generated during calibration procedures to more efficiently quantify application uniformity.

The guidelines for calibrating dry or granular spreaders are outlined in the American Society of Agricultural and Biological Engineers (ASABE), Standard S341.4 (2009), Procedure for Measuring Distribution Uniformity and Calibrating Granular Broadcast Spreaders. An International Standards Organization (ISO 5960-1) (ISO Standards, 1985), also exists that is

similar to ASABE S341.4. This standard provides a uniform method to test, analyze, and report performance data for spinner spreaders. Guidelines are established for test setup, size of collection devices, test procedures, and calculation of application rate and effective swath width. A few important standard test setup parameters include conducting tests with the following criteria: ground slope <2%, wind velocity <8-km/h, and hopper fill level at least 40% to 50% capacity (ASABE Standards, 2009). The International Organization for Standardization (ISO) has also provided a standard for calibrating dry or granular spreaders entitled ISO 5690-1 (ISO Standards, 1985), Equipment for distributing fertilizers--Test methods--Part 1: Full width fertilizer distributors.

The Alabama Cooperative Extension System (ACES) published an article identifying calibration procedures for poultry litter spreaders (Mitchell and Tyson, 2001). Factors such as ground speed, power takeoff (PTO) speed, discharge opening, and swath width need to be monitored during calibration. Mitchell and Tyson (2001) discussed three methods of calibration. The first method included applying litter over a field of known area and measuring the amount applied by weighing the spreader before and after application. The amount applied is divided by the applied area to compute the actual rate (T/ha) which is then compared to the target rate. Spreader adjustments are then made accordingly based on manufacturers recommendations to ensure the actual and target rates are close. The next method utilizes a tarp placed on the ground with the litter spreader then making three equally spaced passes (equal to swath width) over the tarp. The material caught on the tarp is weighed then divided by the tarp area to compute the application rate. Again, the computed rate is compared to the target rate with spreader adjustments made accordingly until these two are close. One point about these two methods, as described, is that spread uniformity cannot be computed; only application rate is evaluated.

The last method that Mitchell and Tyson (2001) describe includes setting 11 pans out in the field. Pans should be spaced 3-ft apart and pans on either side of the center pan should be spaced 6-ft apart to allow room for the tires of the tractor and spreader. By making three passes over the pans, both application rate and distribution uniformity can be evaluated. Material caught in each pans is weighed and plotted to determine the material distribution and uniformity. Hammond et al. (1994) of The University of Georgia Cooperative Extension proposes similar calibrating procedures as the ACES. However, one major difference is that they propose using multiple tarps evenly spaced in a line perpendicular to the travel of the spreader instead of collection pans to determine pattern uniformity and swath width.

Parish (2000) used three commercial fertilizer spreaders and two products to compare delivery rates calculated from using collection trays during the calibration tests. Pattern tests were conducted on all the spreaders and pans were set out to conform to the ASABE S341.3 standard (ASABE Standards, 2009). The spreaders passed over the collection pans three times with the application rate determined by converting the mass in each pan to a rate (kg/ha). A calibration of the delivery system was then conducted for each spreader. This calibration was performed by removing the distribution mechanism from each spreader to allow material to be caught in a bucket and the application rate computed after each test. Results indicated that half of the comparisons between rates determined by pattern data versus those computed through calibration were significantly different. In most cases, the rates from pattern data were higher. The difference was assumed to be caused by particles bouncing into collection pans off the hard surface. This study confirmed that significant spreader delivery rate errors can be generated from pattern tests when conducted on a smooth surface; however, errors may or may not occur

on a rough surface. Parish (2000) suggested that rate calibration be conducted after an effective swath width is determined through pattern testing.

2.2.2 Impact of Spreader Components on Material Distribution

The hardware components of a spinner-disc spreader control how the material is conveyed and distributed. The primary components include the gate, conveyor, divider, spinner discs, and vanes mounted on the discs. Each of these components serves a different function in metering, conveying, and distributing material during application. Several studies have been performed to evaluate the impact each component has on the ability of the spreader to perform effectively in distributing material.

2.2.2.1 Gate Height and Conveyor Settings

Metering of material out of the hopper for a spinner spreader is controlled by conveyor speed and gate opening. To achieve certain flow rates, different combinations of conveyor speed and gate height can be used. Wilhoit and Ling (1999b) observed that there was often a cyclic variation in material falling onto the spinner discs. They hypothesized that this flow variation was due to material falling off the conveyor in large chunks rather than in a continuous, uniform stream. This result was more likely to happen with larger gate heights. Tests were conducted to investigate the effects of gate height and conveyor speed on material metering using two flow rates of 0.45 and 1.78-m^3/min with four combinations of gate height and conveyor speed at each flow rate. Material metering was evaluated by measuring the pressure drop across the hydraulic motor powering one of the spinners. Results showed that the variation in pressure dropped increased with increasing gate height over all of the flow rates. The increase in pressure variation was greatest at the lowest flow rate with the variation decreasing as conveyor speed

increased. It was concluded that a combination of low gate height and high conveyor speed would produce less pressure drop variation onto the spinner-discs.

Cunningham (1963) concluded in his performance analysis of bulk spreaders that variation due to conveyor performance may be eliminated by reducing the conveying-time lag to zero or making the conveying velocity proportional to ground speed. Glover and Baird (1973) evaluated some modifications in spreader design that might improve the spread pattern. It was concluded that a reduced gate height setting for narrower swath widths will improve the pattern and a triple overlap, using a swath width which is one-third as wide as the total pattern, will provide uniform distribution for almost any spreader. Consequently, smaller swath widths require more passes resulting in more expense.

Wilhoit et al. (1994) found problems with a gravity flow/agitator method of metering poultry litter. Gravity flow metering uses gravity to force the litter out of the hopper. The litter passes through an agitator which is used to prevent material bridging in the hopper while metering the litter through the opening or orifice. Larger gate heights resulted in litter free-flowing with little or no metering effect from the agitator. When the gate was closed enough to restrict flow, litter clumps completely block flow from the hopper. The application rate fluctuated cyclically in the direction of travel when the floor chain with individual chain flights was used. When a mesh chain was used, the cyclic fluctuations were eliminated and good uniformity achieved in the direction of travel.

2.2.2.2 Flow Divider and Drop Location

The function of a flow divider is twofold. First, it evenly splits the flow of material falling off the conveyer so equally delivered to the two spinner-discs. Secondly, the divider

controls the drop location of material onto the spinner-discs. Cunningham (1963) noted the importance of flow dividers which deliver fertilizer to boom or spinner distributors. He indicated that flow dividers have a critical influence on distribution and must be designed to prevent excessive changes in position of delivery due to spreader motion and field slope. Wilhoit and Ling (1999b) stated that the adjustment by standard deflectors or flow dividers that come with commercial spreaders is very coarse at best. Even with the little adjustment, it is difficult to tell what effect the adjustment will have on the actual material drop location onto the spinner discs. Glover and Baird (1973) stated that even with the best adjustments available, each of the five spreaders they evaluated failed to perform satisfactorily with wet lime and that flow divider adjustments must be made with different application rates.

Wilhoit and Ling (1999b) performed extensive testing to evaluate the effect of drop point location on uniformity and effective swath width over a range of spinner speeds and material flow rates. They concluded that the most effective spread patterns, based on both uniformity and effective swath width, were achieved at the 90° and 135° drop point locations (measured from the front end of the spinners).

Pezzi and Rondelli (2002) also evaluated drop location onto the spinner disc. The drop location varied from 0-mm (center of discs beneath hopper outlet) to 200-mm. They found that adjusting the delivery point was significant. At a spinner speed of 58.6-rad/s, four drop locations, from +40 to +200-mm, showed that the throwing width was slightly influenced by this parameter. However, the distribution pattern and the possibility of overlapping changed remarkably. When the point of delivery was closer to the center of the spinner discs (40-mm), manure distribution was mainly localized in two bands and did not allow overlapping because

the CV was never less than 40%. The best distribution was obtained at +170-mm from the center of the spinner discs, with an acceptable swath width up to 8.5-m and CV less than 10%.

Parish and Chaney (1986) looked at pattern sensitivity to location of the drop point onto the spinner discs for fertilizer. Five drop locations, 20° apart, were tested. The first drop location was -40° from the centerline of the disc and the fifth drop location was +40° from the centerline of the disc. Results indicated that rotating the drop point of material counterclockwise onto a clockwise rotating disc shifted the pattern from side-to-side and helped overcome skewing problems, but was not able to correct all pattern problems.

2.2.2.3 Discs and Vanes

Wilhoit and Ling (1999b) reported that 625-rpms was the approximate disc speed for the litter spreader they tested. However, they also indicated that this disc speed was standard with most poultry litter spreaders of that time. Lower and higher values were used in their tests so the effect spinner disc speed on spreader performance could be evaluated. Results showed that for all flow rates and drop point locations, the higher the spinner speed, the better the uniformity and the greater the swath width. Wilhoit and Ling (1999b) stated that these results were expected for the higher application rates because higher disc speed would reduce the spinners from being overloaded with material at higher material flow rates. For low application rates, the higher spinner speed can be used to throw material further with wider swath widths attainable. These results produced lower application rates for a given flow rate of material onto the spinners indicating that the spinner discs should be operated at the highest possible speed. Pezzi and Rondelli (2002) found that an increase in spinner disc speed improved the throwing width and thereby effective swath width.

Yildirim and Kara (2003) attempted to determine the vane height which provided the best distribution uniformity for a given disc speed at different flow rates. Five different vane heights of 25, 35, 45, 44, and 65-mm were used during these tests. A vane length of 120-mm remained constant for all vane treatments. Four orifice diameters of 30, 35, 40, and 45-mm were used to drop fertilizer onto the discs providing the different flow rate treatments. Triple superphosphate (TSP) and calcium ammonium nitrate (CAN) were the selected fertilizers. Results showed that the most uniform distribution was obtained with a vane height of 35-mm and an orifice diameter of 35-mm for both fertilizers. The mean CV values varied from 7% to 20% for different combinations of vane height and orifice diameter for TSP. Variations of CVs were minimized with a vane height of 65-mm. For CAN, the mean CV values varied from 6% to 17% for different combinations of vane height and orifice diameter. A vane height of 45-mm produced the least amount of variation in the CV values.

Parish (2003) studied the effect of impeller (disc) angle on pattern uniformity using a professional walk-behind turf spreader. He found that as the front of the impeller was angled downward, relative to horizontal, the spread pattern skewed more to the left. Angling the impeller upward caused the pattern to skew more to the right. Impeller angles as-small-as 5° produced significant changes in spread pattern quality. Srivastava et al. (2006) stated that forward-pitched vanes give greater carrying distances for free-flowing materials, while rearward-pitched vanes unload sticky material more readily. Duhovnik et al. (2004) stated that the tangential speed of a piece of manure as it departs the disc is influenced by the size of the disc and its rotational speed. Through theoretical calculations, results indicated that disc rotational speeds should be between 300 and 700-rpms. Reumers et al. (2003) concluded that an increase in vane length resulted in an increase of both tangential and radial velocity of the particles when

leaving the vane. Cunningham and Chao (1967) stated that vane pitch significantly influenced the velocity vector; specifically the direction imparted on granular fertilizer. Their results indicated that the use of two values of vane pitch on a disc, with alternate vanes set at the same value, should provide a positive means of imparting divergent velocities on fertilizer granules. Glover and Baird (1973) evaluated design changes to the spinner disc and vanes. They reported that discs that are dished and tilted have a higher particle trajectory which increases the swath width while reducing interferences from terraces and rough terrain. For a wet-lime or multi-purpose spreader, vanes that were retarded approximately 10° had less tendency to buildup lime deposits. They also concluded that a 10° retarded vane angle had little effect on the spread pattern if the flow divider was adjusted to place material properly on the discs with discs having a 60.96-cm diameter producing the best performance.

2.3 Discrete Element Modeling

The processing and handling of particulate material is a significant factor in production costs in many industries. Some of the means in which these costs can be reduced is by increasing production efficiency, reducing product waste, or increasing processing through-put. In each of these cases, new designs and/or operational techniques are required. Curry et al. (2009) stated that by achieving a small percentage improvement in performance, a large amount of savings may be gained. To assess the benefits of new designs, testing must be performed in either an experimental or simulated mode. By using simulations to minimize the number of design options, substantial savings may be achievable. Discrete Element Modeling (DEM) is an available tool for modeling particulate flow and processes.

DEM is a numerical technique that allows the mechanical static and dynamic behavior of granular materials to be simulated. DEM was developed by Cundall and Strack (1979) and is

based on an explicit numerical scheme in which each particle of a system is individually simulated; a requirement when simulating granular materials. The material flow is modeled using laws of motion. Newton's second law of motion is usually used to describe translational movement with the general rotational dynamics equation used to describe rotational movement. Particles are assumed to be rigid but, in their movement, they are deemed to overlap, producing contact between them. The interaction between particles is monitored by each contact that takes place using a force-displacement law which relates the force involved in the contact between particles with their overlap. DEM has commonly been used in many industrial sectors, such as pharmaceutical, mining and food, to describe the conveyance of materials. DEM has also been used in the design of construction, earth-moving and agricultural machinery. The study of granular material behavior of in silos and hoppers is another common area where DEM has been used (Gonzalez-Montellano et al., 2011). They were able to analyze pressures exerted by the stored material, flow patterns, segregation phenomena, flow modification by the inclusion of inserts, and discharge rate.

The main intention of DEM is to adequately represent a particle's actual behavior within a system. It therefore requires the use of contact models that represent the characteristics of the simulated material as reliably as possible. It also requires the use of values that describe the properties of material(s) under evaluation. These values can be determined through direct measurements or by calibration procedures. However, the material properties must be obtained at a particle (microscopic) level and it sometimes makes direct determination difficult. Few procedures to measure material properties at the particle level have been described within scientific literature and additionally, little information about material properties values is available to adequately use within DEM or similar material simulation models.

2.3.1 Model Setup

Setting up the DEM model is important to attaining an accurate simulation of the mechanical processes and material interactions. Setting up the model involves establishing material properties and interaction parameters, importing geometry and applying necessary dynamics, establishing how particles are to be generated, performing the simulation, and finally analysis. A challenge common to most studies involving the use of DEM is choosing the appropriate input parameters. Contact models are used to characterize the behavior of the particles as they interact with other particles and surrounding geometry. Landry et al. (2009) used two common contact models in his use of DEM to model manure conveyance. The linear contact model was defined by the shear and normal stiffnesses of the two entities that are in contact with each other. Contact stiffnesses are computed assuming that the stiffnesses of the two contacting entities act in series. The linear-contact model can be used to relate the cohesion between contacting bodies using the elastic material properties. The second contact model used by Landry et al. (2009) was the Hertz-Mindlin contact model which represents a non-linear contact model defined by the shear modulus and the Poisson's ratio. The Hertz-Mindlin contact model is not defined for spheres that are in tension and is not compatible with contact bonding. For particle-to-particle interactions, the elastic properties are mean values. For particle-to-geometry interactions, the geometry is assumed to be rigid and elastic properties of the particle are used (Landry et al., 2009).

2.3.2 Model Calibration

When modeling organic fertilizers, such as poultry litter, calibration of the DEM simulation must be performed to account for irregularly shaped particles and variations in

material properties, especially when using spherical particles within the model. Specification of particle shape and physical properties can be a challenge with any DEM software (Curry et al., 2009). In many cases, experimentally derived material properties will not reproduce the desired material behavior in a DEM simulation to the level of accuracy that is required to produce realistic results. In addition, simple tests may not provide the insight into which parameters significantly influence the final result of interest. The purpose of simulating a particulate process with DEM is to achieve an accurate representation of material bulk behavior. Curry et al. (2009) stated that accurate representation was achieved by defining material properties that affect material behavior at the particle scale which consequently creates the overall bulk behavior. When the physical particle size was small relative to the volume of bulk material, further assumptions and scaling were needed to make the problem computationally achievable.

Since direct experimental measurement of these material properties is not clearly defined, and particle scaling reduces the precision of these properties, extracting the correct material properties from a single experiment or simulation and applying it to another becomes difficult to accomplish. In most cases, the direct measurement of particle properties from a bulk process is not possible. Likewise, measuring individual particle properties and applying them to a simulation of a bulk material process may not yield accurate results. Much of this complication is because a DEM simulation will usually consist of uniform particles (spheres or a combination of spheres to build a shape) that are intended to approximate actual particle shapes. Curry et al. (2009) stated that for bulk flows, perfectly matching the sizes and shapes of the entire particle was not possible and further increased the approximation errors of the simulation.

Curry et al. (2009) created an approach to material characterization by defining properties through a series of tests within the EDEM^{TM} software package and an experimental lab test to

measure the objective function for an optimization routine. This optimization routine varied all of the input parameters through multiple EDEM simulations and compared the predicted results to the objective function. This process was repeated until optimized parameter values resulted in simulations that accurately matched empirical experiments. However, creating a computer algorithm is not the only way to calibrate a DEM model.

Dintwa et al. (2004a) calibrated their simulation model by quantifying the dependence of particle landing area parameters on a variety of spreader settings under controlled environmental conditions using Kemira calcium ammonium nitrate (CAN) 27% N as the fertilizer. The spreader settings investigated included orifice properties (shape, dimension and location relative to the spreader disc), vane properties (shape, length, pitch), and disc properties (radius, cone angle, distance between the two spinning discs, angular speed, height above ground). The calibration results confirmed and described the influence of various spreader adjustments on the shape of the distribution patterns. The landing area of the fertilizer was found to be dependent upon the mass flow rate. An increase in mass flow rate increased the size of the landing area on the disc. An increase in rotational speed decreased the landing area on the disc and rotated the position of the landing area clockwise with respect to the travel direction. When the radius of the disc increased, the landing area increased and the position of the landing area rotated counterclockwise but never rotated beyond the direction of travel. Dintwa et al. (2003) stated that ideally the disc radius and rotational speed should not have any influence on the particle landing area as they represent phenomena that occur after the particles have landed on the disc. With an increase in landing area, there is more space and time for particle interactions on the disc. Shifting the orifice opening radially away from the disc center rotated the position of the landing area counterclockwise until the position was in-line with the direction of travel.

Landry et al. (2006b) recreated direct shear and triaxial tests within DEM simulations to calibrate the model. Several numerical direct shear tests were carried out to perform a sensitivity analysis (Table 1) for the various parameters defining the linear and Hertz-Mindlin contact models used in the simulations.

Table 1. Summary of the sensitivity analysis on the parameters defining the linear and Hertz-Mindlin contact models (Landry et al., 2006b).

Contact Model	Young's Modulus E (MPa)	Shear Modulus G(MPa)	Poisson's Ratio ν	Friction Coefficient μ	Contact Stiffness K	Contact Bonds Strength (N)	Regression Equation[a]	R^2
Linear	2.0	n.a.[b]	n.a.	0.5	0.86	n.a.	y=1.2x+76.4	0.95
	0.9						y=0.70x+54.1	0.92
	0.5						y=0.47x+34	0.94
	0.3						y=0.61x+19.8	0.99
	0.15						y=0.60x+16.5	0.97
Linear	0.3	n.a.	n.a.	1.5	1.50	n.a.	y=0.73x+19.6	0.98
					1.20		y=0.71x+18.8	0.99
					1.00		y=0.64x+19.0	1.00
					0.86		y=0.58x+18.8	1.00
					0.75		y=0.47x+20.8	0.96
Linear	0.3	n.a.	n.a.	1.6	0.86	n.a.	y=0.63x+28.5	0.95
				0.8			y=0.51x+25.6	0.97
				0.4			y=0.59x+16.0	0.96
				0.2			y=0.55x+11.8	0.92
Linear	0.3	n.a.	n.a.	0.8	0.86	1.5[c]	y=0.62x+33.5	0.99
						1.0	y=0.72x+27.8	0.99
						0.75	y=0.61x+30.1	1.00
						0.5	y=0.57x+25.8	0.96
						0.1	y=0.52x+24.7	0.95
Linear	0.3	n.a.	n.a.	0.5	0.86	3.0[d]	y=0.62x+10.5	0.93
						1.5	y=0.76x+3.3	0.98
						0.75	y=0.71x+1.6	1.00
						0.25	y=0.58x-0.11	0.90
Hertz-Mindlin	n.a.	2	0.35	0.5	n.a.	n.a.	y=1.25x+16.1	0.98
		1					y=0.93x+13.1	0.96
		0.8					y=0.75x+12.4	0.98
		0.6					y=0.69x+10..2	0.97
		0.4					y=0.39x+2.7	1.00
		0.2					y=0.31x+2.7	0.98
Hertz-Mindlin	n.a.	0.4	0.45	0.5	n.a.	n.a.	y=0.32x+4.9	0.98
			0.35				y=0.39x+2.7	1.00
			0.2				y=0.41x+1.9	1.00
			0.1				y=0.44x+1.1	1.00
			0.05				y=0.42x+1.46	1.00

[a] In the regression equations, y corresponds to the maximum shear stress and x represents the normal stress.
[b] Not applicable (n.a.)
[c] Bonds applied to the whole assembly of particles.
[d] Bonds linking the clustered particles.

2.3.3 Sensitivity Analysis-Effects of Model Parameters on Estimates

Even though the use of DEM modeling is relatively new, information has been published in regards to how material properties affect a simulated distribution pattern. The published literature on this topic was reviewed.

2.3.3.1 Particle Size and Distribution

In their study to model machine-manure interactions of two types of conveying systems, Landry et al. (2006a) found that using clustered particles affected the results of DEM simulations. The clusters were found to be a good means of mimicking clumps present in actual manure and their effect on flow characteristics. Unbreakable clusters caused artificially contact forces in the case of the simulated 4-auger conveying system. The scraper conveyor was less affected by cluster strength. Van Liedekerke et al. (2009) found that larger particles congregate along the vane edge away from the disc center whereas smaller particles are highly concentrated along the vane towards the disc center. Large particles were found to be forced to leave the disc at lower outlet angles than the smaller particles. In agreement with lab experiments, segregation occurred in the simulations, as larger particle tended to leave the disc earlier than the smaller fractions.

2.3.3.2 Coefficient of Friction

Coetzee and Lombard (2011) used a single set of spreader settings to experimentally measure the reference spread pattern of a fertilizer spreader. A sensitivity study was performed to determine the most accurate set of DEM parameters to simulate a fertilizer spreader. It was found that the model was not sensitive to particle stiffness or contact damping. Particle-wall friction influenced the results the most, followed by the particle-particle friction coefficient. An

increase in the friction coefficients caused the particles to stay on the disc longer and rotated the spread pattern in the same direction as the disc rotated.

Van Liedekerke et al. (2006) modeled the path of a single particle on a spinning disc using DEM simulations. They found that the friction coefficient plays an important role in the rotational velocity of the particle. For a friction coefficient of 0.1, the rotational velocity component against the vane was observed to drop by a factor of 0.5 and the particle was sliding across the vane. Another effect of the lowered friction coefficient was that the particle left the disc earlier. In principle, less friction implied less dissipation of energy (e.g. kinetic energy). When the friction coefficient equaled 0.35, the particle-vane contact resulted in a rolling contact with no dissipation of energy. The particle-disc contact on the other hand was found to be a sliding contact and there was dissipation of energy. A coefficient of friction of 0.1 resulted in sliding and thereby dissipated energy for the particle-vane and particle-disc contacts, yet their combined effect was lower than the dissipation in the particle-disc contact with the friction coefficient equaling 0.35. It was concluded that the relationship between the friction coefficient and the final radial velocity was found to be nonlinear but in agreement with the reasoning of less friction results in faster particle motion.

Tijskens et al. (2005) found that friction properties have a larger influence during higher particle flow rates since more energy is dissipated between individual particles. Landry et al. (2006b) concluded that the static coefficient of friction is mostly related to the apparent cohesion of the particles. The increase in the apparent cohesion was proportional to the change in the friction coefficient. Landry et al. (2006c) stated that organic fertilizers, such as manure, has similar characteristics to organic soils and, therefore, used coefficient of friction values of 0.60 and 0.63 for dry and regular compost, respectively. Van Liedekerke et al. (2009) concluded that

the more spherical the particles are, the less sensitive the particle flow is for higher wall-to-particle friction. Internal particle friction has little influence on the spread pattern compared to the particle-to-particle friction. For higher flow rates, the wall-to-particle friction becomes more important, and higher wall-to-particle friction caused particles to spread further in the field.

2.3.3.3 Coefficient of Restitution

In Van Liedekerke et al. (2009), the coefficient of restitution was among other material properties evaluated to study their impact on the simulated distribution pattern. Particles with a high restitution coefficient (0.8) had higher exit velocities when leaving the disc and appeared to have a greater dispersion. This study rationalized that the observed behavior was caused by the fact that elastic particles gained more speed after interacting with the disc and vane. The pattern width was higher when the particles were more elastic (high coefficient of restitution). Reasoning for this observation was that the larger initial area on the disc, associated with the more elastic particles, caused the particles to lose less energy when colliding with the disc and therefore spread farther.

2.3.4 Model Validation

Van Liedekerke et al. (2009) used two methods to validate their DEM model. The first method measured the cylindrical spread pattern (CSP) by using a device that surrounds a single disc with a circular collector tray (Figure 6a). The collector tray was divided into sectors of 30° and positioned 0.5-m from the center of the disc (Figure 6b). NPK fertilizer particles were fed onto the disc by a plastic funnel with an orifice diameter of 0.029-m. The funnel was placed at a height of 0.11-m above the disc and 0.1-m from the disc center. This method provided

information about the tangential mass distribution, but not about the particle exit velocities when they left the disc.

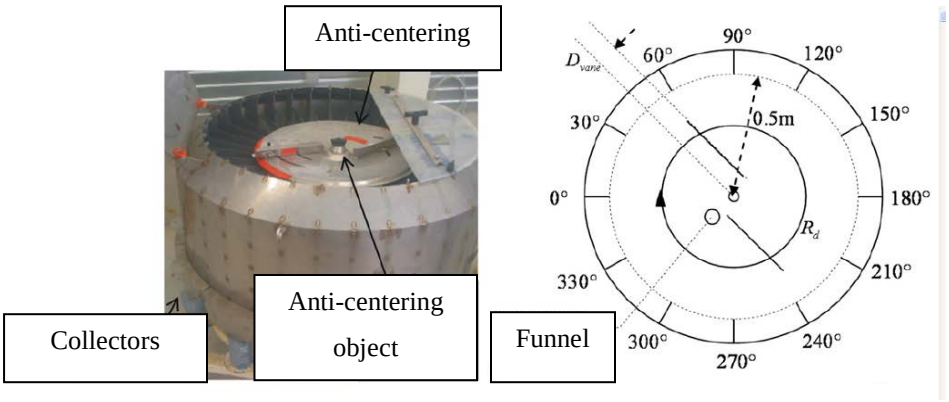

(a) (b)

Figure 6. (a) Testing device for measuring the tangential mass distribution pattern; (b) Geometry of the testing device for measuring the tangential mass distribution pattern (top view) (Van Liedekerke et al., 2009).

The second method measured the transverse spread pattern (TSP) and the total transverse spread pattern (TTSP) produced by a single spinning disc in a large measuring hall. Sixteen baskets were aligned at a distance vector (X,Y,Z) from the disc center (Figure 7) where X is the transverse distance, Y is the longitudinal distance, and Z is the height between the baskets and the disc. The TSP was measured over different Y distances to obtain the TTSP. Y distances were 0-m, -0.5-m, -1-m, -1.5-m, and -2-m relative to the disc center. Values for Y distances of -0.25-m, -0.75-m, -1.25-m, and -1.75-m were interpolated between the measured lines.

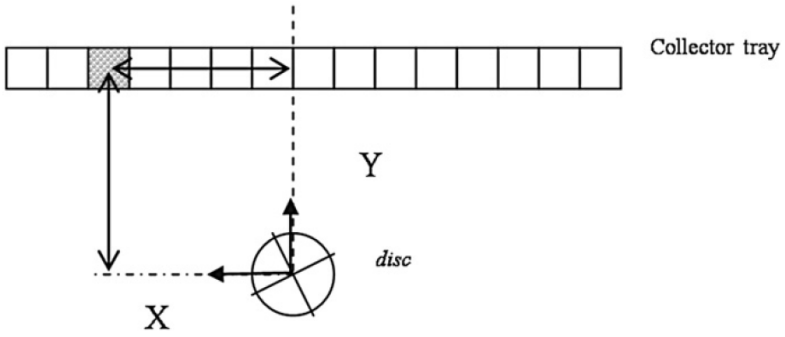

Figure 7. Schematic of the transverse spread pattern (TSP) experimental setup (Van Liedekerke et al., 2009).

Two types of discs were used for the experimental tests. Type A was a flat disc for a lawn spreader with a 0.15-m radius, four vanes and no horizontal flaps. Type B had a conical inclination of 9°, a radius of 0.29-m, and two L-shaped vanes. The vanes had a length of 0.3-m, height of 0.036-m, and were offset 0.045-m relative to the center of the disc. The CSP method used both discs with rotational velocities for disc Type A being: 300-rpm and 400-rpm. Rotational velocities for disc Type B were: 300, 500-rpm, and 650-rpm. At each speed, the test was replicated 5 times. The TSP method only used the Type A disc with rotational velocities of 300-rpm and 400-rpm.

Once the two experimental methods were performed, simulations replicating both experiments were run. To compare experimental versus simulated data, three variables were calculated for the CSP experiment. Average distribution angle was defined as:

$$\bar{\alpha} = \sum_i f_i \alpha_i \quad (2)$$

where α_i is the angle of each *i*-th compartment and $f_i = \frac{M_i}{M_{tot}}$ the fraction of particles. The width of the pattern, β, was calculated as:

$$\beta = \sum_i f_i \left| \alpha_i - \bar{\alpha} \right| \quad (3)$$

Comparisons between simulation output and experiment data were made by using Olieslagers deviation function RD (Olieslagers, 1997):

$$RD(exp,sim)=\frac{\sum_i(|M_{i,exp}-M_{i,sim}|)}{M_{tot,exp}+M_{tot,sim}}100 \quad (4)$$

The TSP experiment used a modified version of the Olieslagers deviation function to compare the mass of particles from experimental results to simulated data for the different Y distances.

$$RD_Y(exp,sim)=\frac{\sum_x(|M_{XY,exp}-M_{XY,sim}|)}{M_{Y,exp}+M_{Y,sim}}100 \quad (5)$$

For the CSP measurements, the experimental and simulation values for disc Type A were close, yielding RD(exp,sim) values less than 5%. For disc Type B, the RD values for 300-rpm and 500-rpm were less than 10% and less than 19%, respectively. At 600-rpm, RD values were approximately 21%. For the TSP measurements, the relative average deviation (RD) values at 400-rpm were approximately 25% and around 21% at 300-rpm. Van Liedekerke et al. (2009) stated that overall, the DEM simulations performed well when the comparison to the experiments was made qualitatively. Deviations for the CSP experiment grew with higher disc rotational speeds and the simulations lost their quantitative predictive value. A similar conclusion was made for the TSP experiment even though the disc speeds were relatively low. It was concluded that the deviations were mainly due to an over concentration of fertilizer mass in the radial direction compared to the experiments, especially at higher disc speeds. A similar effect was observed by Reumers et al. (2003) who conducted experiments in a spreader hall and tried to predict the spread patterns by means of a ballistic model and measurements of the particle outlet velocities at the edge of the disc. Van Liedekerke et al. (2009) stated that one could link these deviations to the conclusions made by Reumers et al. (2003) and that was

plausible to assume that the deviations are due to miscalculation of the velocities, especially the vertical component, at the disc edge.

Reumers et al. (2003) performed similar tests to that of Van Liedekerke et al. (2009) to evaluate the cylindrical distribution pattern, which represents the tangential and vertical mass distribution of the granular flow, transverse, and static distribution patterns. Two types of fertilizer used were—calcium ammonium nitrate (CAN) 27% N and a NPK 16-16-16 prilled product. Two series of tests were conducted for each of the two types of fertilizer. One series used long vanes mounted on the disc and the second series used short vanes. The test apparatus for the cylindrical distribution pattern consisted of 36 compartments, each 10° wide. The compartments were arranged circularly at 1-m from the center of the disc. Weighing the collected fertilizer, the tangential distribution pattern was determined from the mass of particles leaving the disc during each 10° angular rotation of the disc. To obtain the horizontal directions in which the particles were leaving the disc, the horizontal outlet angles of flight, β, needed to be determined (Figure 8).

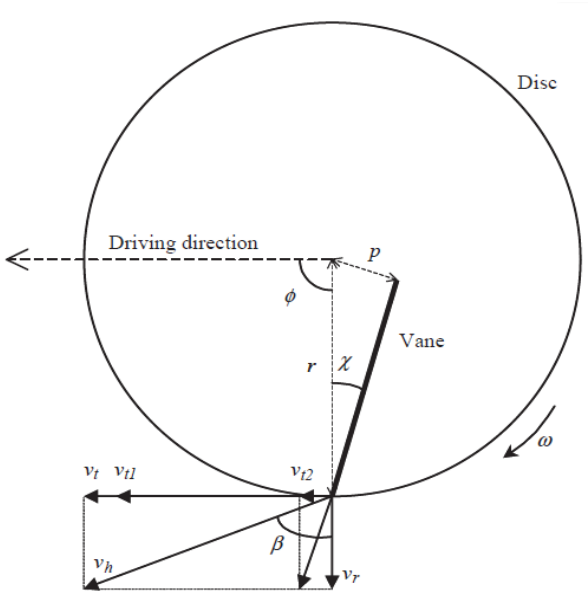

Figure 8. Schematic of vectors and angles on the rotating disc for an exiting particle; p, perpendicular distance from the disc center to the vane; r, disc radius; v_h, horizontal component of the particle outlet velocity; v_r, radial component of particle outlet velocity; v_t, resulting tangential component of the particle outlet velocity; v_{t1}, tangential component of the particle outlet velocity resulting from the disc rotational velocity; v_{t2}, tangential component of the particle outlet velocity resulting from the non-radial vane position; β, particle outlet angle with respect to the radial direction through the vane end; χ, vane position angle with respect to radial; ϕ, particle position angle at the disc edge with regard to spreader driving direction; w, disc rotational velocity (Reumers et al., 2003).

Reumers et al. (2003) measured the horizontal directions of particle using four cameras mounted in the apertures of the cylindrical testing device. On the photographs, particles appeared as straight lines because of their high speed. Horizontal positions were measured at several angular positions at the disc edge. To determine the transverse and static distribution patterns, the cylindrical distribution was projected to the tangential and vertical particle distributions at the disc edge. The projection was based on the measured horizontal flight directions, the dimensions of the disc and test apparatus, and basic assumptions. The horizontal and vertical components of the velocity vectors of the particles were then computed. Ballistic flights could then be calculated which resulted in a simulation of the static distribution pattern.

To validate this model, static distribution patterns were measured in a spreading hall that consisted of a double row of collection pans. Each row was 56-m in length and contained 224 bins. A spreader was driven at a constant ground speed perpendicular to the rows of bins. The captured mass within each bin were weighed to determine the transverse distribution pattern. The static distribution pattern was measured by executing subsequent transverse measurements with a stationary spreader. Between each test, the relative distance between the spreader and the rows of bins was increased by 2-m. Every test resulted in one of the odd rows of the overall matrix representing the static distribution pattern. The even rows of the matrix were obtained through interpolation.

Differences between the simulated and measured distributions were quantified using the following formula to compute the relative error, e_R, Reumers et al. (2003):

$$e_R = \frac{\sum_j \sum_i \left(M_m(i,j) - M_s(i,j)\right)^2}{\sum_j \sum_i M_m^2(i,j) + \sum_j \sum_i M_s^2(i,j)} \quad (6)$$

where M_m represents the matrix containing the normalized measured distribution; M_s the matrix containing the normalized simulated distribution; and i and j indicating the row and column number, respectively. There was better agreement for distributions with short vanes compared to the long vane and for distributions of the granular product compared to the prilled product (Table 2). Reumers et al. (2003) concluded that it was possible to draw qualitative conclusions using simulations; however, an improvement in the model was determined necessary before the model could predict distribution patterns with sufficient accuracy to replace empirical testing in the spreading hall.

Table 2. Relative error, e_R, of the simulated distribution patterns (Reumers et al., 2003).

	Relative Error (e_R), %	
Fertilizer Type	Short Vane	Long Vane
Granular Product	11.8	13.1
Prilled Product	11.0	14.5

2.4 Summary

The use of organic fertilizers, such as poultry litter, has been used for several years as a soil amendment and substitute for inorganic fertilizers. Due to rising cost of inorganic fertilizers, poultry litter has become popular for application to cropland. Applying poultry litter uniformly has always been a challenge due to the inherent variability of its physical properties. However, over-application near production facilities along with continued concerns of N and P movement from cropland has led to environmental concerns resulting in regulations such as USDA-NRCS Code 590 (2011) and the USDA-NRCS P-Index (2001) to establish guidelines on how and when to apply fertilizers. The spinner-disc spreader has been an economical (cheap) and conventional way to apply poultry litter for years. In general, there has been little or no research and development on litter spreaders by manufacturers while scientific information is limited to help litter spreader manufacturers to improve their product. However, spreader hardware involved in the conveyance and distribution processes impacts application uniformity of litter. Therefore, it remains important to have the correct hardware designs to avoid material flow obstructions of the spinning discs. New design testing requires extensive field testing and large amounts of litter. As time moves forward, accurate placement will be required to minimize over-application. A new technology has emerged recently known as discrete element modeling (DEM). This approach allows the spreader and its hardware configurations to be virtually evaluated. To use DEM to its full potential, material properties of poultry litter must be established as inputs into

the DEM software. Like other modeling software, the DEM software needs to be calibrated and validated through empirical tests. From review of previous studies, DEM has shown that while the model does not perform well quantitatively all the time, it does provide good qualitative results in predicting trends and spread pattern shifts with a change in spreader hardware design or setup.

CHAPTER THREE

MATERIALS AND METHODS

Setup of a DEM simulation model is important to ensure accurate results. An initial challenge of DEM is establishing the correct material properties and parameters for poultry litter. Particle size, moisture content, bulk density, and other important physical properties can be difficult to measure and quantify. In some cases, parameters must be assumed when modeling biological materials but can be based on previous research. The initial effort of this research entailed quantifying the bulk density and particle size distribution of litter at three moisture contents (MC): 18%, 24%, and 30%. These moisture contents were based on previous research. The 18% MC treatment represents a dry sample, 24% MC represents a sample at a common moisture content, and the 30% MC represents a wet sample. The second step consisted of establishing the parameters that influence the single-disc spread pattern the most, through a parameter sensitivity analysis. Next, the physical parameters of uniform, plastic BBs used during calibration and validation were quantified. The following steps involved calibrating the DEM model for bulk litter and then validating the DEM simulation model used in this research. Figure 9 presents a general overview of the setup process for a DEM software package illustrating the needed steps.

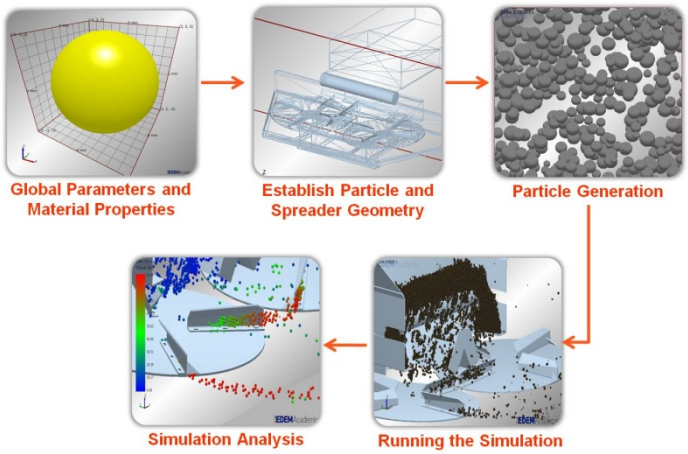

Figure 9. Overview of steps needed to implement DEM.

3.1 Material Properties

3.1.1 Broiler Litter

Before a DEM model could be setup, basic material properties of broiler litter needed to be established. These material properties included bulk density and particle size distribution. Before measuring the particle size distribution and bulk density, the broiler litter was separated into three piles; one for each moisture content treatment (18%, 24%, and 30%). Each pile was hydrated or dried until the nominal MC of the treated litter was within 1% of the desired treatment. A 300-g sample from each treatment pile was obtained and its bulk density calculated by filling a 500-mL beaker and measuring its mass. Dividing the measured mass by 500-mL yielded the bulk density of the sample. Four replications were performed for each treatment.

Particle size distribution for each treatment was determined by running 300-g of litter through a Camsizer (Model 216753 Retsch Technology GmbH, Germany). Results reported diameter size probabilities at d_{16}, d_{50}, and d_{84}. Four replications were performed with a mean and standard deviation of these diameters. The granulometric spread index (GSI) was also calculated

for each replication using equation 7. GSI represents how much the diameters of the particles vary within a sample.

$$GSI = \frac{d_{84} - d_{16}}{2 x d_{50}} x100 \quad (7)$$

where d_{16}, d_{50}, and d_{84} are the diameter size probabilities at the 16, 50, and 84 percentiles, respectively.

Since litter consists of a wide range of particle sizes, dust to large chunks, the bulk litter at the 24% MC treatment was segregated into three size classification ranges: small, medium, and large. Segregating the litter into size classifications allowed the variability of litter to be studied and documented. This segregation was performed using a Ro-Tap testing sieve shaker, Model B (Tyler Combustion Engineering Inc.) and ASTM sieve No.'s 4, 40, and pan. Material retained on the No. 4 sieve ($x>4.75$-mm) was considered to be composed of large particles. Likewise, material collected on the No. 40 sieve ($0.425<x<4.75$-mm) was labeled as medium size particles. Material that ended up in the pan ($x<0.425$-mm) was considered small particles. The bulk density, size distribution, and GSI values were measured for each size classification. Four replications were performed with a mean and standard deviation calculated for bulk density, d_{16}, d_{50}, and d_{84} and GSI values. Statistical analyses were performed on the litter material properties in SAS® v.9.1 statistical analysis software with a confidence interval of 95%.

3.1.2 Plastic BBs

Since broiler litter is a highly variable material, the model was evaluated using a uniform material for comparison. It was decided to use plastic BBs since all of the BBs are manufactured to a uniform size, shape, and mass. The BBs provided a uniform material with "particles" of equivalent size. Each plastic BB had a mass of 0.12-g and a diameter of 6-mm. The bulk

density of the BBs was obtained using the same methods to obtain the bulk density of the broiler litter. Three replications were performed and a mean value was calculated. Particle density was calculated to be 1,061-kg/m^3 by dividing the particle mass (0.00012-kg) by its volume ($1.13e^{-7}$-m^3).

3.2 Litter Spreader Description and Calibration

A Chandler Litter Spreader (Gainesville, GA) (Figure 10) used in this research and had a maximum gate opening of 35.6-cm, 86.4-cm wide slatted conveyor chain, two spinner-discs with diameters of 76.2-cm, and four vanes per spinner-disc with each vane having a height of 7.6-cm and length of 27.9-cm (see Appendix A). Two Brand Hydraulics electronically adjustable proportional pressure compensated flow control valves (see Appendix B) were used to in conjunction with a Topcon Precision Agriculture (Livermore, CA) X20 console (see Appendix C) to control conveyor speed and spinner-disc speed.

Figure 10. Chandler Equipment Co. litter and shavings spinner-disc spreader.

Prior to testing, both hardware and software calibration procedures were performed based on the manufacturer's published literature. Pan testing for spread pattern uniformity was performed per ASABE S341.4 (2009). The calibration of the rate controller and spreader hardware settings is recommended by manufacturers. A single-row of 19 pans, uniformly spaced

at 0.9-m, were used during calibration. The pans were 50.8-cm long, 40.6-cm wide, and 10.2-cm tall. The pan on either side of the center pan was removed to allow the tractor and spreader to pass unobstructed. Calibration was conducted at an application rate of 4,483-kg/ha, representing a common application rate for litter in Alabama. Adjustments were made to the flow divider location and disc speed until the most uniform application was accomplished. An effective swath width of 9.1-m was determined for this spreader.

After several spread pattern tests using bulk litter, varying flow divider location and spinner-disc speed, the most uniform single-pass spread pattern (Figure 11a) and simulated multiple-pass spread pattern (Figure 11b) were achieved using a gate height of 34.9-cm, divider location of 2.54-cm forward of the divider guide-rail edge, and a disc speed of 650-rpm. The mean multiple-pass application rate was calculated at 5180-kg/ha with a CV of 20%. Even though the single-pass pattern formed a "W" shape, the results were considered adequate for a litter spreader.

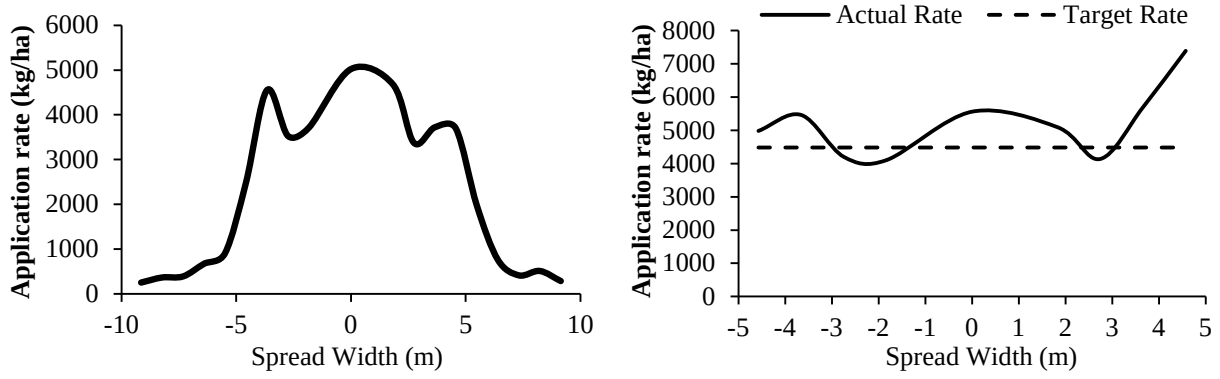

Figure 11. Single-pass (a) and simulated multiple-pass (b) spread patterns for the calibrated litter spreader.

3.3 DEM Setup

Once the values of bulk density and particle size distribution were established, they were used to construct the DEM model. This process entailed inputting the measured and assumed

material property values along with importing the spinner-disc spreader geometry. The amount of particles to generate was based on the number of plastic BBs and volume of litter used for the experimental tests. Since limited information exists for using DEM to model spinner-disc spreaders, it was required to properly setup features and menus within the EDEM software to establish the litter and spinner-disc spreader parameters. In doing this setup, it was also required to select the appropriate contact models for particle-to-particle and particle-to-geometry interactions. For this research, the select models were based on previous research and recommendations by EDEM's manufacturer (DEM-Solutions). These models are discussed in the following sections while Appendix F contains more information regarding EDEM setup.

3.3.1 Particle-to-Particle Interactions

EDEM provided two previously coded contact models for particle-to-particle interactions. The first model was the linear-cohesion contact model. This model is governed by the values of normal and shear stiffnesses of the bodies that are in contact with each other. It was selected because cohesion strength is incorporated into the interaction between particles. However, the linear-cohesion model is limited in that the cohesion is assumed to be uniform between the particles that are in contact. Cohesion is derived from energy density values and the overlap area of the two bodies in contact (Landry et al., 2006b). Energy density is the scaling function for the cohesiveness of the material and is an input that the user must define.

Using a spreadsheet provided by EDEM, the energy density coefficient was initially calculated to be 1e+5-J/m^3 for the litter-to-litter interactions using assumed material properties based on Landry et al. (2006c). Values for other input parameters had to be assumed. These values (Table 3) were based on research by Landry et al. (2006c).

Table 3. Litter material properties based on Landry et al. (2006c) used for the initial setup of the DEM model.

Parameter	Value
Poisson's Ratio	0.25
Young's Modulus (MPa)	2.0
Bulk Density (kg/m^3)	370
Coefficient of Restitution	0.30
Coefficient of Static Friction	0.63

The second contact model used for particle-to-particle interactions was the Hertz-Mindlin, also known as the "no slip" model. The Hertz-Mindlin model represents a non-linear contact model and is defined by the shear modulus (G) and Poisson's ratio (ν). Like the linear-cohesion model, the assumption of uniform behavior for particle-to-particle is made. For particle-to-particle interactions, elastic properties of the particle are used. A material's shear modulus can be calculated from Young's modulus (E) and Poisson's ratio (Landry et al., 2006b). Depending on the material, values for E and ν can be found in literature, but at times must be obtained through experimental means. For this study, values of E and ν (Table 3) were based on recommendations from Landry et al. (2006c).

3.3.2 Particle-to-Geometry Interactions

The linear-cohesion and Hertz-Mindlin contact models were used for particle-to-geometry interactions. The assumption of uniform cohesion and particle-to-geometry behavior is made as with the particle-to-particle interactions. Instead of performing calculations of interactions between particles, calculations were performed between the particles of the material and the geometric surfaces of the spinner-disc spreader. It was important to define the linear-cohesion and Hertz-Mindlin models for interactions of all materials and surfaces present in order to account for all possible contacts that a particle might encounter. For this study, the two discs of the spinner-disc spreader were constructed of stainless steel. An initial energy density value

of 3e+5-J/m^3 was calculated for poultry litter-to-stainless steel interactions using the assumed values from Landry et al. (2006c) and the spreadsheet provided by EDEM.

A third contact model was used for particle-to-geometry interactions. It is known as a "moving plane model" and has already been previously incorporated into the EDEM software. The moving plane model is used to represent the conveyor chain and slats at the bottom of the hopper (Figure 11). The linear velocity for the moving plane was calculated to be 0.0986-m/s in the -y direction so that material would be exiting the hopper in the same way as with an actual spinner-disc spreader. Linear velocity of the conveyor was calculated using Equation 8:

$$\text{Conveyor Speed} = \left(\frac{\text{Application Rate*Tractor Speed*Swath Width}}{\text{Bulk Density*Gate Area*43560}}\right) \quad (8)$$

where application rate = 4,483-kg/ha, tractor speed = 2.23-m/s, swath width = 11-m, bulk density = 370-kg/m^3, and the gate area = 0.302-m^2.

3.3.3 Spinner-disc Spreader Geometry

CAD files of a Chandler Equipment Company spinner-disc litter spreader were modified to only include components which contact litter during the spreading process. The CAD files were reduced into components (e.g. discs, gate, and hopper) which impacted conveyance and material distribution, then imported into EDEM using the IGES (.IGS) format. However, complex geometries of the spinner-disc spreader such as the conveyor chain links, made up of several parts, could not be successfully imported. Therefore, the geometry for these components were established using EDEM's predefined geometry which best represented each component required to convey litter. For example, the conveyor shaft was replaced with a rotating cylinder (Figure 12). Simplifying the final geometry was done to reduce simulation time. The final geometry of the spinner-disc spreader is presented in Figure 12. The two discs (including vanes)

were assigned material properties of stainless steel with the remaining geometry assigned material properties of high-stiffness steel. The next step was to apply component dynamics to the necessary geometry. The only dynamics applied were for the two rotating spinner-discs and the cylinder representing the rotating conveyor shaft. The discs were assigned to rotate at 600-rpm and the cylinder at 14-rpm to match the conveyor speed of 0.0986 m/s.

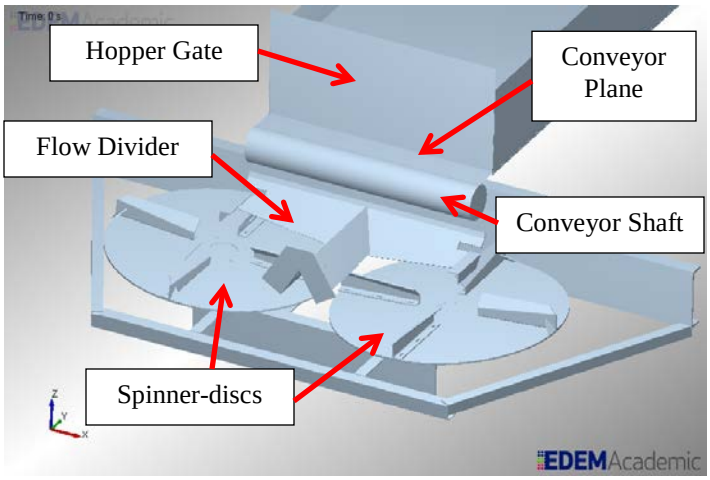

Figure 12. Representation of spinner-disc spreader geometry within EDEM.

3.4 DEM Calibration

Empirical experiments and simulations were performed using 6-mm plastic BBs to gain a better understanding of how to calibrate the DEM model to empirical tests. In order to establish values for the coefficients of static friction and rolling friction, two methods of characterizing material behavior were performed for both the plastic BBs and litter. The first method was a tilt test (Figure 13a). The purpose of the tilt tests was to establish the particle-to-geometry interactions so that they could be replicated within the DEM model. The tilt tests involved placing approximately 100 BBs (multi-colored in Figure 13a) on a 20.32-cm x 25.4-cm stainless steel plate and elevating one end of the plate until the BBs started to slide. This angle

was measured and recorded. Four replications were performed and a mean tilt angle calculated. For bulk litter, 100-g was used in each replication (Figure 14a).

(a) (b)

Figure 13. Tilt tests (a) and angle of repose tests (b) performed in the lab to establish material interactions of 6-mm plastic BBs.

(a) (b)

Figure 14. Tilt tests (a) and angle of repose tests (b) performed in the lab to establish material interactions of broiler litter.

The second characterization method performed was an angle of repose test Figure (13b). The measured angle of repose established the particle-to-particle interactions. Testing for the angle of repose involved pouring 1200-g of BBs (approximately 10,000 BBs) into a plastic bin. After allowing the BBs to settle, a flap in the bottom of the bin was removed allowing the BBs to "free flow" through the opening. As a result, the angle of repose was formed by the remaining BBs (green material in Figure 13b) in the bin. Once the BBs stopped flowing, the angle of repose was measured. For litter, measuring the angle of repose involved filling a 0.95-L funnel that was suspended 15.2-cm over a flat stainless steel plate. The funnel was opened with the litter accumulating on the plate. The height and width of the pile was measured to compute the

angle of repose using equation 9. Four replications were performed for both the BBs and the litter with a mean angle of repose and standard deviation calculated.

$$\theta = \tan^{-1}\left(\frac{\text{height of pile}}{\text{radius of pile}}\right) \quad (9)$$

where *height of the pile* is measured from the base to the highest point of the peak and *radius of pile* is half of the diameter of the pile at its base.

The coefficient of restitution of the plastic BBs was measured by suspending a single BB 30.5-cm above both a stainless steel and plastic surface. A ruler was placed directly behind the BB so the bounce height could be measured (Figure 15). The BB was released with bounce height recorded. The coefficient of restitution was calculated using equation 10. The same procedure was used for measuring the restitution for the bulk litter. Fifteen replications were performed for both the plastic BBs and the bulk litter.

$$\text{Coefficient of Restitution} = \sqrt{\frac{\text{Mean Bounce Height}}{\text{Drop Height}}} \quad (10)$$

where *Mean Bounce Height* is the mean of fifteen replications measuring the rebound height of the particle and *Drop Height* is the height above the surface in which the particle made contact.

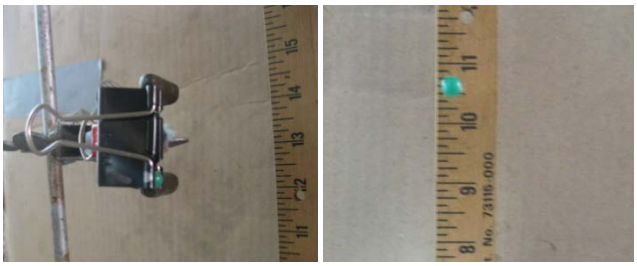

Figure 15. Method of calculating the coefficient of restitution by dropping a single BB onto a stainless steel and plastic surface.

Results from the tilt, angle of repose, and restitution tests were used in setting up the model with simulations created replicating the empirical tests. Another required parameter by

the model was particle density, the density of a single particle. The particle density for the bulk litter could not be established within the model since the model's capability was limited by the number of particles that is created within the simulation. Therefore, it was determined to use the same particle density as the BBs in order to achieve the desired amount of simulated mass. The coefficients of static friction, rolling friction, restitution were adjusted through trial-and-error until the equivalent tilt angle, angle of repose, and bounce height were attained. As with the plastic BBs, results from the tilt, angle of repose, and restitution tests of broiler litter were input into the model and simulations performed by adjusting the coefficients of static friction, rolling friction, and restitution until the equivalent tilt angle, angle of repose, and bounce height were reached. Means and standard deviations of the tilt angle and angle of repose were calculated within Microsoft Excel.

3.4.1 Parameter Sensitivity Analysis

A sensitivity analysis was conducted as part of the model calibration. This analysis was performed by varying individual parameters while holding all others constant. The parameters evaluated were: particle density, coefficient of restitution, coefficient of static friction, coefficient of rolling friction, energy density coefficient, and particle diameter. For each parameter, a simulation was performed using a low, medium, and high value to assess the impact on the distribution pattern. Within the simulation, 8-L (approximately 25,000) of particles was dropped onto a single rotating disc at 600-rpm (Figure 16) and broadcasted over an array of simulated pans. The "ground" was not included in the simulation in order to reduce particles being counted multiple times within virtual pans. The number of particles captured in each simulated pan was transformed into a 2D surface map using Surfer® mapping software (v. 8).

The parameter sensitivity analysis provided the "controls" of the model. These controlling parameters reflect longitudinal and transverse translations of the spread pattern along with particle concentration within the spread pattern.

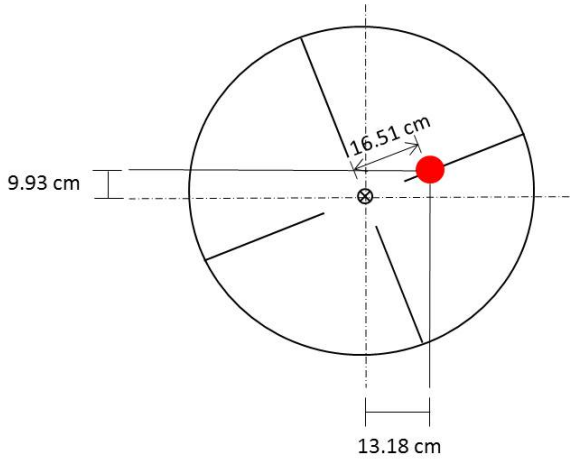

Figure 16. Drop location 1 of BBs onto a single rotating disc for DEM model calibration to particle trajectory tests.

3.4.2 Particle Trajectory Tests

As part of the calibration process, field trajectory tests were performed to generate single-disc spread patterns. Plastic BBs were used as the material along with the results from the parameter sensitivity analysis to evaluate the needed adjustments for the model to produce similar spread patterns. Symmetry was assumed between the two discs, hence the use of a single disc. Preliminary field tests were conducted to determine the amount of BBs needed and the appropriate collection pan arrangement. BB's were poured down the PVC pipe until enough BB's were captured in the collection pans to calculate the spread pattern. It was determined that approximately 1200-g of BBs (10,000) were needed for each replication. One drop location on the disc was used with respect to the inside edge of the disc vane. A 7.6-cm diameter PVC pipe was fitted with a funnel that narrowed from 7.6-cm to 2.5-cm. For the drop location, the PVC pipe was fixed 7.62-cm above the disc so that the pipe opening was 13.18-cm to the right, 9.93-

cm forward of disc center and 16.51-cm radially from the disc center (Figure 16). The PVC pipe and funnel assembly are presented in Figure 17 with the simulated setup presented in Figure 18. A single disc speed of 400-rpm was used for all three replications. Wind speed was checked during each test to ensure that the wind velocity did not exceed more than 8 km/h as outlined by ASABE standard 341.4 (2009). There were occasional gusts that exceeded 8 km/h with testing performed when gusts were not occurring.

Figure 17. PVC pipe and funnel assembly attached to litter spreader for BB particle trajectory testing.

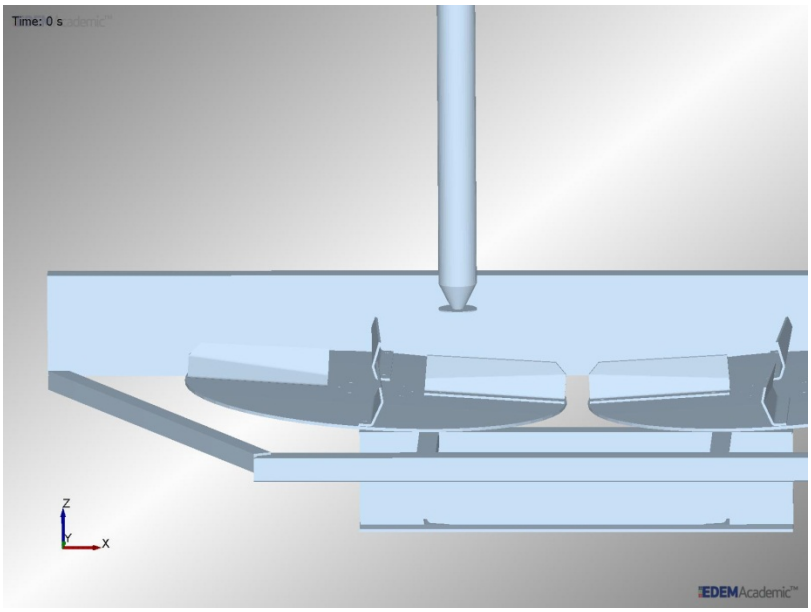

Figure 18. Simulated PVC pipe and funnel for BB trajectory tests within EDEM software.

The pan configuration consisted of 65 pans that met the requirements in the ASABE standard 341.4 (2009). All pans were evenly spaced 1.83-m apart (Figures 19 and 20).

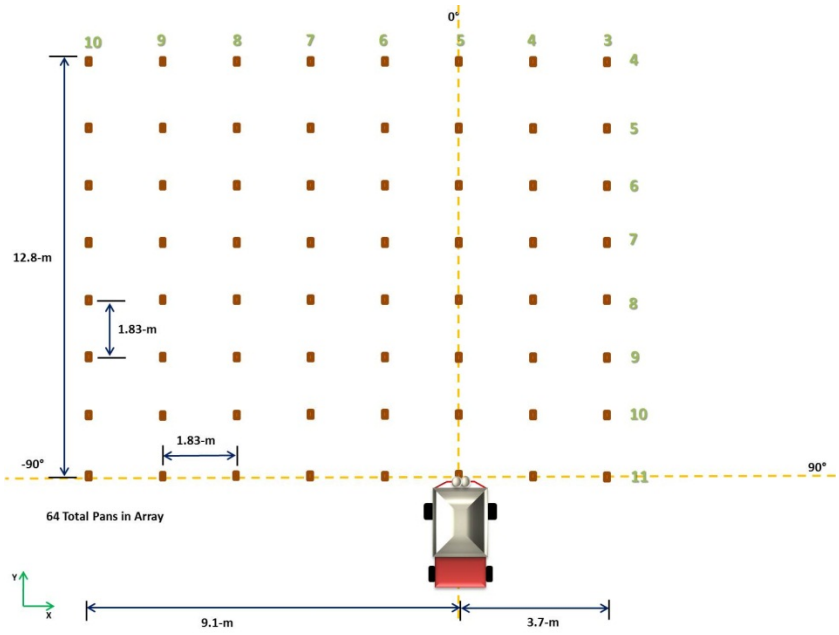

Figure 19. Pan configuration of 64 pans for static particle trajectory tests using plastic BBs.

Figure 20. Pan array for BB particle trajectory tests.

An average of the three replications was calculated to produce a mean number of BBs caught in each pan for the field tests. Simulations were created to replicate static trajectory tests performed in the field. Each virtual pan calculated the number of BBs that it captured within the simulation. Results from the simulation were compared to field results by computing the standard deviation of reduced mean errors (SDRME; equation 11), relative deviation (RD; equation 13), root-mean-square error (RMSE; equation 14), and the coefficient of determination (R^2). Plots along with a least squares linear regression fit were generated using Microsoft Excel to compare field and simulation results. The relative deviation (RD) was calculated using a modified version of Olieslager's deviation function similar to equations 4 and 5. Mass was used in the deviation function when calibrating the model to litter, and the number of particles collected was used when calibrating the model to plastic BB's.

$$\text{SDRME}=\sqrt{\frac{1}{n}\sum_{i=1}^{n}\left(\frac{\hat{Y}(s_i)}{\hat{\sigma}\left(\hat{Z}(s_i)\right)}-\text{SME}\right)^2} \tag{11}$$

where SME is the standardized mean error (equation 12), $\hat{Y}(s_i) = Z(s_i) - \hat{Z}(s_i)$ the prediction error associated with estimating the number of BBs at a spatial location s_i, $Z(s_i)$ the number of observed BBs, $\hat{Z}(s_i)$ the number of simulated BBs, $\sigma\left(\hat{Z}(s_i)\right)$ the simulated standard deviation associated with the simulated BBs, and n represents the sample size.

$$\text{SME} = \frac{1}{n}\sum_{i=1}^{n}\frac{\hat{Y}(s_i)}{\hat{\sigma}\left(\hat{Z}(s_i)\right)} \tag{12}$$

$$\text{RD(exp,sim)} = \frac{\sum_j \sum_i \left(|M_{ij,exp} - M_{ij,sim}|\right)}{M_{total,exp} + M_{total,sim}} 100 \tag{13}$$

where M_{ij}(exp) represents the experimental mass (g) captured in each collection pan, M_{ij}(sim) the mass (g) captured in individual simulated collection pan, M_{total}(exp) the total collected mass (g) from the experiment, and M_{total}(sim) the total simulated mass (g) collected within the DEM model.

$$\text{RMSE} = \sqrt{\frac{\sum_{i=1}^{n}(\hat{y}_i - y_i)^2}{n}} \tag{14}$$

where y_i represents the observed value for the i-th observation and $\hat{y}_i$ the predicted value.

Visual comparisons of the number of BBs captured in each pan were made by producing two-dimensional surfaces for the simulation and field data using the mapping software Surfer® (v. 8). The number of BBs collected at each spatial location was imported into Surfer 8 and overlaid onto the interpolated surface to produce 2D plots. A surface plot was generated to present the difference in number of BBs captured between the virtual and experimental collection pans.

Several simulations were performed altering input parameters until the model results generated good visual and statistical correlations to the experimental data. This method required a lot of time since it simply was trial-and-error. The energy density coefficient and the

coefficients of static friction and restitution were adjusted within the DEM to replicate the spatial location and concentration of the spread pattern from experimental tests. Appendix J contains a summary of the simulations performed along with statistical data. Once the model was considered calibrated for the BB's, the simulation was replicated two more times to evaluate the model's repeatability. The standard deviation of the field replications was obtained in Microsoft Excel and plotted within a surface map using the Surfer® software to present the variability between replications. Transverse and longitudinal patterns for the field data, initial parameters, and calibrated parameters were generated in Microsoft Excel to compare the simulated patterns to the field data. The transverse patterns were formed by summing the number of BBs captured within each column of pans where the longitudinal patterns were formed by summing the number of captured BBs within each row of pans.

Model calibration for litter required performing particle trajectory tests using bulk litter and using the same methods outlined with the plastic BBs. The same drop location was used with a disc speed of 600-rpm, which is considered a median spinner-disc speed for litter application. The amount of bulk litter used for each replication was 8-L. The funnel at the end of the PVC pipe was removed for the litter tests because the 2.5-cm opening was too narrow for the litter to freely flow. A different pan configuration was used for the bulk litter tests due to higher concentrations collecting near the spreader. The pan configuration consisted of 87 total pans (Figure 21). An inner array of 35 pans was spaced 0.9-m apart in the area where most of the litter landed. The remaining 52 pans were spaced 1.8-m apart.

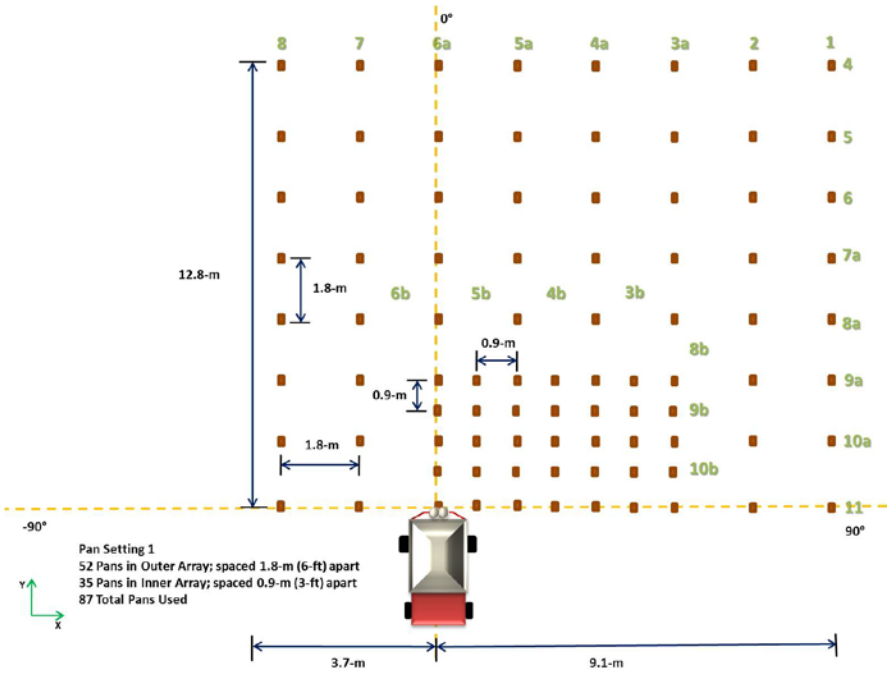

Figure 21. Pan configuration for particle trajectory tests using bulk litter.

Three replications were performed for the field tests yielding a mean mass of litter captured in each pan. Within the simulation, the amount of particles generated was based on the amount of litter used for each replication. Approximately 25,000 simulated particles were needed to equal the 8-L of litter used. Each virtual pan calculated the mass of litter captured. As with the plastic BBs, results from the simulation were compared to field results using the reduced mean errors (SDRME; equation 11), relative deviation (RD; equation 13), root-mean-square error (RMSE; equation 14), and the coefficient of determination (R^2). A surface map was created, as with the plastic BBs, to present the standard deviation of the replications. Transverse and longitudinal patterns were generated in Microsoft Excel in the same method as the plastic BBs.

3.5 DEM Validation

The validation process was divided into two methods: conveyance and particle trajectory tests. Experiments performed included field tests followed by simulations with each analyzed and compared to determine simulation performance with respect to the experimental field data. The following sections outline the methods used to validate the model.

3.5.1 Divider (Conveyance) Accuracy Tests

Litter conveyance onto the rotating discs is important to achieving the desired application rate and ultimately the desired spread pattern. As part of this conveyance process, the litter falls from the conveyor onto a flow divider which, theoretically, divides the flow of litter into two, but equal, flows onto the spinner-discs. Both discs were removed and a wooden box constructed to channel the litter from each side of the divider into separate collection bins (Figure 22).

(a) (b)

Figure 22. Wooden box (a) used to funnel litter that fell on each side of the flow divider (b) into two collection bins.

While the spreader remained stationary, the conveyor was allowed to run for approximately twenty seconds at an application rate of 560-kg/ha and approximately ten seconds at application rates of 4,483-kg/ha and 6,725-kg/ha. Application rates were selected to test a low, common, and high application rate for litter. The conveyor speeds for each application rate

were 1.6-cm/s, 12.6-cm/s, and 20.0-cm/s, respectively. The target application rate for each test was programmed into the X20 rate controller. The gate height was set at 17.8-cm above the bed of the hopper and remained constant for all tests. The accumulated mass of litter captured in each bin was weighed using a set of Triner Scales with tests replicated three times. A simulation within EDEM was created to replicate these tests using the input parameters from the model calibration to bulk litter. The amount of simulated particles was based on the mean weight of the total collected litter for each application rate during the experimental tests. Simulated collection bins were used to calculate the amount of mass accumulated on each side of the divider. Percent difference (Equation 15) was computed between the simulated and experimental results for each collection bin. An analysis of variance (ANOVA) at the 95% confidence interval was also conducted using SAS® (v.9.1) to compare the right versus left bins.

$$\text{Percent Difference } (\%) = \left(\frac{\text{abs}(\text{Experimental Wt.-Simulated Wt.})}{\text{Experimental Wt.}}\right) 100 \qquad (15)$$

where *Experimental Wt.* represents the mean collected weight (kg) for each bin and *Simulated Wt.* the simulated weight (kg) measured based on the simulation for individual bins.

3.5.2 Particle Trajectory Tests

Preliminary tests were conducted to determine the amount of BBs needed and how collection pans needed to be arranged behind the spreader. It was determined that approximately 1,200-g of BBs (approximately 10,000) were needed for each replication. Again, 6-mm plastic BBs were used as a uniform material for the basis of comparison. Two drop locations (termed Location 1 and Location 2) on the disc were used with respect to the disc center. The PVC pipe, with attached funnel, was fixed above the disc as during the calibration process for the first drop location (Figure 16).

The second drop location placed the BBs 25.35-cm to the right, 19.10-cm forward, and 31.75-cm radially from the disc center (Figure 23). Treatments included three disc speeds of 500, 600, and 700-rpm and were replicated three times. A summary of the treatments for the particle trajectory tests are listed in Table 4.

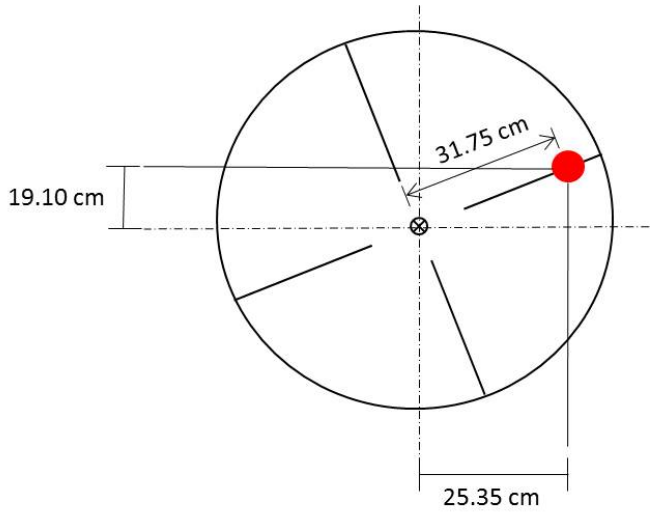

Figure 23. Drop location 2 used for DEM validation.

Table 4. Particle trajectory tests (validation) for plastic BBs and bulk litter. Drop locations measured radially from disc center.

	Disc Speed			
	500-rpm	600-rpm	700-rpm	
Drop Location 1 (16.51-cm)				
Bulk Litter	3	3	3	
6-mm BBs	-	3	3	
Drop Location 2 (31.75-cm)				**Total Number of Tests**
Bulk Litter	-	-	-	
6-mm BBs	-	3	3	
Total Tests per Disc Speed	3	9	9	**21**

The pan configuration shown in Figure 24 was used for both drop locations using plastic BBs. All collection pans were evenly spaced 1.83-m apart.

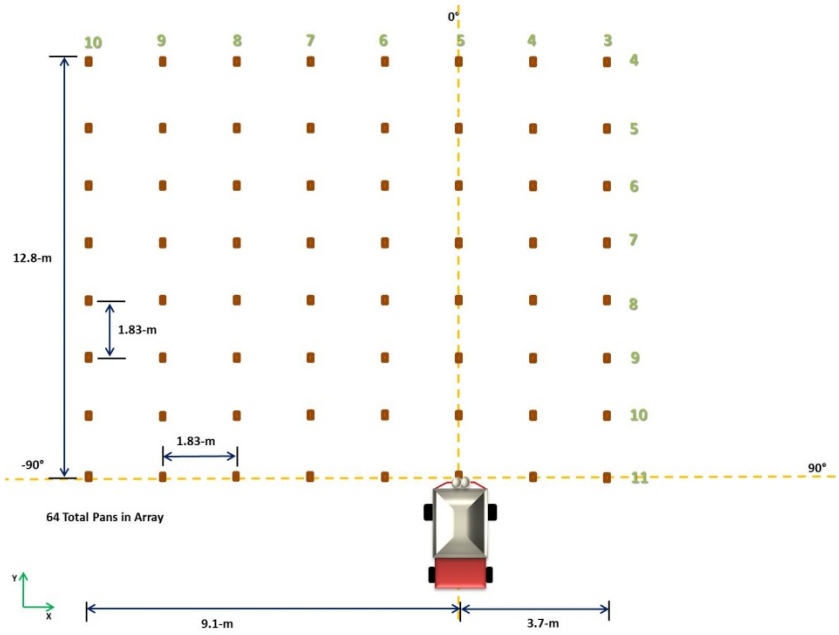

Figure 24. Pan configuration of 64 pans for static particle trajectory tests using plastic BBs.

Model validation for bulk litter consisted of particle trajectory tests (Table 4) using the same methods as with the plastic BBs. Only the first drop location was used along with the three disc speeds for the litter. The pan configuration used for the bulk litter particle trajectory tests consisted of 87 total pans (Figure 25). An inner array of 35 pans was spaced 0.9-m apart in the area where most of the litter landed. The remaining 52 pans were spaced 1.8-m apart. Within the simulation, approximately 25,000 particles were generated in order to meet the equivalent 8-L from the experimental tests. The simulated "ground" within EDEM was removed from the simulation so that particles would pass through the virtual pans and not roll or bounce into another virtual pan.

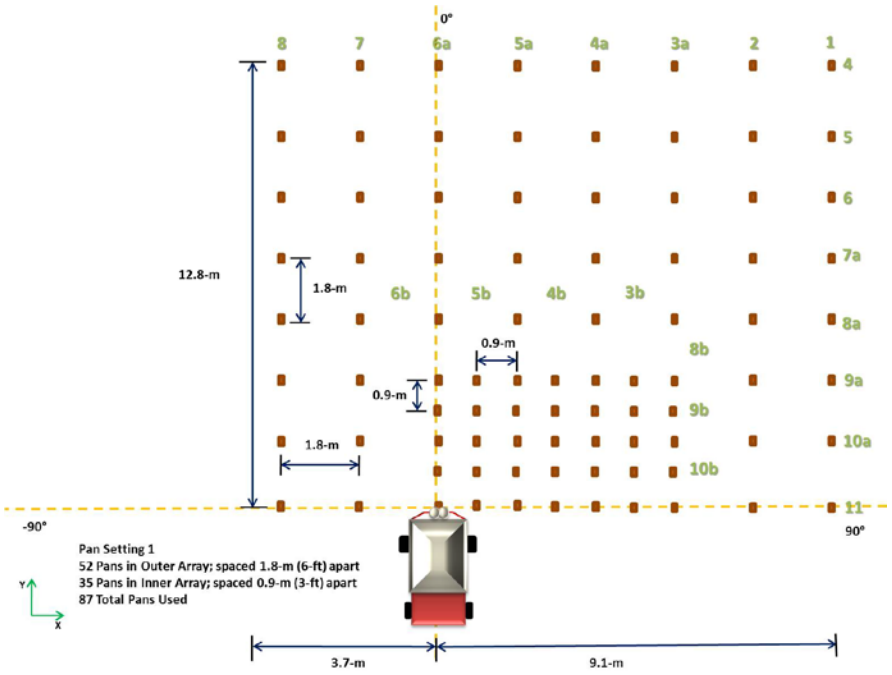

Figure 25. Pan configuration for drop location 1 of the trajectory tests using bulk litter.

3.5.2.1 Statistical Summary and Analysis

For the plastic BBs and bulk litter, the reduced mean errors (SDRME; equation 11), relative deviation (RD; equation 13), root-mean-square error (RMSE; equation 14), and the coefficient of determination (R^2) were used to compare the results from the simulations and field tests. Visual comparisons of the experimental and simulated spread patterns were made using the Surfer® 8 mapping software. The standard deviation among the replications was plotted as a surface map. Results from the simulations were compared to field results using transverse spread patterns which were generated in Microsoft Excel.

The steps taken to setup, calibrate, and validate the DEM simulation were important to ensure that the plastic BBs and litter were simulated as accurately as possible. Knowing the material properties of the BBs and bulk litter were essential in setting up the DEM model. Properties were either assumed or measured through experimental tests. Calibration involved a

parameter sensitivity analysis to understand which input parameters acted as the controls of the single-disc spread pattern. These input parameters were adjusted to replicate the single-disc spread patterns measured in experimental particle trajectory tests. Finally, validation of the model involved replicating litter conveyance testing and particle trajectory tests of BBs and bulk litter.

CHAPTER FOUR

RESULTS AND DISCUSSION

4.1 Material Physical Properties of Broiler Litter and Plastic BBs

The particle size distribution, bulk density, and GSI results for the three litter MC treatments are listed in Table 5. As the moisture content of the litter increased from 18% to 24%, the mean bulk density also increased. This result was expected since adding water increases sample weight for an equivalent volume. Further, the median particle distribution (d_{50}) increased with moisture content indicating that the cohesion of the particles increased with moisture content, thereby, increasing the median particle size. The standard deviations of the d_{50} values showed an increasing trend as well. Overall, the GSI values tended to be high. These high GSI values were attributed to the variable nature of the litter and the large range of particle sizes. The GSI values indicated that variation in particle size decreased with increasing moisture content with less variation existing in particle size at the 30% MC treatment. As with bulk density, the added water caused the particles to cluster together reducing the range of particle sizes. The ANOVA at the 95% confidence level resulted in p-values <0.05, which indicated that all of the values within each column were significantly different from each other.

Table 5. Means of particle size distribution, bulk density, and GSI values for three MC treatments.

Target MC	Nominal MC[1] (%)	d_{16} (mm)[1]	d_{50} (mm)[1]	d_{84} (mm)[1]	Bulk Density (kg/m^3)[1]	GSI[1]
18%	18.5^c (0.7)	0.7^c (0.0)	1.8^c (0.2)	5.8^c (0.6)	351.0^c (2.0)	147.6^a (3.5)
24%	23.3^b (0.5)	0.8^b (0.0)	2.3^b (0.2)	7.2^b (0.5)	380.3^b (1.2)	136.7^b (5.6)
30%	30.4^a (0.8)	1.7^a (0.1)	3.7^a (0.3)	8.7^a (0.9)	404.3^a (2.9)	93.7^c (3.5)

1) Mean values with different letters within each column indicate they are statistically different at the 95% confidence level and standard deviations provided in parentheses.

Results associated with the particle size distribution of bulk litter at the 24% MC are listed in Table 6. Bulk densities decreased with increasing size classification. This trend can be explained in that smaller particles have less void space between them; therefore, the amount of measured mass at the given volume was higher for the smaller particles. It is important to note that the GSI value for the medium size classification was higher than the other two size classes. Observations of the medium size classification indicated more wood shavings, small feathers, etc. causing the GSI to be the highest. Appendix E contains images of the small, medium, and large size classifications. The ANOVA at the 95% confidence level resulted in all values within each column being statistically different from each other except for the bulk and medium d_{16} ($p=0.7982$) and the small and large GSI values ($p=0.0878$) being similar.

Table 6. Mean particle size distribution, bulk density, and GSI values for segregated litter at 24% MC.

Size Classification	d_{16} (mm)[1]	d_{50} (mm)[1]	d_{84} (mm)[1]	Bulk Density (kg/m^3)[1]	GSI[1]
Bulk	0.8^b (0.0)	2.3^b (0.2)	7.2^b (0.5)	380.8^b (1.3)	136.7^a (5.6)
Small (x<0.425-mm)	0.6^c (0.0)	1.1^c (0.1)	1.9^d (0.1)	530.0^a (10.0)	56.3^c (1.9)
Medium (0.425<x<4.75-mm)	0.8^b (0.0)	1.9^d (0.1)	4.3^c (0.2)	340.0^c (12.2)	90.5^b (2.2)
Large (x>4.75-mm)	3.9^a (1.1)	7.9^a (0.8)	14.6^a (1.7)	272.5^d (8.3)	67.8^c (9.5)

1) Mean values with different letters within each column indicate they are statistically different at the 95% confidence level. Standard deviations provided in parentheses.

The basic physical parameters measured for the litter provided a starting point for initial model setup. These data incorporated the actual differences between particle sizes and provided the actual physical properties; however, adjustments to the model setup for these parameters would be necessary during calibration. The actual physical measurements should represent relative differences which exist once the model is calibrated. Table 7 includes the bulk density results for the plastic BBs. The calculated particle density was 1,061-kg/m^3.

Table 7. Bulk density results for the plastic BBs. Standard deviation presented in parentheses.

	Bulk Density (kg/m^3)
Rep 1	532.8
Rep 2	543.2
Rep 3	532.4
Mean	536.1 (6.1)

4.2 DEM Model Calibration

4.2.1 Particle Interactions

Initial calibration parameters for the plastic BBs are listed in Tables 8 and 9. Table 8 includes parameters for particle-to-geometry interactions while Table 9 includes parameters for particle-to-particle interactions. The experimental tilt tests produced a low mean tilt angle of 2.3° with the experimental angle of repose tests generated 17.2°. Since the BBs are smooth and spherical, a low amount of friction exists against the surface of the stainless steel plate. Similar thoughts existed for the amount of friction between BBs in the angle of repose tests. With a low coefficient of static friction, the BBs had less friction between each other resulting in BBs rolling off of each other. Within the DEM model, the coefficient of static friction did not have to be adjusted to reproduce the same tilt angle, however, the coefficient of static friction had to be lowered from the calculated value of 0.31 to 0.06 to replicate a similar angle of repose of 17.2°.

It is unknown to why there was a drastic change in static friction; however, the model's ability to replicate particle interactions might be of significance. The experimental tests calculating the coefficient of restitution for the BBs yielded a mean coefficient of restitution of 0.87 at a bounce height of 22.9-cm for the stainless steel surface. A coefficient of restitution of 0.82 was calculated for a measured bounce height of 20.3-cm for the plastic surface. To replicate the same bounce height against the stainless steel surface, the coefficient of restitution within the DEM model was equivalent to 0.88. The coefficient of restitution (0.82) did not have to be adjusted to achieve the same bounce height for the plastic surface.

Table 8. Initial calibration parameters based on tilt tests for 6-mm plastic BBs against a stainless steel surface.

Parameter	Measured[a]	DEM[b]
Mean Tilt Angle (degrees)	2.29 (0.06)	---
Coefficient of Static Friction	0.04	0.04
Coefficient of Rolling Friction	0.10	---
Coefficient of Restitution	0.87	0.88

Standard deviation in parentheses.
[a]Measured values under laboratory conditions.
[b]Values determined within the DEM model.

Table 9. Initial calibration parameters based on angle of repose tests for 6-mm plastic BBs against a plastic surface.

Parameter	Measured[a]	DEM[b]
Mean Angle of Repose (degrees)	17.2 (0.80)	---
Coefficient of Static Friction	0.31	0.06
Coefficient of Rolling Friction	0.10	---
Coefficient of Restitution	0.82	0.82

Standard deviation in parentheses.
[a]Measured values under laboratory conditions.
[b]Values determined within the DEM model.

Tables 10 and 11 include the initial calibration parameters for the bulk litter. Table 10 includes parameters for particle-to-geometry interactions while Table 11 presents parameters for

particle-to-particle interactions. The bulk litter achieved a higher tilt angle (23.6°) and angle of repose (35.5°) than the plastic BBs. This result is due to the litter particles not being perfectly spherical in nature with more cohesion existing between particles. There was no bounce of the litter particles during the tests for restitution. Therefore, the coefficient of restitution was 0.00 for the bulk litter. No measurable bounce of the litter does not suggest that litter is absent of elastic properties. Litter, being a biological material, exhibits visco-elastic properties.

Table 10. Initial calibration parameters based on tilt tests for bulk litter against a stainless steel surface.

Parameter	Measured[a]	DEM[b]
Mean Tilt Angle (degrees)	23.6 (0.80)	---
Coefficient of Static Friction	0.44	0.55
Coefficient of Rolling Friction	0.10	---
Coefficient of Restitution	0.00	0.00

Standard deviation is in parentheses.
[a]Measured values under laboratory conditions.
[b]Values determined within the DEM model.

Table 11. Initial calibration parameters based on angle of repose tests for bulk litter.

Parameter	Measured[a]	DEM[b]
Mean Tilt Angle (degrees)	35.5 (1.21)	---
Coefficient of Static Friction	0.71	0.12
Coefficient of Rolling Friction	0.10	---
Coefficient of Restitution	0.00	0.00

Standard deviation is in parentheses.
[a]Measured values under laboratory conditions.
[b]Values determined within the DEM model.

4.2.2 Parameter Sensitivity Analysis

Results from the parameter sensitivity analysis (Table 12) indicated which parameters spatially controlled the longitudinal and transverse aspects of the spread pattern as well as the concentration of particles within the spread pattern.

Table 12. Summary of the parameter sensitivity analysis.

Parameter	Effect on Simulated Single-disc Spatial Spread Pattern
Static Friction	Transverse movement and rotation
Energy Density Coefficient	Longitudinal movement
Coefficient of Restitution	Concentration of particles within spread pattern

The particle-to-geometry friction values were found to control the transverse location of particles using the coefficient of static friction. Increasing values of static friction shifted the pattern from left to right of the centerline (Figures 26a, 26b, and 26c). Higher static friction also caused the pattern to rotate in the same direction as spinner-disc rotation (Figure 27) since the residence time of the particles on the vane increased. The particle-to-particle friction values had similar effects on the spread pattern, but did not impact the pattern as much as the particle-to-geometry friction values.

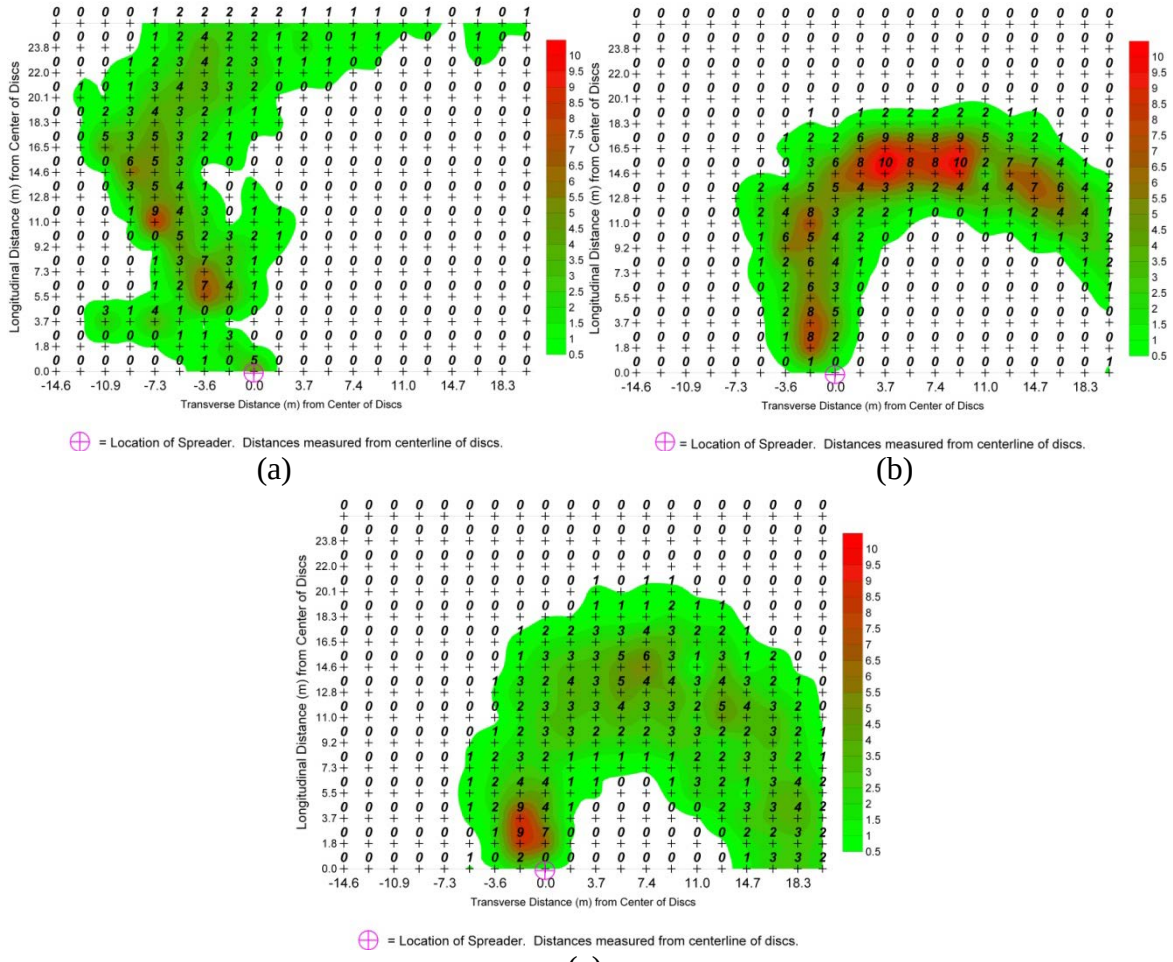

Figure 26. Single-disc spread patterns with a coefficient of static friction equal to 0.0 (a), 0.5 (b), and 1.0 (c) using a spinner-disc speed of 600-rpm. Increasing the coefficient of static friction shifted the pattern to the right and rotated it in the same direction of the spinning disc (clockwise).

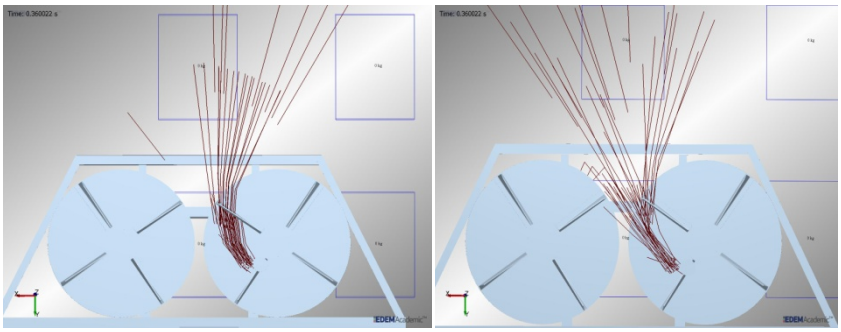

Figure 27. Paths of simulated particles after interacting with the spinning disc and vanes using coefficient of static friction values = 0.0 (a) and 1.0 (b). Disc speed = 600-rpm.

The energy density parameter within the EDEM software accounts for material cohesion. Based on the parameter sensitivity analysis, the particle-to-geometry energy density was found to affect the longitudinal location of the particles. Higher values of the energy density coefficient affected the interaction between particles and geometric surfaces shifting the pattern longitudinally towards the disc. This result is represented in Figures 28a, 28b, and 28c as well as in the longitudinal spread patterns (Figure 29). As the energy density increased, the highest concentration of particles moved from 14.6 m to approximately 12.8 m, longitudinally. As with the friction values, the particle-to-particle energy density had similar effects on the spread pattern as the particle-to-geometry energy density, but did not affect the pattern as much.

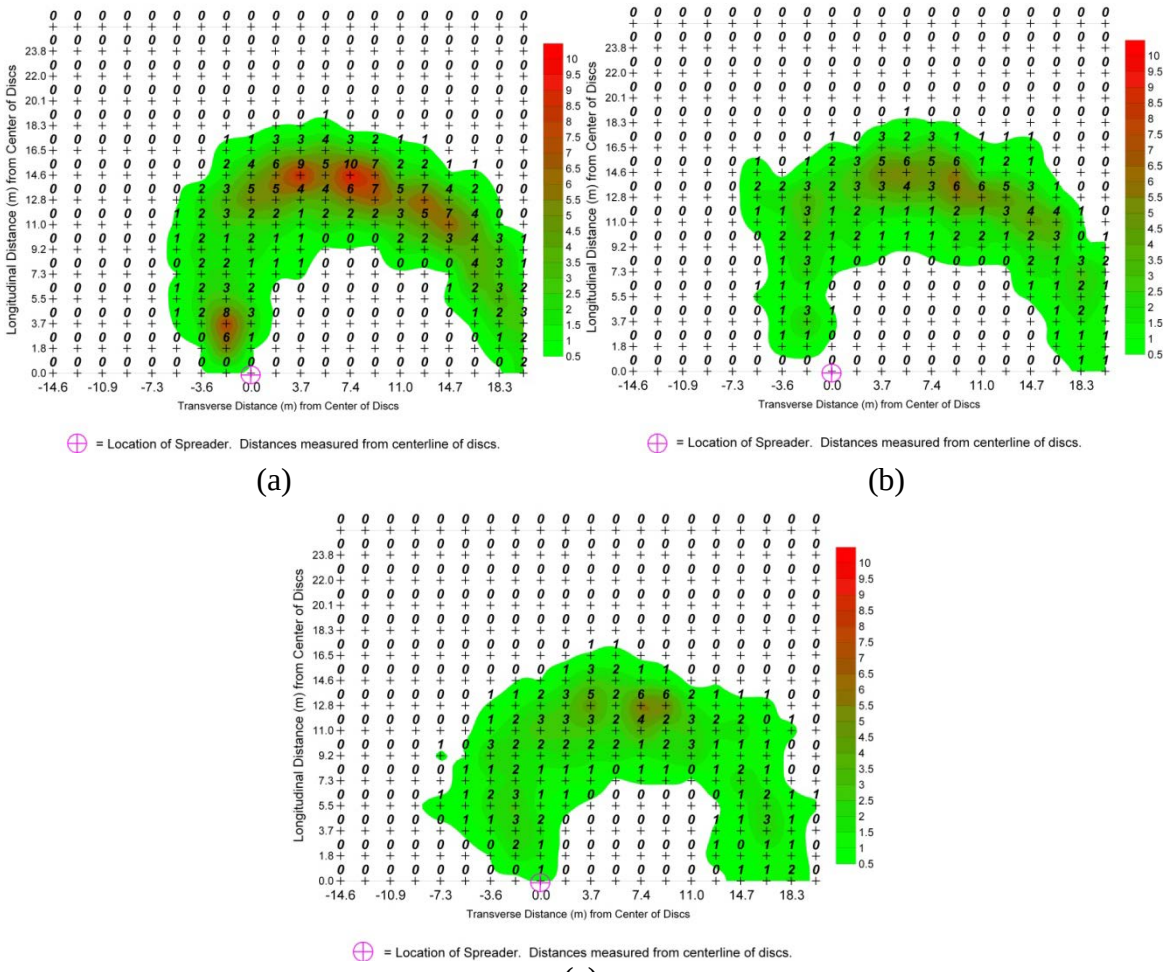

Figure 28. Single-disc spread patterns with a particle-to-geometry energy density coefficient equal to 0-J/m^3(a), 2e+3-J/m^3 (b), and 2e+5-J/m^3(c) using a spinner-disc speed of 600-rpm. Lower values of energy density resulted in more longitudinal travel of the particles. Increasing the energy density coefficient decreased the travel of the particles longitudinally from the disc.

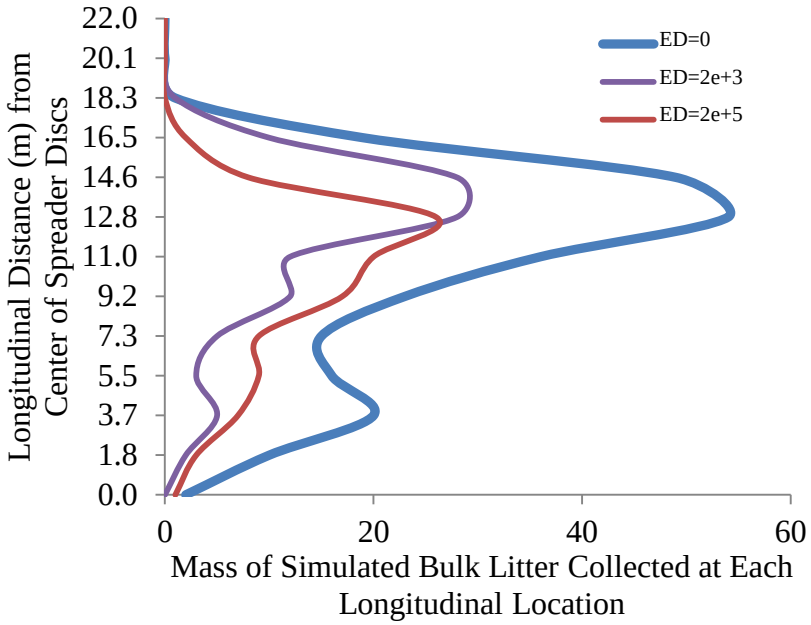

Figure 29. Longitudinal spread patterns at energy density values of 0, 2e+3, and 2e+5-m^3 using a spinner-disc speed of 600-rpm.

The coefficient of restitution was found to impact particle dispersion within the spread pattern. Higher values of restitution caused material to have more bounce when impacting the disc and vanes and thereby generating more dispersion (Figures 30a, 30b, and 30c). A lower value of restitution generated a higher concentration of particles within the spread pattern (Figure 30a). Interactions within the model are presented in Figures 31, 32, and 33. Figure 31 illustrates the effect that the coefficient of restitution has on a single simulated particle dropped onto a stainless steel plate. Figures 32 and 33 highlight the simulated behavior of particles being dropped on a stationary disc and rotating disc (600-rpm), respectively. In Figure 32, the particles had little to no bounce when contacting the vane and simply rolled along the disc surface. The concentration of the particles leaving the disc decreases with increasing restitution, noted by the particle trajectories in Figure 33.

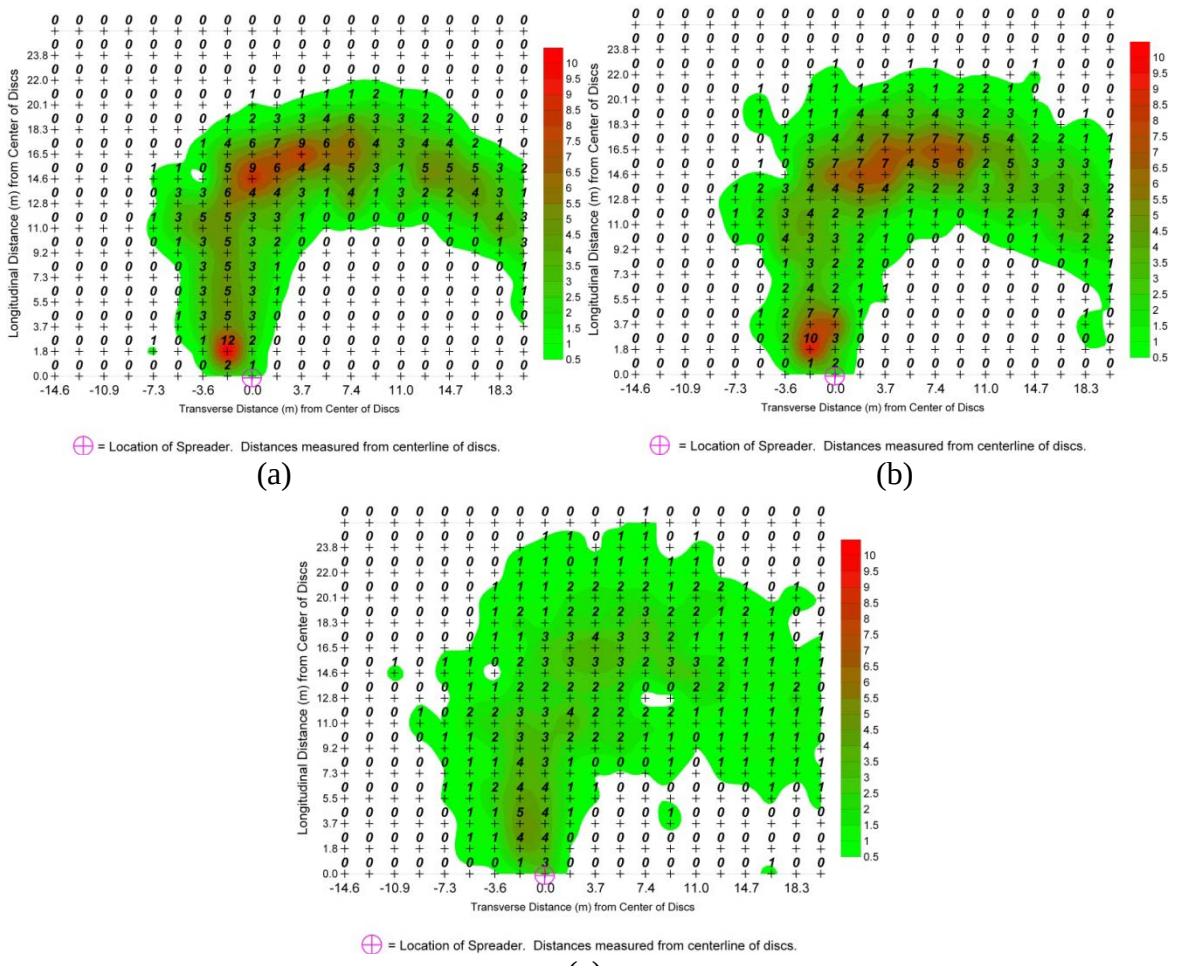

Figure 30. Single-disc spread patterns with a particle-to-geometry coefficient of restitution equal to 0.0 (a), 0.5 (b), and 1.0 (c) using a spinner-disc speed of 600-rpm. As restitution increased, particle concentration decreased.

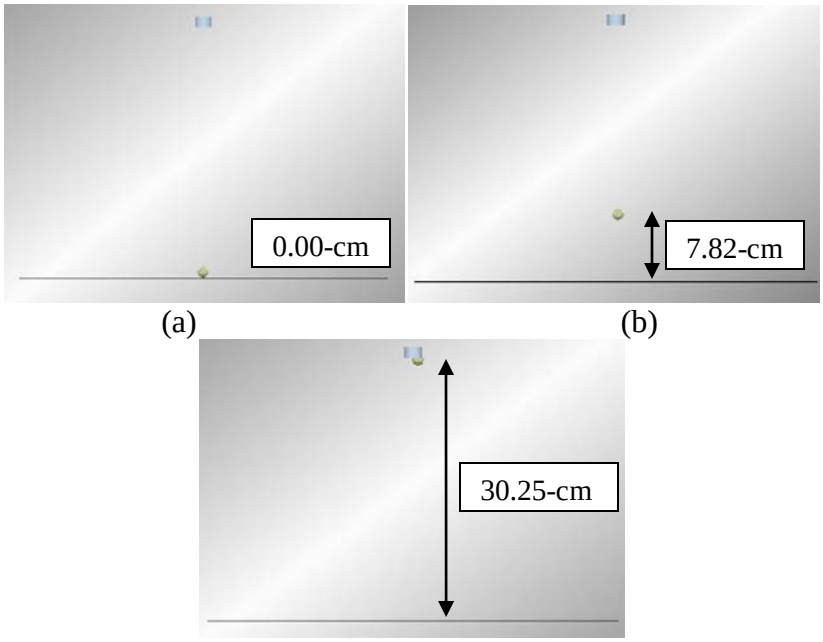

(a) (b) (c)

Figure 31. DEM results illustrating the bounce of a single simulated particle dropped 30.48-cm above a simulated stainless steel plate using a coefficient of restitution = 0.0 (a), 0.5 (b), and 1.0 (c). Bounce heights were 0.0-cm (a), 7.82-cm (b), and 30.25-cm (c).

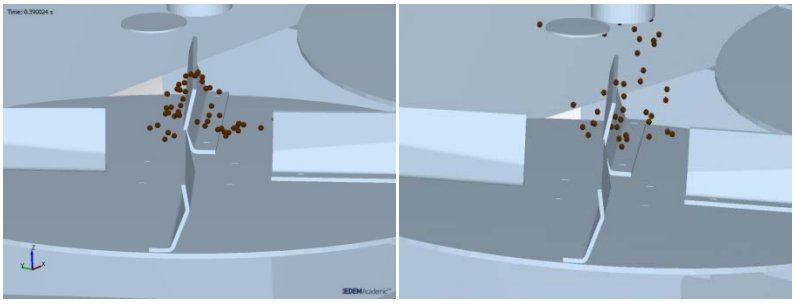

(a) (b)

Figure 32. Interaction of simulated particles with disc and vane using coefficient of restitution values = 0.0 (a) and 1.0 (b). Disc speed = 0-rpm. Scatter of particles increased with increasing restitution.

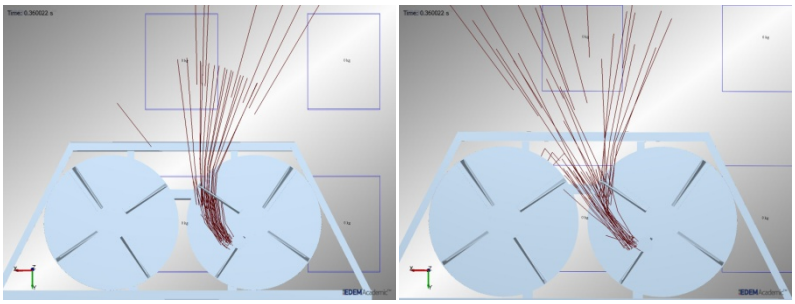

(a) (b)

Figure 33. Paths of simulated particles after interacting with the spinning disc and vanes using coefficient of restitution values = 0.0 (a) and 1.0 (b). Disc speed = 600-rpm. Dispersion of particles increased with increasing restitution.

An important result was the limitation of particle size. It was discovered that the smallest particle diameter that the model could handle was 6-mm. When particle diameters less than 6-mm were used, the particles appeared to "explode" upon generation or the simulation would "freeze up." The total number of generated particles also affected EDEM in the same way. When a large quantity (>50,000) of particles of the same diameter (6-mm) was set to be generated, EDEM would "freeze up" or crash completely. Quantity of particles was dependent upon particle size. The smaller the particle size, the quantity of particles that could be created without overwhelming the simulation decreased. This limitation was most likely due to the computational power of the computer (four processors) on which the EDEM software was installed. Therefore, the particle density parameter defined in the material properties section of the model was impacted. Since the d_{50}(mm) of the bulk litter was less than the diameter of the plastic BBs (6-mm), the particle density for the bulk litter decreased, requiring more particles to be generated to achieve the desired mass of simulated litter. The required amount of simulated litter particles was more than what the model could simulate. Thereby, the particle density of the litter was set to be the same as the plastic BBs for the model to work. Domain size, volume

of space in which the simulation occurred, was another limiting factor in the performance of the simulation. As domain size increased, the performance of the simulation decreased.

4.2.3 Particle Trajectory Tests

Results for the static trajectory tests performed in the field using the plastic BBs is presented in Figure 34a. Figure 34b illustrates the standard deviation of each collection pan from the three field replications. It was observed, while performing field tests, that the BBs ricocheted off of the disc vanes. Most of this ricocheting resulted in BBs landing around a single pan approximately 3.7-m left of the spreader centerline and 5.5-m behind the spreader. All of the particles landed within -7.3 to 9.1-m transverse with maximum longitudinal distance of 14.6-m. After several observations within EDEM simulations, this result was attributed to the BBs ricocheting off the vanes during initial contact once dropped from the conveyor (Figure 35). This result is an example of how DEM can be utilized in evaluating the performance of litter spreaders and their components.

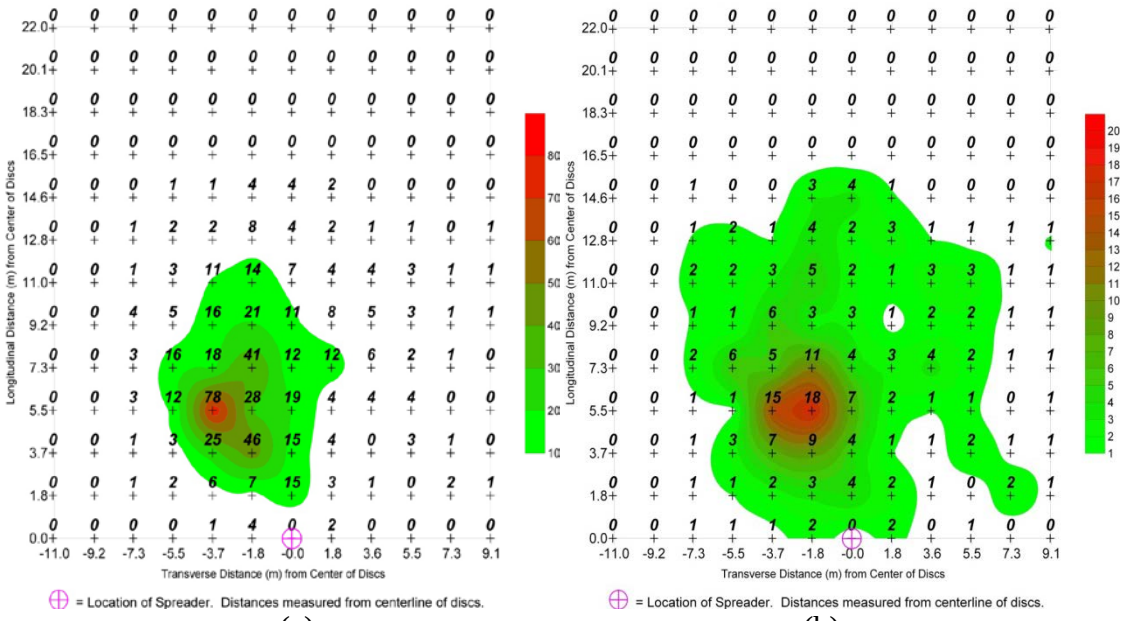

(a) (b)

Figure 34. Interpolated surfaces overlain with mean number (a) and standard deviation (b) of BBs captured in each collection pan for the field trajectory tests.

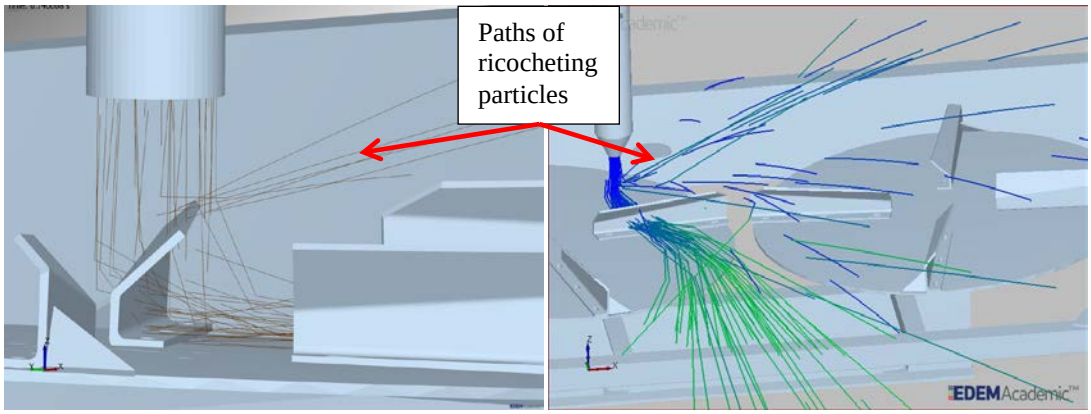

(a) (b)

Figure 35. Simulated plastic BBs ricocheting off of top surface of disc vane (a). The paths traveled by the BBs are shown to highlight the ricocheting effect (b).

After calculating the particle-to-geometry and particle-to-particle input parameters from the tilt, angle of repose, and restitution tests, a simulation was initiated using these values. However, with the particle-to-particle static friction of 0.31, the simulated BBs never exited the pipe opening. Therefore, the particle-to-particle static friction had to be lowered to 0.1 for the

BBs to exit the pipe opening. The resulting simulated spread pattern (Figure 36a) was not as concentrated as the spread pattern from the field data (Figure 34a), evident by comparing the transverse and longitudinal dimensions that the patterns cover.

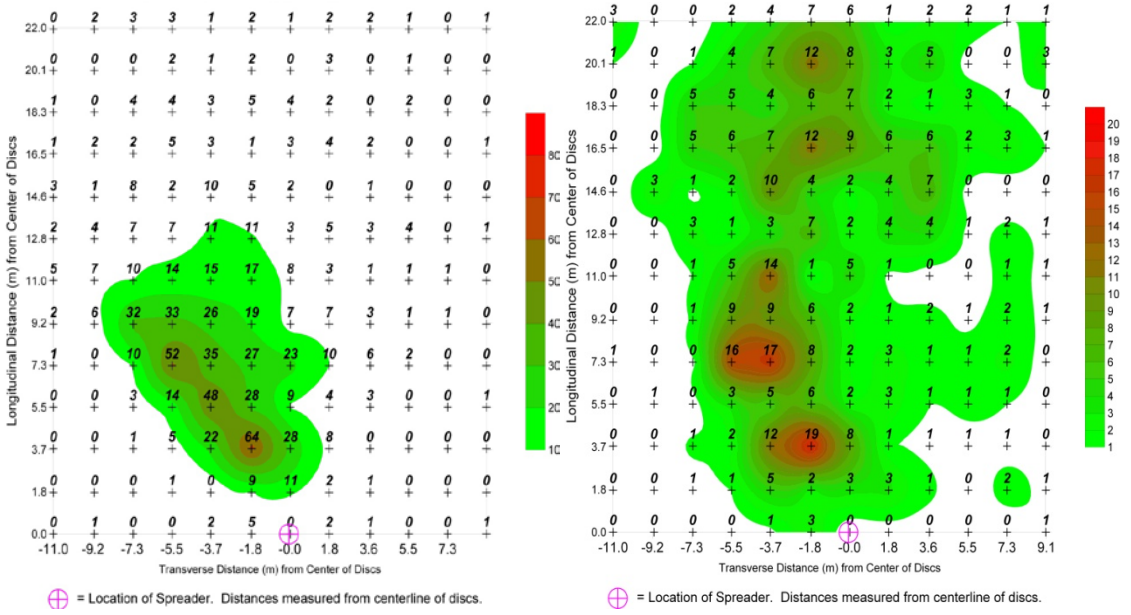

(a) (b)

Figure 36. Interpolated surfaces overlain with simulated number of BBs captured in each virtual pan (a) and the difference in number of BBs captured in the simulated collection pans versus the experimental collection pans (b) using initial input parameters for plastic BBs.

Table 13 and Figure 37 summarize the initial parameters values along with statistics comparing field and simulation data. The R^2 (0.6) was low with the SDRME (0.6) higher than desired. Figure 37 compares the simulated number of BBs captured in the virtual pans using the calculated input parameters to the actual number of BBs captured during field tests. The least squares linear fit with no y-intercept yielded an R^2 value of 0.59. From the plot, there are BBs captured in the simulation where no BBs were captured in the field. Ideally, the data points would be grouped around the 1:1 line. Reasoning for this occurrence might be that the DEM model exaggerated the number of BBs landing near the spreader. This indication leads to the conclusion that the DEM model did not accurately simulate the chaotic behavior of the BBs

while in contact with the spinning disc, thereby impacting particle trajectories. The parameters that are involved in the interactions between the particles and the disc surfaces are the coefficients of friction, restitution, and energy density. The DEM model keeps these parameters constant while in reality, these parameters are likely to vary between particles due to their elastic nature.

Table 13. Initial input values and comparison of simulation results to field data for BBs. [a]The calculated value of static friction (0.31) could not be used within the simulation. 0.1 was used for the simulation to run.

	Particle-to-Geometry	Particle-to-Particle
Coefficient of Static Friction	0.04	0.10
Coefficient of Restitution	0.87	0.82
Energy Density Coefficient (J/m^3)	2.0E+05	9.0e+4
Comparison to Field Data		
Coefficient of Determination	0.59	
RMSE (# of BBs)	6.3	
Relative Deviation	44.3	
SDRME	0.6	

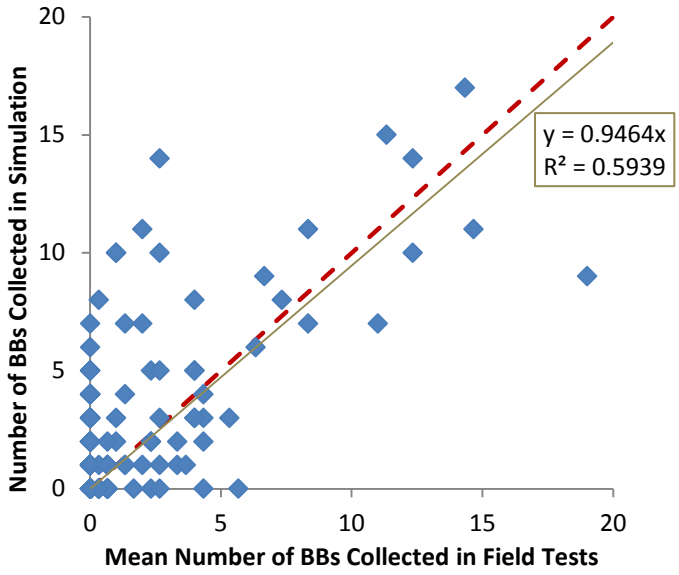

Figure 37. Number of BBs collected within virtual pans vs. actual number of BBs collected during experimental tests using calculated input parameters at a spinner-disc speed of 400-rpm. Dashed red line represents 1:1 line.

Knowledge from the parameter sensitivity analysis was used to adjust the simulated, BB spread pattern until a maximum coefficient of determination was attained. Appendix I contains supporting data for the model calibration to plastic BBs. The adjusted input parameters resulting from the calibration of the DEM to plastic BBs and their comparison to field data are summarized in Table 14.

Table 14. Calibrated input values and comparison of simulation results to field data for the plastic BBs.

	Particle-to-Geometry	Particle-to-Particle
Coefficient of Static Friction	0.10	0.10
Coefficient of Rolling Friction	0.10	0.10
Coefficient of Restitution	0.77	0.81
Energy Density Coefficient	2.0E+05	9.0E+04
Comparison to Field Data		
Coefficient of Determination	0.85	
RMSE (# of BBs)	2.1	
Relative Deviation	39.7	
SDRME	0.3	

The corresponding surface map illustrating the EDEM representation for the calibration simulation is presented in Figure 38a with Figure 38b illustrating the difference in the number of collected BBs between the calibrated and experimental results. Figure 39 illustrates the comparison between number of BBs captured in the virtual pans to the actual number of BBs collected during field tests.

Comparing Figures 34a (field experiments) and 38a (calibrated model), the primary peak of the BBs occurred at about the same location (-3.7-m, 5.5-m) with the overall shape of the simulated spread pattern comparable to the pattern from the field experiments. However, BBs within the calibrated simulation traveled further longitudinally from the disc than in the field data. This difference was evident in Figure 37a from the three circular areas shaded green

between distances of 14.6-m and 20.1-m. It was unknown as to why this result occurred, but this observation was noticed among several of the other simulations during the calibration process. An explanation could be that the model does not accurately simulate the particle interactions on the spinning disc and vane surfaces.

Another observation when comparing Figures 34a and 38a was that two secondary peaks occurred in the field data where only one secondary peak occurred in the calibrated simulation. A possible explanation to this occurrence might be found in comparing the experimental and simulated secondary peaks. The experimental data in Figure 34a begins to show an arced-shaped pattern with the two secondary peaks (42 and 47) to the right of the primary peak (78). From the simulated data in Figure 38a, this arced pattern was not as prevalent and the primary peak of 83 and secondary peak of 65. During the field experiments, the BBs were noticed to ricochet off of the top surface of the disc vanes. The same behavior was noticed during the simulations (Figure 35). The model appeared to exaggerate this behavior, thus forming only one secondary peak during the simulation.

In Figure 39, results indicate that, even after calibration, there are still BBs being estimated in the simulation where there were no BBs captured in the field data. The previous hypothesis of the DEM model not being able to accurately simulate the chaotic behavior of the BBs seems to be supported by the existence of this observation through the calibration process.

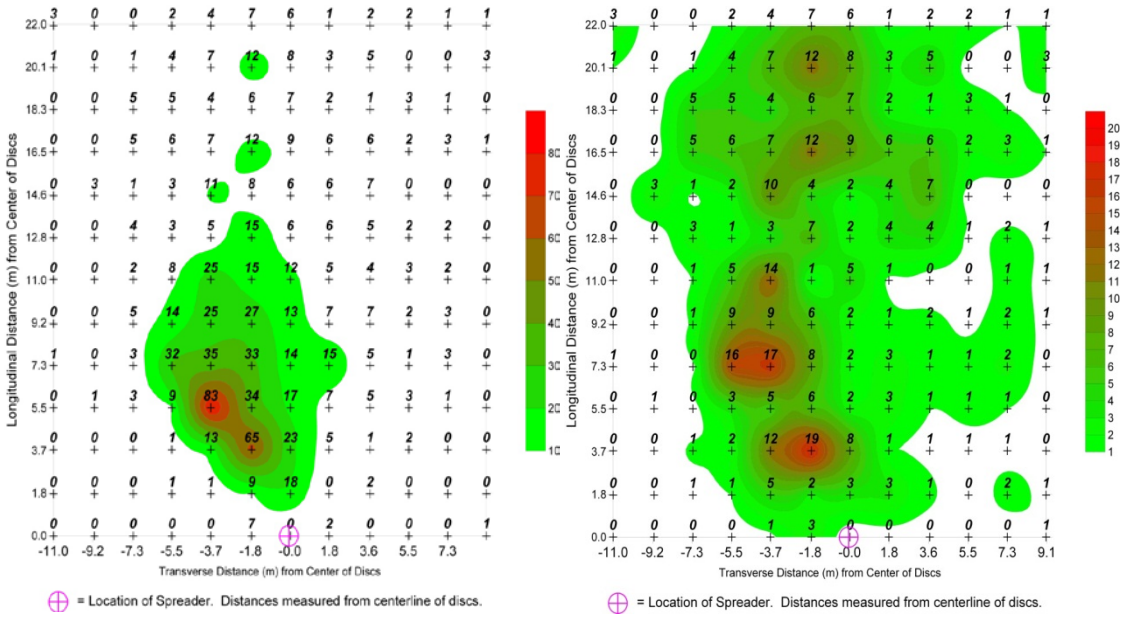

Figure 38. Interpolated surface overlain with simulated number of BBs captured in each virtual collection pan for the calibrated DEM model (a) and surface map illustrating the difference in number of BBs captured in the simulated collection pans versus the experimental collection pans for the calibrated simulation (b).

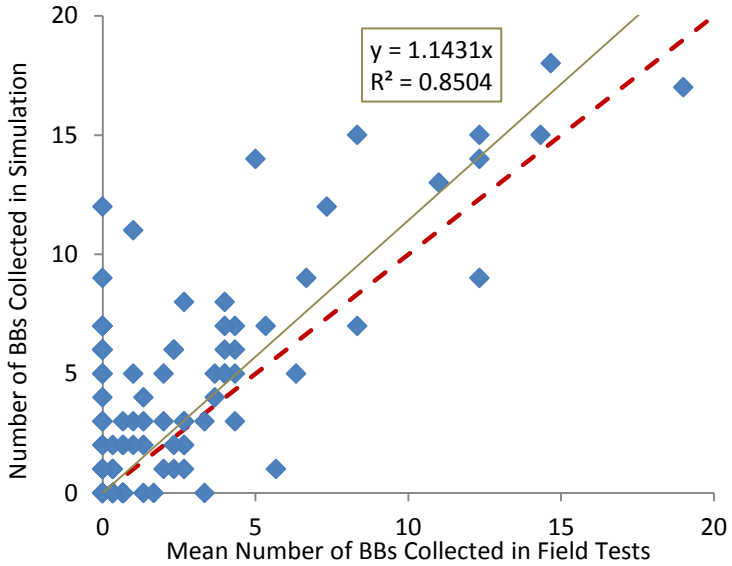

Figure 39. Number of BBs collected within virtual pans vs. actual number of BBs collected during experimental tests using calibrated input parameters. Dashed red line is the 1:1 reference line.

Figures 40a and 40b are plots of the transverse and longitudinal single disc spread patterns, respectively, for the field data, initial parameters, and calibrated parameters. Comparing the transverse patterns, the "calibrated" parameters produced more captured particles than the experimental field data and initial parameters. In the simulations, the virtual pans were not identified as geometric objects. Instead, they are referred to as "grid bins" that measure an assigned query or queries. These grid bins counted the number of particles that entered within their defined boundaries. In reality, BBs were observed to bounce off of the front face of the collection pans and/or bounce out of the pan after making contact with the grid inserts. Within the simulations, this behavior was not accounted for, which could have resulted in the higher number of particles (819) measured in each virtual pan (grid bin) than the actual number of particles (564) collected during the field data. The difference between the initial and calibrated parameters patterns was that the calculated parameter simulation placed particles too far to the left, hence the skew to the left. When the model was calibrated, this skew was eliminated, but reducing the transverse width of the pattern caused the center peak to increase. The calibrated parameter simulation measured 798 BBs within the virtual pans compared to 819 BBs measured in the initial parameter simulation, a difference of 21 BBs which was considered small since approximately 10,000 BBs were used per simulation.

Comparing the single-disc longitudinal spread patterns in Figure 40b, the difference in the magnitude of the patterns was not as distinct as in the transverse patterns. The calibrated parameter and field data patterns have similar shapes; however, the calibrated parameter pattern was slightly skewed in the direction away from the spreader. This observation coincided with the previous based on the calibrated parameter surface plot (Figure 38a) where particles were observed to travel too far in the longitudinal direction.

Even though the quantifiable relationship between the field and simulated results was not precise, it was considered good and representative for a uniform material, such as the plastic BBs. The model was able to predict expected trends in the spread pattern (Figure 40). Van Liedekerke et al. (2009) reported similar results.

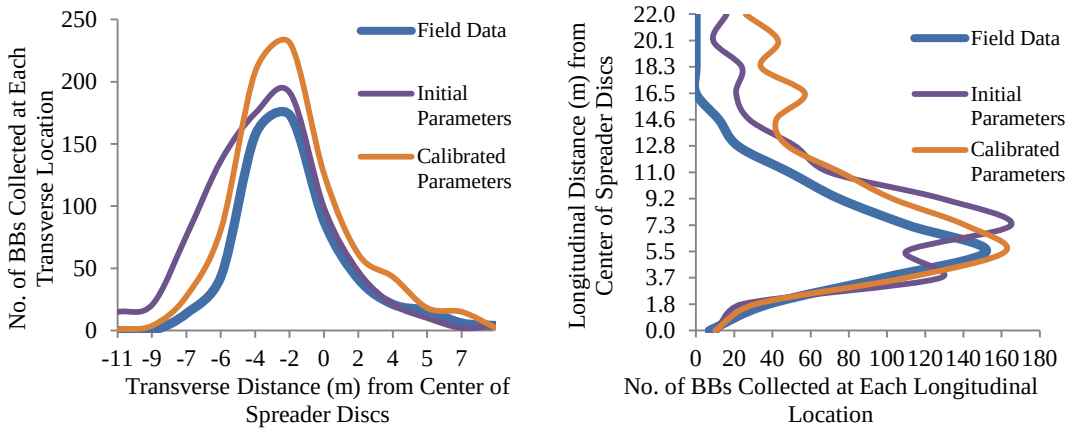

Figure 40. Single-disc transverse spread patterns (a) and longitudinal spread patterns (b) for the field data, initial parameters, and the calibrated parameters using plastic BBs.

Results for the static trajectory field tests using bulk litter are shown in Figure 41a with the standard deviation of each collection pan for the three replications presented in Figure 41b. The funnel, which was attached to the bottom of the PVC pipe, had to be removed during the bulk litter tests in order for the material to flow out of the pipe. This change to the exit aperture increased the landing area of the bulk litter onto the spinning disc. As a result, the behavior of the litter upon contact with the spinning disc and vanes changed to more of a bulk behavior than that of individual particles. Applied litter was highly concentrated near the disc, approximately 1.8-m left to 5.5-m right of the spreader centerline and 5.5-m behind the spreader. The majority of the particles landed within -3.7 to 9.1-m transverse with a maximum longitudinal distance of 11-m. After interacting with the spinning disc, the fine particles formed a dust cloud directly behind the spreader, somewhat limiting observations of the litter-disc interactions.

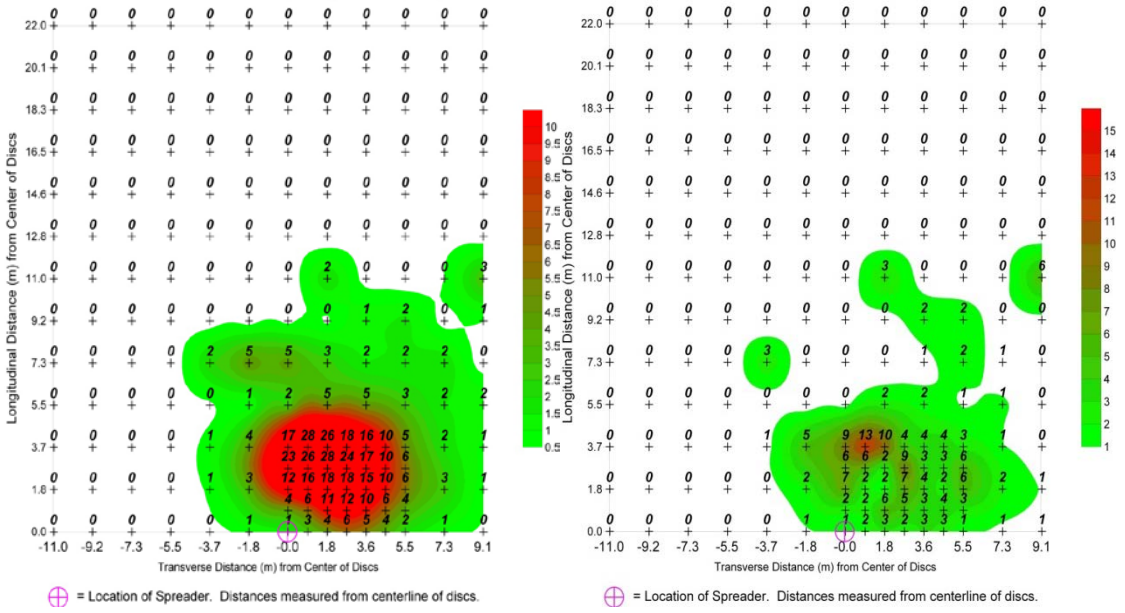

(a) (b)

Figure 41. Interpolated surfaces overlain with mean mass (a) and standard deviation (b) of bulk litter captured in each collection pan for the field trajectory tests.

A simulation using the calculated litter input parameters from the tilt, angle of repose, and restitution tests was performed. Table 15 and Figure 42a summarize these values along with statistics comparing the simulation results to the field data. Figure 42b represents the difference in the mass of litter captured in the simulated collection pans versus the experimental collection pans for the calculated input parameters. Figure 43 illustrates the comparison between mass of litter captured in the virtual pans to the actual mass of litter collected within pans during field tests. Simulated results were expected to be similar to the experimental data based on the plastic BBs results. There was an observable difference between the experimental data and the simulated data using the calculated litter values. The simulated particles in Figure 42a exhibited a broadcasted pattern unlike the experimental spread pattern in Figure 41a. It is important to note that the simulated particles were of the same diameter and mass. Therefore, the model was unable to consider the large particle size distribution and the associated variation in litter particle

interactions into account. The assumption that all particles behave the same when interacting with the spinning disc and vanes was incorrect. If it were possible to model the entire particle size distribution and the variation in particle interactions of the bulk litter, it is plausible to expect the simulated pattern to be closer to that of the experimental.

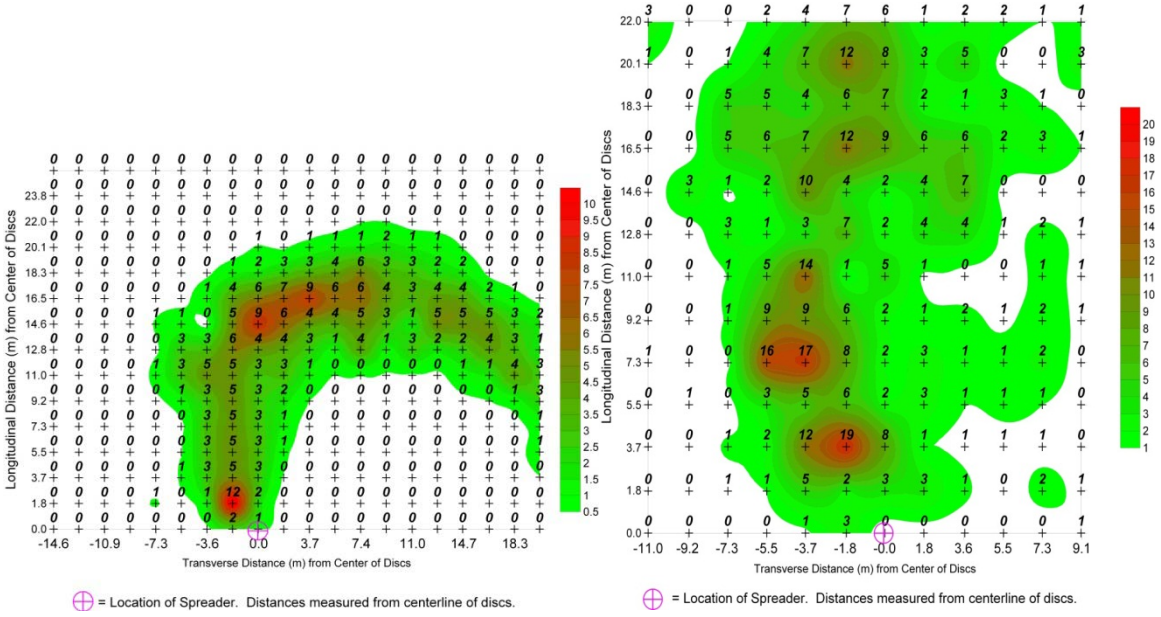

(a) (b)

Figure 42. Interpolated surface overlain with simulated mass of bulk litter captured in each virtual pan using calculated (considered best) input parameters (a) and surface map illustrating the difference in number of BBs (b) captured in the simulated versus experimental collection pans. The DEM simulation represents the calculated input parameters.

Table 15. Calculated bulk litter input values and comparison of simulation results to field data.

	Particle-to-Geometry	Particle-to-Particle
Coefficient of Static Friction	0.44	0.71
Coefficient of Restitution	0.00	0.00
Energy Density Coefficient (J/m^3)	2.0E+04	8.0e+3
Comparison to Field Data		
Coefficient of Determination	-0.41	
RMSE (g)	6.9	
Relative Deviation	50.3	
SDRME	2.7	

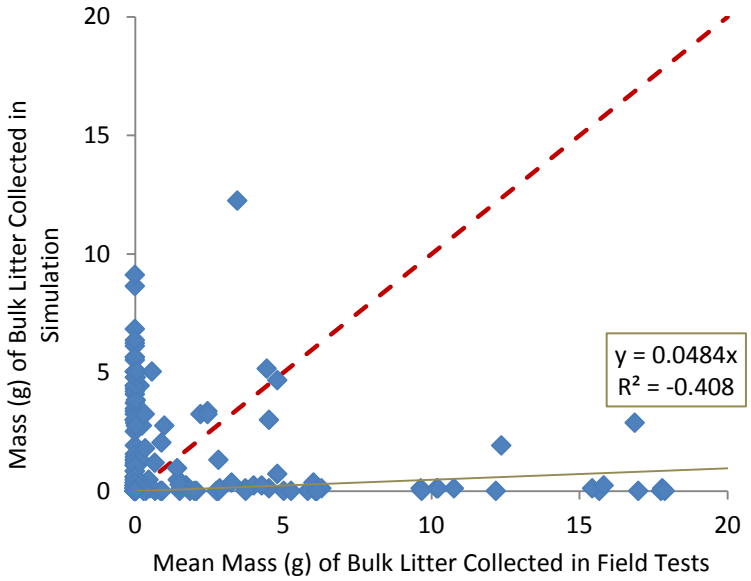

Figure 43. Mass of bulk litter collected within virtual pans vs. actual mass of bulk litter collected during experimental tests using calculated input parameters. Dashed red line represents 1:1 line.

The simulation using the calculated parameters was better than any of the other simulations performed during the calibration process for litter. The input parameters were adjusted over several simulations, but a spread pattern similar to the experimental results (Figure 41a) could not be achieved for the bulk litter. Appendix I contains supporting data for the model calibration to bulk litter. The spread pattern never deviated from the "broadcasted" pattern regardless of what changes were made to the input parameters. Again, this inability to replicate the field data was attributed to the model's limitation in modeling the particle size distribution and particle interactions of the bulk litter. Therefore, the calculated input parameters were considered to be the best performing parameters.

Figures 44a and 44b are plots of the transverse and longitudinal single-disc spread patterns, respectively, for the bulk litter field data and calculated parameters. Collection pans located at 0.9-m, 2.7-m, and 4.6-m transversely and at 0.9-m and 2.7-m longitudinally were omitted from the transverse and longitudinal spread patterns since they did not make up entire

rows and columns of pans. The calculated pattern for both the transverse and longitudinal spread patterns are skewed to the left and aft, respectively, of the curve for the experimental data. This limitation to match the transverse and longitudinal patterns to the pattern resulting from the field data is reflective of the inability to calibrate the model for bulk litter.

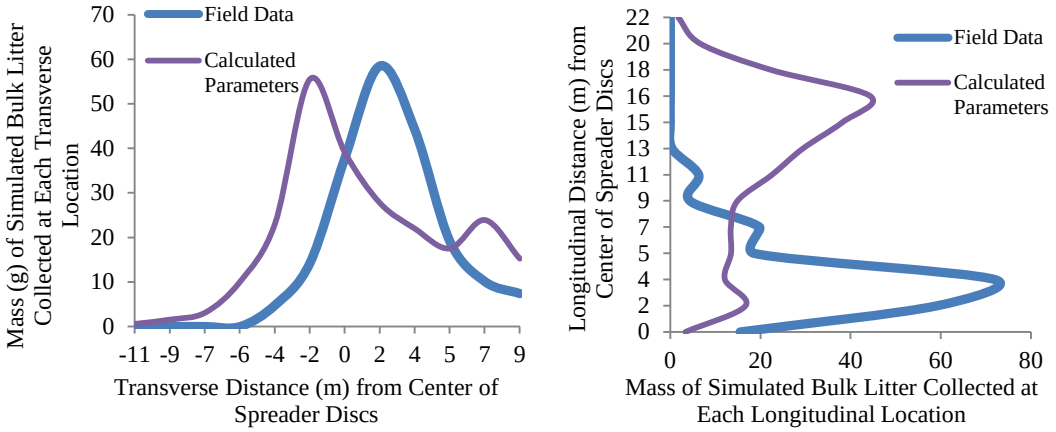

Figure 44. Single-disc transverse (a) and longitudinal (b) spread patterns for the field data and calculated parameters using bulk litter.

Even though the "controls" were discovered through the sensitivity analysis, finding the right combination of parameters for both BBs and bulk litter proved difficult and time consuming. However, this process allowed more understanding of EDEM's abilities and limitations for modeling uniform materials, such as the BBs, and variable materials, such as the broiler litter.

4.2.4 Model Repeatability

Table 16 summarizes the three replications of the calibrated simulation for plastic BBs by comparing the coefficient of determination of each replicated simulation. The results from each replication were not expected to be the exactly same due to the random particle generation within the particle factory. The number of particles captured in each virtual pan differed between the

three replications (Figures 45). The differences between the three replications of the simulation indicated that this DEM software was not deterministic in nature.

Table 16. Results for simulation repeatability of the calibrated model for plastic BBs.

Replication	R^2
1	0.84
2	0.77
3	0.79

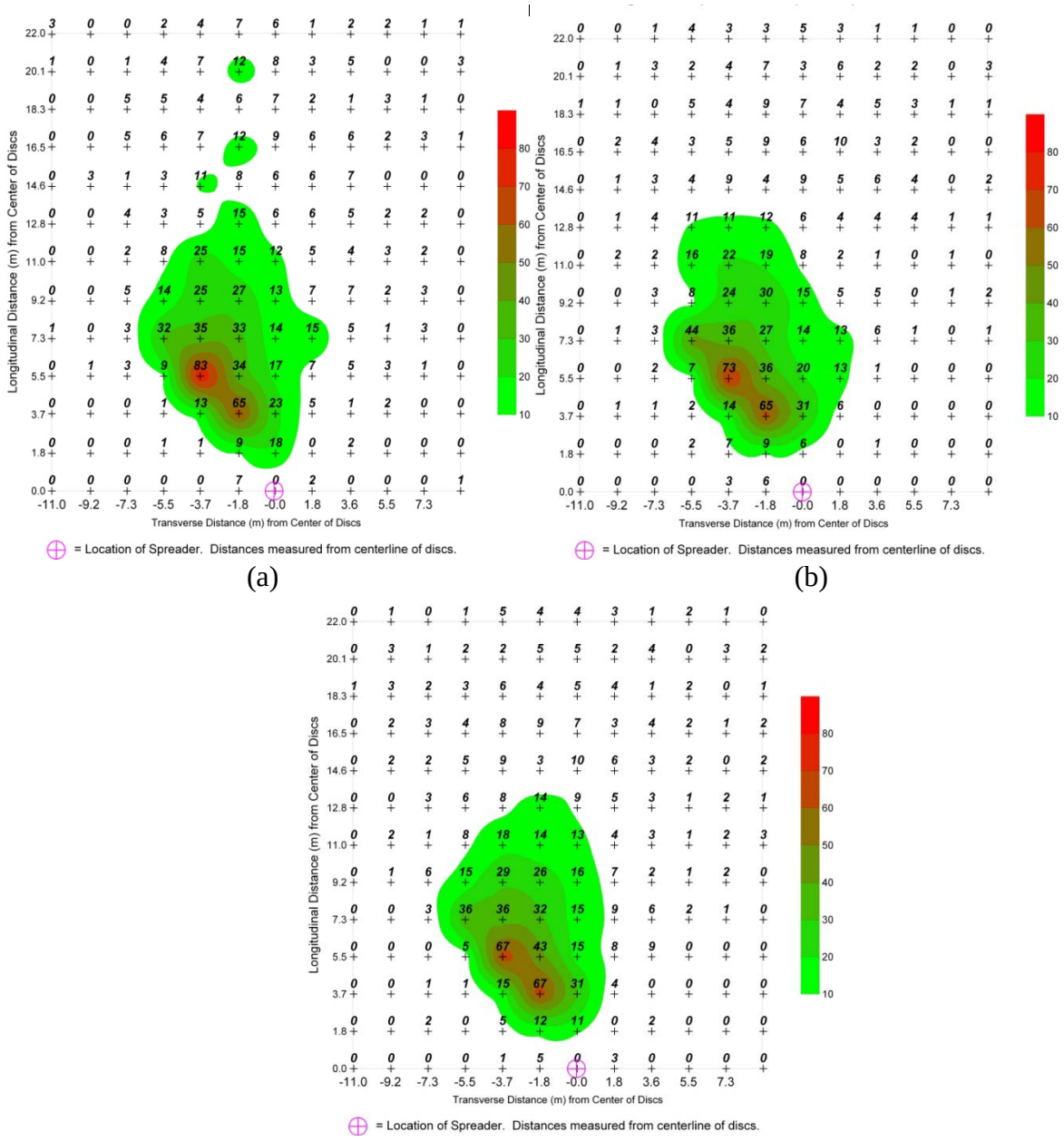

Figure 45. Resulting surface plots for three replications of the calibrated simulation for plastic BB's.

4.3 Validation of DEM Simulations

4.3.1 Divider Accuracy Tests

Summary of the experimental and simulated static divider accuracy tests are presented in Table 17. As expected, the material flow, for the most part, during the experimental tests was evenly divided as it passed over the flow divider. There were some differences in mass between the left and right sides, but considering the variability of the litter, this result was considered acceptable. There was less variability (3.2%) at the highest rate of 6,725-kg/ha possibly due to the higher conveyor speed resulting in a more uniform flow. Slower conveyor speeds have the tendency to generate a cyclic flow. There is less chance of build-up on the divider at higher conveyor speeds. The material flow during the simulations was divided more evenly than during the experiments resulting in lower errors between the two bins most likely due to the fact that perfect spheres with uniform shape and size were used during the simulations. Percent difference between the simulated and experimental results for each side never exceeded more than 2.0%. Similar to the experimental results, the least amount of variability (0.9%) occurred at the highest application rate of 6,725-kg/ha for the simulated results. Appendix I contains the supporting data for the divider accuracy tests. The ANOVA at the 95% confidence level resulted in both bins being similar for all three application rates. The p-values for the 560, 4483, and 6725-kg/ha application rates were 0.6981, 0.3394, and 0.7605, respectively.

Table 17. Summary of experimental and simulated divider accuracy results.

	Application Rate		
	560-kg/ha	4483-kg/ha	6725-kg/ha
Experimental Results[1]			
Left Bin (kg)[1]	14.4[a] (2.3)	50.8[a] (2.0)	58.4[a] (7.5)
Right Bin (kg)[1]	14.7[a] (1.5)	52.5[a] (5.5)	57.2[a] (12.0)
Percent Difference (%)	2.1	3.3	2.1
Simulated Results			
Left Bin (kg)	14.5	51.7	57.9
Right Bin (kg)	14.4	51.5	57.7
Percent Difference (%)	0.7	0.4	0.3
Comparison of Experimental and Simulated Results			
Left Bin Percent Difference (%)	0.7	1.8	0.9
Right Bin Percent Difference (%)	2.0	1.9	0.9

[1]Mean values with different letters within each column indicate they are statistically different at the 95% confidence level. Standard deviation presented in parentheses.

4.3.2 Particle Trajectory Tests

The experimental results of the static particle trajectory tests for the plastic BBs at drop location 1(near disc center) at disc speeds of 600 and 700-rpm are shown as surface maps in Figures 46a and 47a, respectively. Of note, calibration was performed at 400-rpm. Results are reported as the mean number of BBs (3 replications) captured in each collection pan (Figures 46a and 47a) with standard deviation illustrated in Figures 46b and 47b. Increasing spinner-disc speed resulted in the pattern becoming more concentrated and shifting the peak away (radially) from the disc. This change in peak position was an expected trend since there was an increase in the spinner-disc speed.

Figures 48 and 51 present the surface maps of the simulated single-disc spread patterns for the 600-rpm and 700-rpm tests, respectively. It is important to note that the same number of simulated particles was used in both simulations. With that being noted, there are a different number of particles captured by the simulated pans when comparing Figures 48 and 51. The

number of particles captured by the simulated pans changed with alterations to spinner-disc speed due to the shift in the spatial location and shape of the spread pattern. Another important observation from comparing the simulated surface maps is that the simulated particles at the spinner-disc speed of 700-rpm did not travel further than the simulated particles at the spinner-disc speed of 600-rpm. This can be attributed to the loss of predictability when changing spinner-disc speed. Figures 49 and 52 illustrate the comparison between number of BBs captured in the virtual pans to the actual number of BBs collected within pans during field tests at drop location 1 for spinner-disc speeds of 600 and 700-rpm, respectively.

By comparing the simulated results (Figures 48 and 51) to the experimental results (Figures 46a and 49a), the simulated results do not represent the experimental tests. The simulated patterns are more elongated with most of the BBs landing closer to the disc. The simulated spread pattern was calibrated to a specific disc speed of 400-rpm. When changing the disc speed within the DEM, the behavior of the simulated particles changed. Tables 18 and 19 summarize the results from comparing the simulated and experimental spread patterns at 600 and 700-rpm, respectively, for drop location 1 using plastic BBs. The transverse spread patterns of the simulated and experimental results are compared in Figures 50 and 51 for spinner-disc speeds of 600 and 700-rpm, respectively, for drop location 1.

Table 18. Comparison of simulation results to field data for drop location 1 at 600-rpm using plastic BBs.

Comparison to Field Data	
Coefficient of Determination	0.28
RMSE (# of BBs)	5.8
Relative Deviation	47.3
SDRME	0.8

Table 19. Comparison of simulation results to field data for drop location 1 at 700-rpm using plastic BBs.

Comparison to Field Data	
Coefficient of Determination	0.22
RMSE (# of BBs)	5.1
Relative Deviation	50.3
SDRME	0.9

These results were somewhat unexpected based on the calibration results indicating a good relationship (Table 14). However, the model was calibrated at a single disc speed (400-rpm) and at the first drop location. The only difference between the calibration and the tests at the first drop location was the spinner-disc speed. These results indicated that the model loses its predictive ability when the spinner-disc speed is changed. Calibration of the model would be necessary for each disc speed if testing over a range of disc speeds. In this study, calibration was not performed for the disc speeds used in validating the model since this research is focused on the capabilities and potential limitations of using DEM for material distribution.

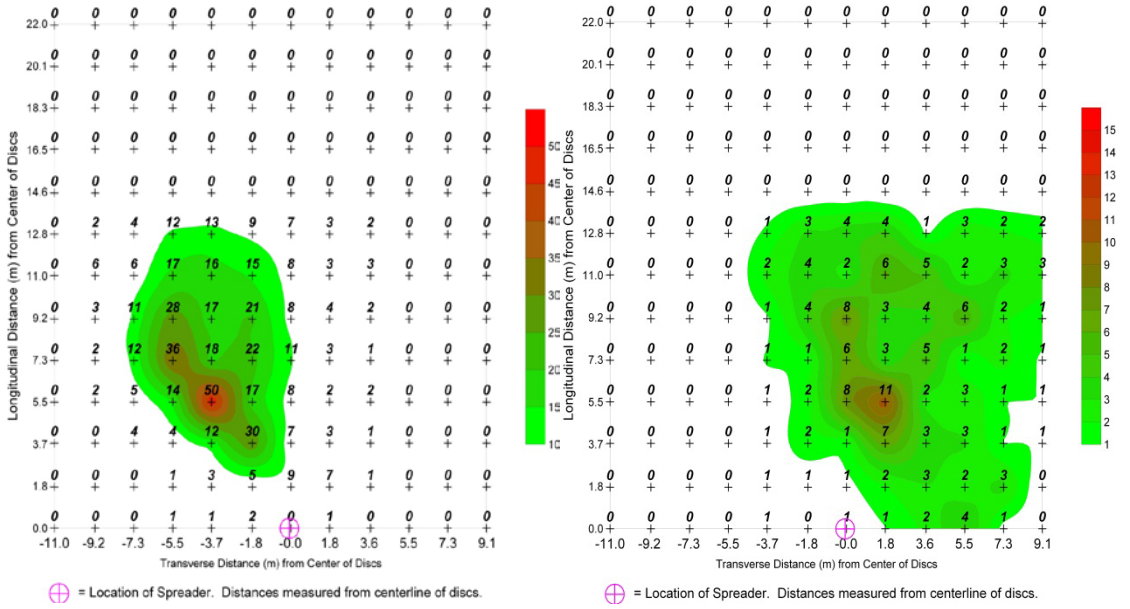

(a) (b)

Figure 46. Interpolated surfaces overlain with mean number (a) and standard deviation (b) of BBs captured in each collection pan for the field trajectory tests at drop location 1 with a disc speed of 600-rpm.

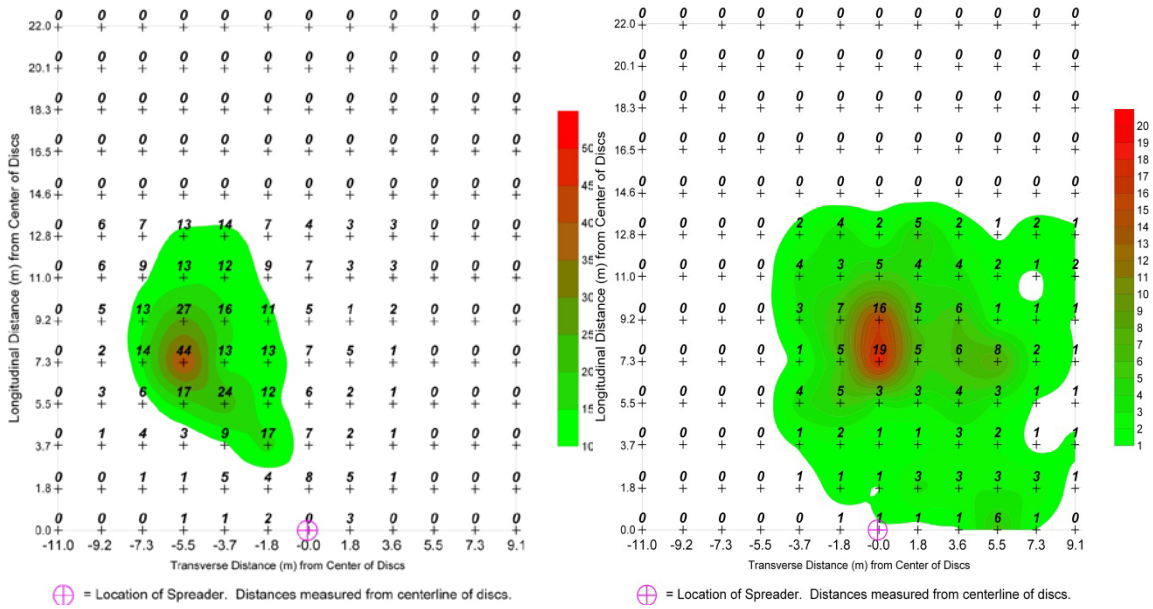

(a) (b)

Figure 47. Interpolated surfaces overlain with mean number (a) and standard deviation (b) of BBs captured in each collection pan for the field trajectory tests at drop location 1 with a disc speed of 700-rpm.

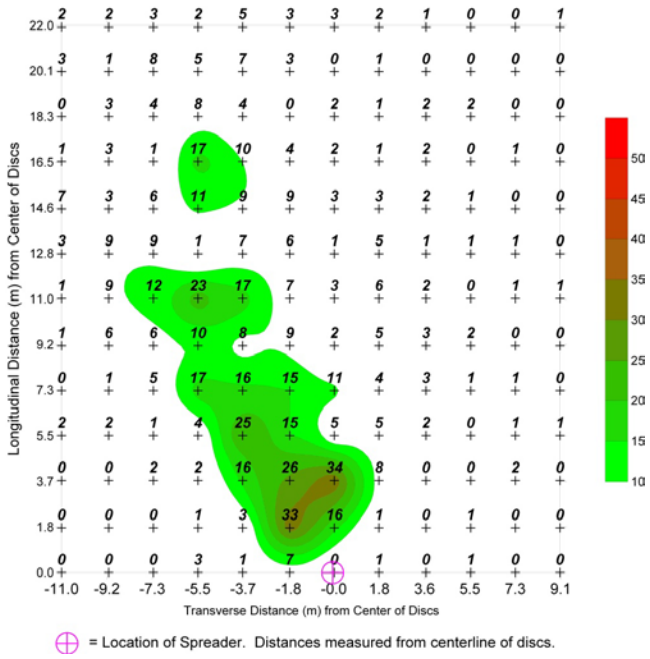

Figure 48. Interpolated surface overlain with simulated number of BBs captured in each virtual collection pan for drop location 1 (near disc center) with a disc speed of 600-rpm.

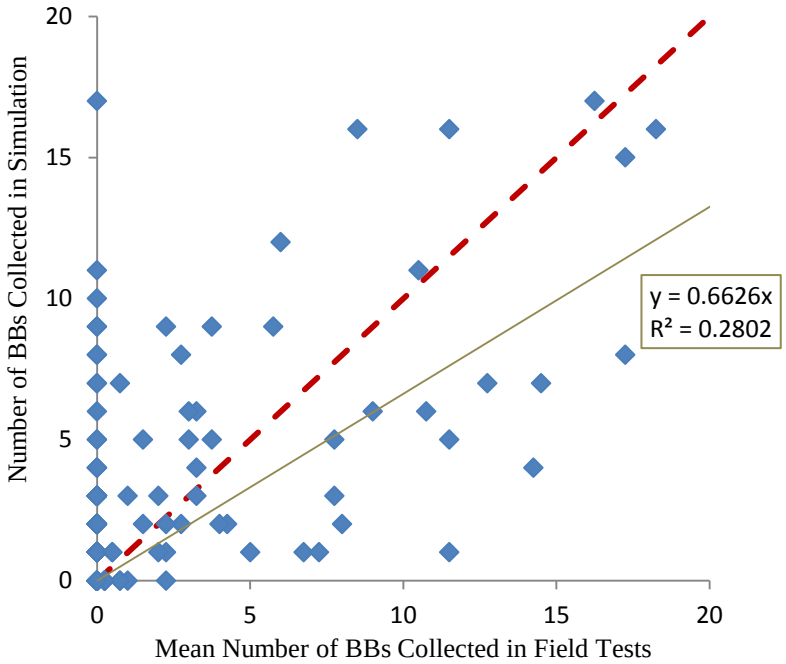

Figure 49. Number of BBs collected within virtual pans vs. actual number of BBs collected during experimental at drop location 1 with disc speed of 600-rpm. Dashed red line represents 1:1 line.

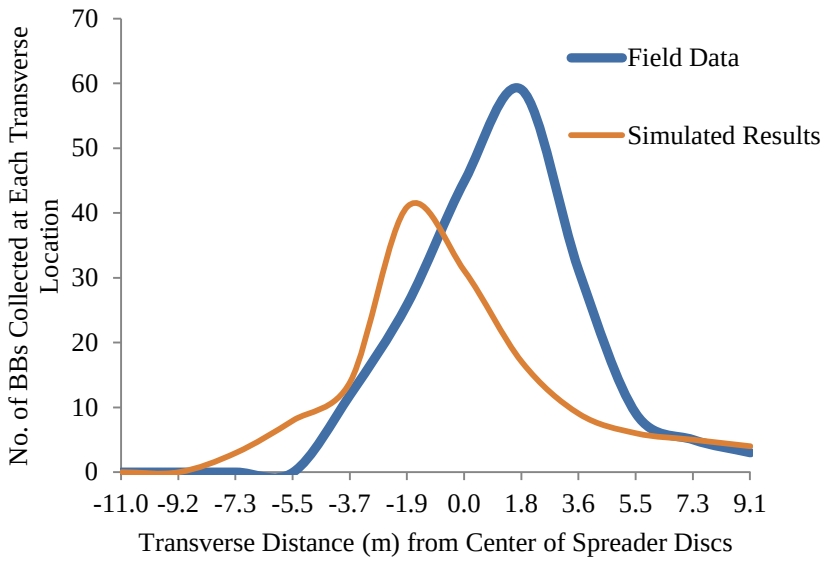

Figure 50. Single-disc transverse spread patterns for the field data and simulated results at drop location 1 with disc speed of 600-rpm using plastic BBs.

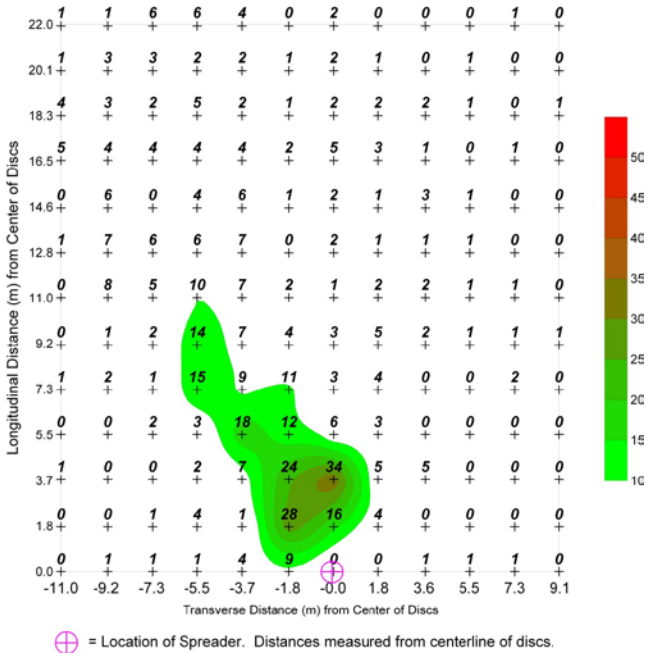

Figure 51. Interpolated surface overlain with simulated number of BBs captured in each virtual collection pan for drop location 1 (near disc center) with a disc speed of 700-rpm.

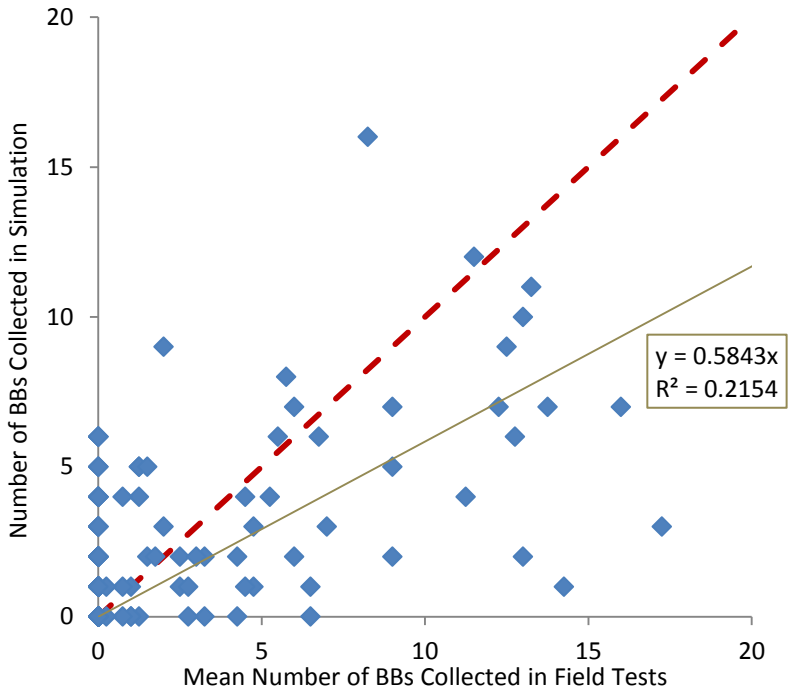

Figure 52. Number of BBs collected within virtual pans vs. actual number of BBs collected during experimental at drop location 1 with disc speed of 700-rpm. Dashed red line represents 1:1 line.

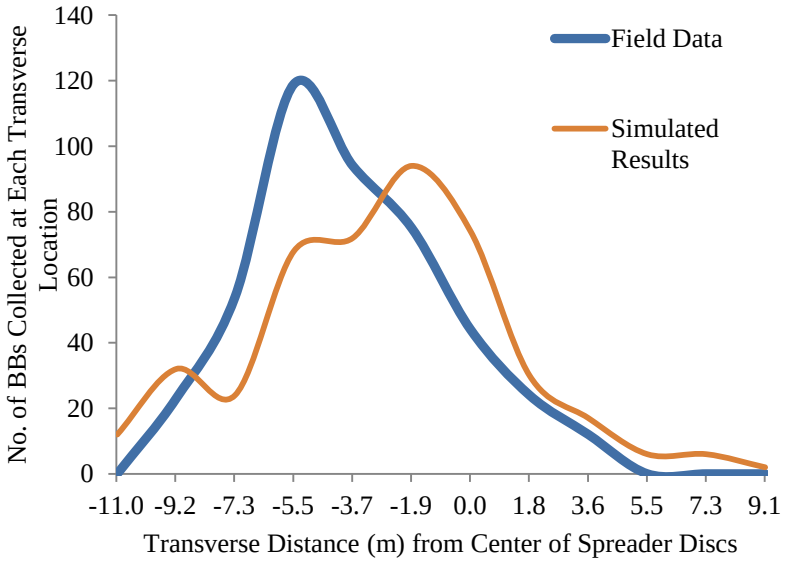

Figure 53. Single-disc transverse spread patterns for the field data and simulated results at drop location 1 with disc speed of 700-rpm using plastic BBs.

Figures 54 and 55 are surface maps of the field data collected at drop location 2 (near disc edge) with spinner-disc speeds of 600-rpm and 700-rpm, respectively. Figures 56 and 59 are surface maps of the simulated single-disc, spread patterns at 600-rpm and 700-rpm, respectively. Like the results from drop location 1, the simulated patterns are different from the patterns generated from the experimental data. Tables 20 and 21 summarize the results from comparing the simulated and experimental spread patterns at 600 and 700-rpm, respectively, for drop location 2 using plastic BBs. Figures 57 and 60 illustrate the comparison between number of BBs captured in the virtual pans to the actual number of BBs collected within pans during field tests at drop location 2 for spinner-disc speeds of 600 and 700-rpm, respectively. The transverse spread patterns of the simulated and experimental results are compared in Figures 58 and 61 for spinner-disc speeds of 600 and 700-rpm, respectively, for drop location 2.

Table 20. Comparison of simulation results to field data for drop location 2 at 600-rpm using plastic BBs.

Comparison to Field Data	
Coefficient of Determination	0.60
RMSE (# of BBs)	4.8
Relative Deviation	49.3
SDRME	0.6

Table 21. Comparison of simulation results to field data for drop location 2 at 700-rpm using plastic BBs.

Comparison to Field Data	
Coefficient of Determination	0.34
RMSE (# of BBs)	6.0
Relative Deviation	58.2
SDRME	0.8

Ironically, the simulated spread patterns for drop location 2 resembled the experimental spread patterns using drop location 1. This similarity can be traced back to the model's inability to simulate the interactions between the particles and the spinning discs. The model inaccurately

predicts the interactions, thus placing the peak(s) of the pattern closer to the disc. This result was more evident at the higher disc speed of 700-rpm.

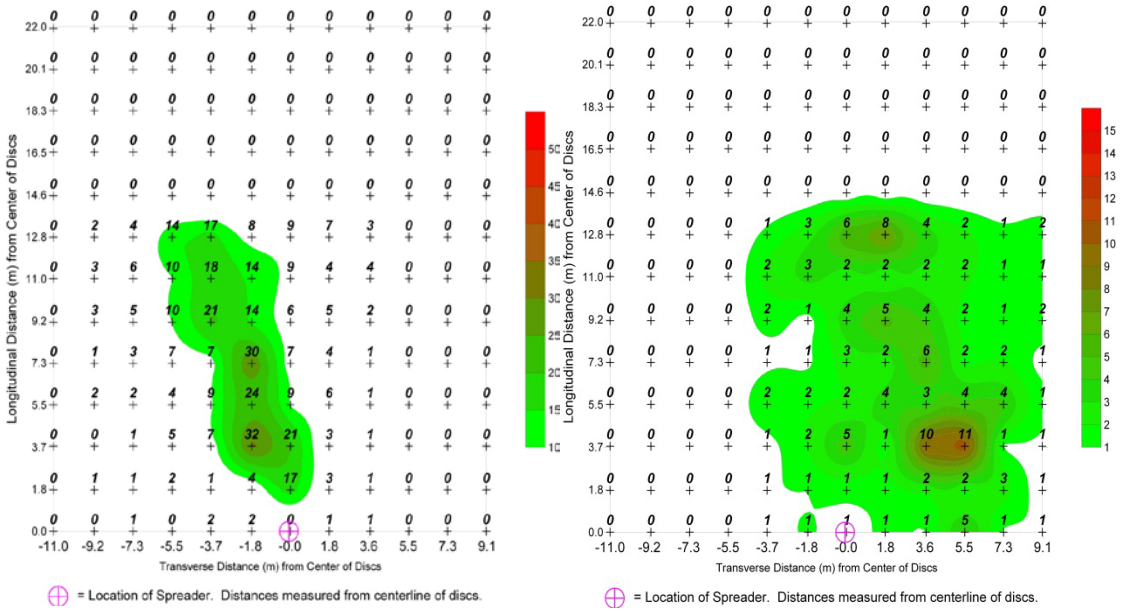

(a) (b)

Figure 54. Interpolated surfaces overlain with mean number (a) and standard deviation (b) of BBs captured in each collection pan for the field trajectory tests at drop location 2 with a disc speed of 600-rpm.

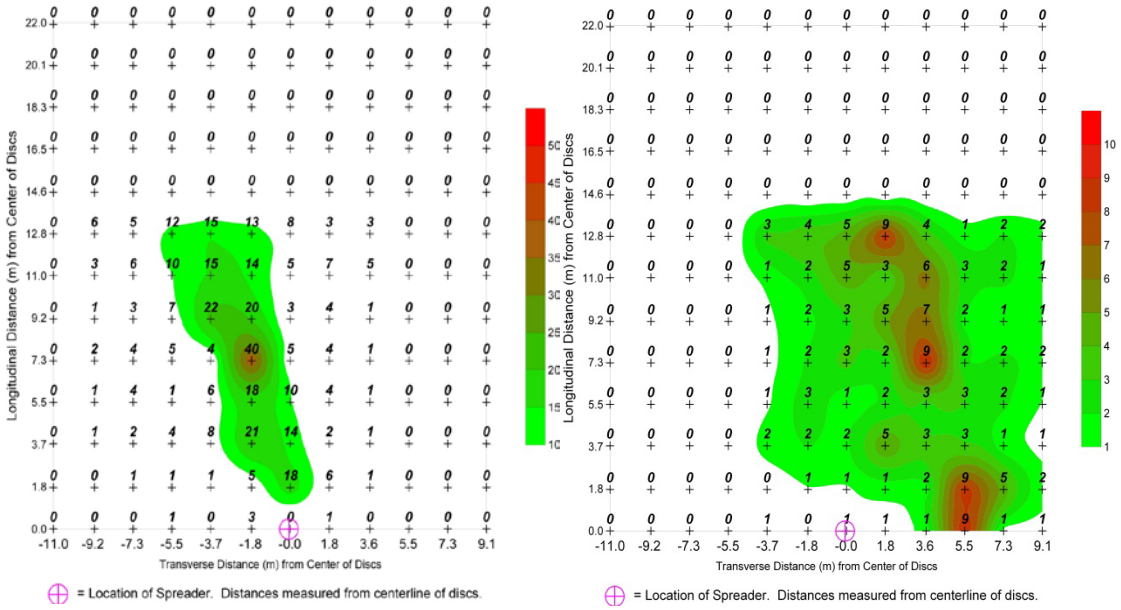

(a) (b)

Figure 55. Interpolated surfaces overlain with mean number (a) and standard deviation (b) of BBs captured in each collection pan for the field trajectory tests at drop location 2 with a disc speed of 700-rpm.

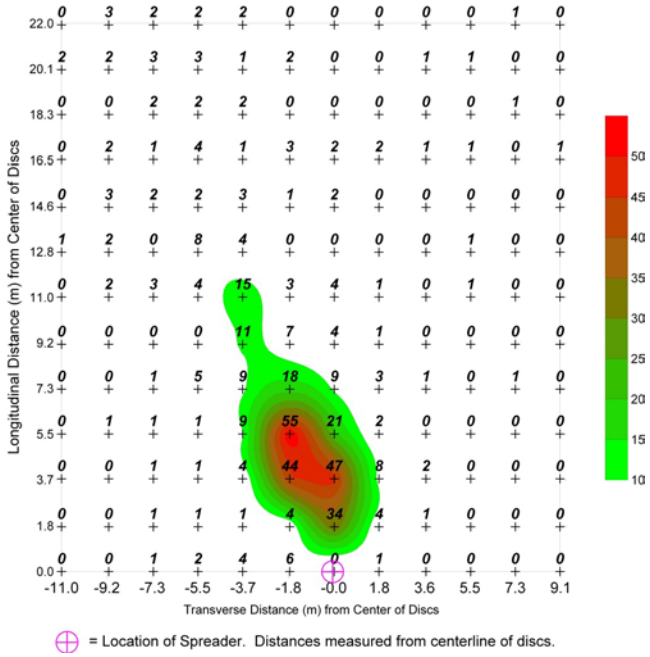

Figure 56. Interpolated surface overlain with simulated number of BBs captured in each virtual collection pan for drop location 2 (near disc edge) with a disc speed of 600-rpm.

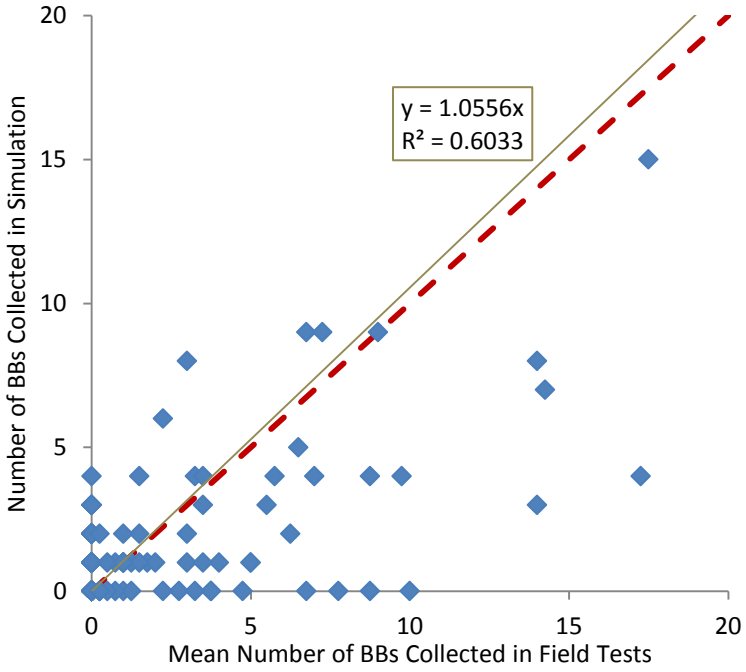

Figure 57. Number of BBs collected within virtual pans vs. actual number of BBs collected during experimental at drop location 2 with disc speed of 600-rpm. Dashed red line represents 1:1 line.

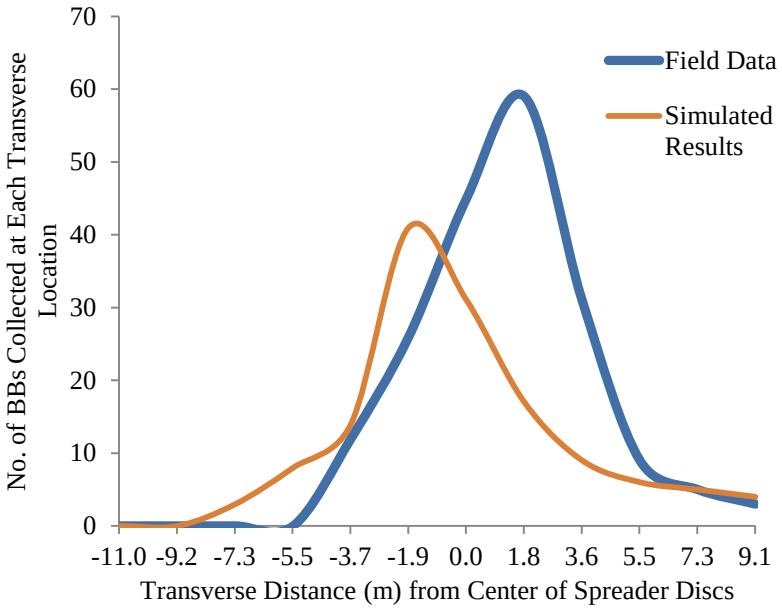

Figure 58. Single-disc transverse spread patterns for the field data and simulated results at drop location 2 with disc speed of 600-rpm using plastic BBs.

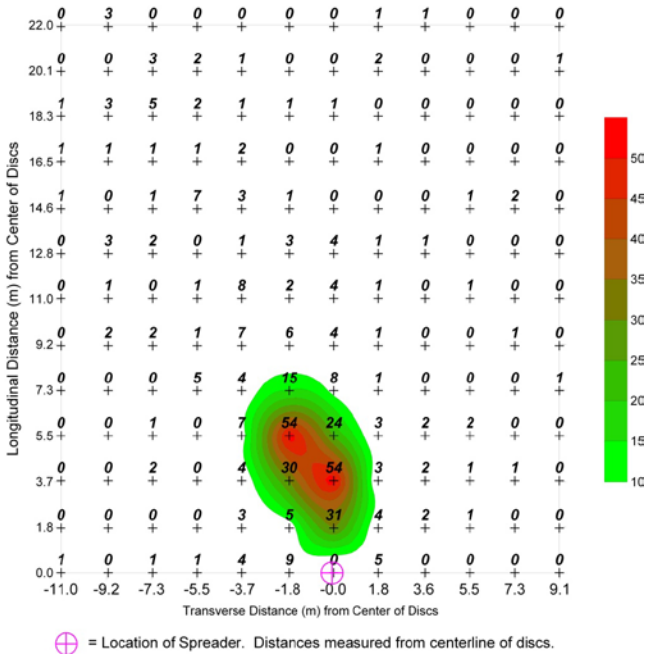

Figure 59. Interpolated surface overlain with simulated number of BBs captured in each virtual collection pan for drop location 2 (near disc edge) with a disc speed of 700-rpm.

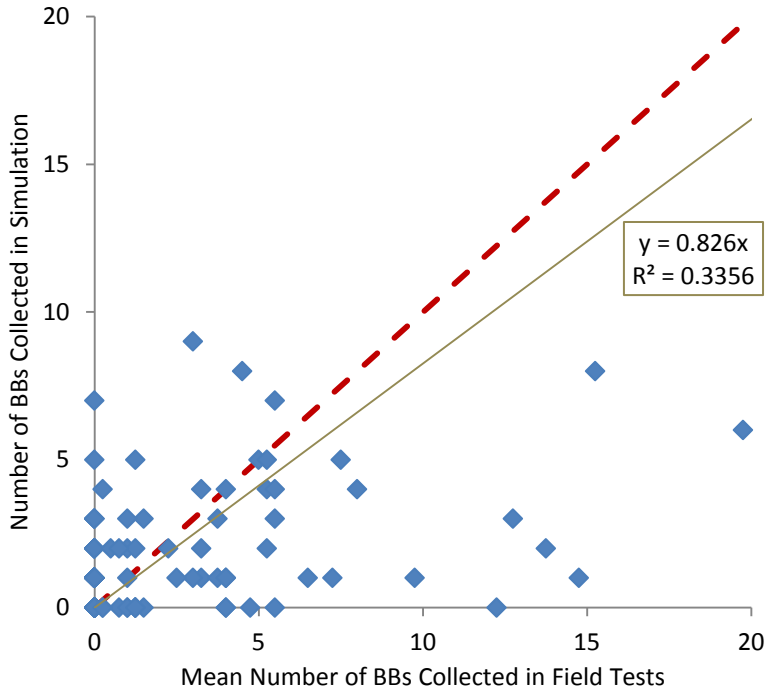

Figure 60. Number of BBs collected within virtual pans vs. actual number of BBs collected during experimental at drop location 2 with disc speed of 700-rpm. Dashed red line represents 1:1 line.

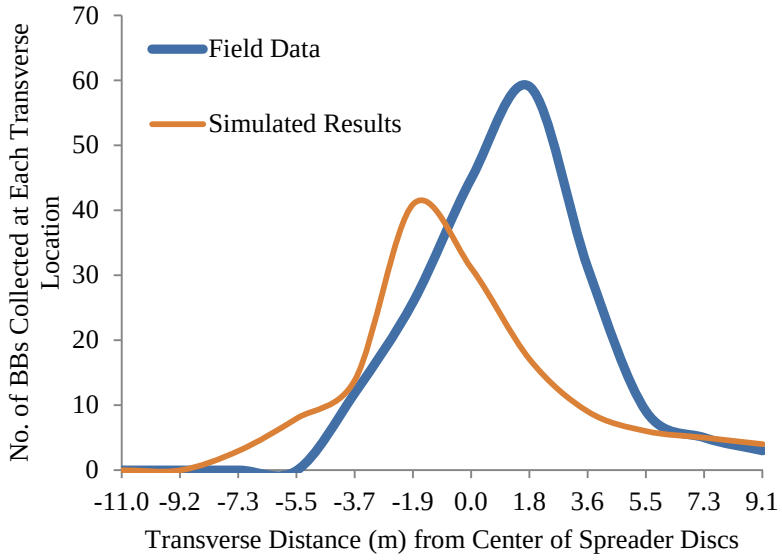

Figure 61. Single-disc transverse spread patterns for the field data and simulated results at drop location 2 with disc speed of 700-rpm using plastic BBs.

Not only did the model lose its predictive ability with a change in spinner-disc speed, it also lost it with change in drop location. Therefore, if one wanted to compare a set of spreader hardware setups, such as different spinner-disc speeds and divider locations, the model would have to be calibrated for each individual setup. Unfortunately, this discovery was discouraging in the sense that there will be significantly more time spent on calibrating the model than using it to evaluate different design setups for distribution uniformity. A possible solution to this problem might be to incorporate a computer program with the DEM model that calibrates the model for a given hardware setup once the input parameters have been established. This way, the input parameters would be optimized by the computer program for a given hardware setup instead of using the trial-and-error approach to find the right input parameters. The calibration of the DEM model as presented in this study would be eliminated.

The experimental results of the static particle trajectory tests (500 and 700-rpm) for bulk litter at drop location 1 (near disc center) are shown as surface maps in Figures 62 and 63. The results for the disc speed of 600-rpm are discussed in the results for model calibration to bulk litter (Figures 41a and 42a). The majority of the litter landed between -1.8-m and 5.5-m transversely of the spreader centerline and up to approximately 5.5-m aft of the disc.

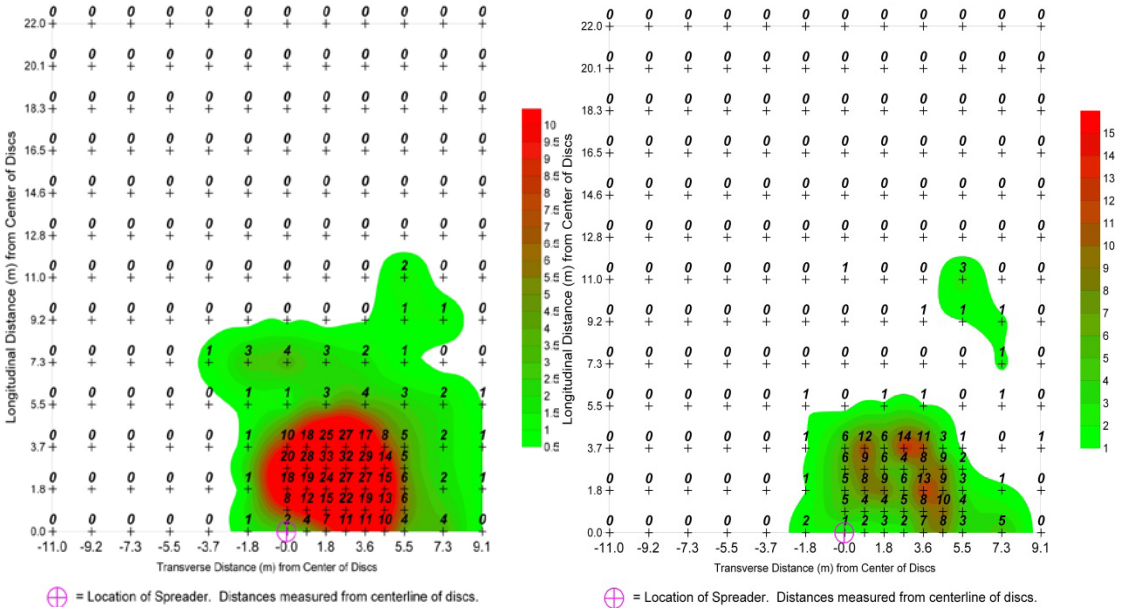

(a) (b)

Figure 62. Interpolated surfaces overlain with mean mass (a) and standard deviation (b) of bulk litter (3 replications) captured in each collection pan for drop location 1 (near disc center) at disc speed of 500-rpm.

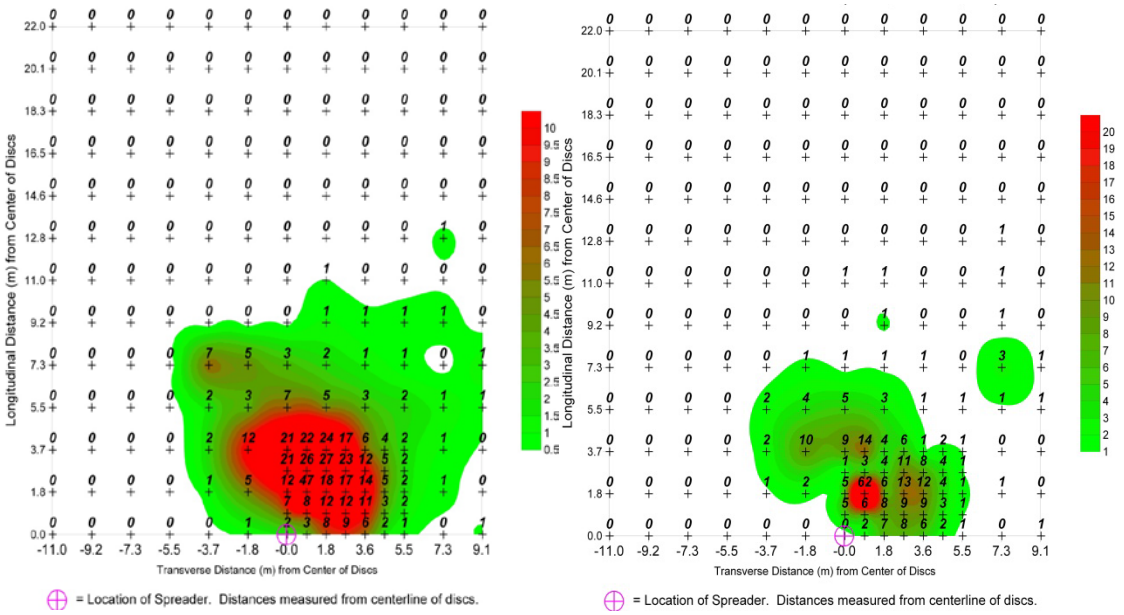

(a) (b)

Figure 63. Interpolated surfaces overlain with mean mass (a) and standard deviation (b) of bulk litter (3 replications) captured in each collection pan for drop location 1 (near disc center) at disc speed of 700-rpm.

Figures 64 and 65 represent the surface maps of the simulated single-disc spread patterns for the 500-rpm and 700-rpm tests, respectively, using bulk litter. Based on the conclusions from the model validation to litter, the simulated surface maps were not expected to correlate to the experimental tests. Tables 22 and 23 summarize the results from comparing the simulated and experimental spread patterns at 500 and 700-rpm, respectively, for drop location 1 using bulk litter. Figures 65 and 68 illustrate the comparison between mass of bulk litter captured in the virtual pans to the actual mass of bulk litter collected within pans during field tests at drop location 1 for spinner-disc speeds of 500 and 700-rpm, respectively. The transverse single-disc spread patterns (experimental and simulated) for bulk litter at spinner-disc speeds of 500-rpm and 700-rpm are illustrated in Figures 66 and 69.

Table 22. Comparison of simulation results to field data for drop location 1 at 500-rpm using bulk litter.

Comparison to Field Data	
Coefficient of Determination	-0.2
RMSE (g)	8.4
Relative Deviation	86.9
SDRME	2.4

Table 23. Comparison of simulation results to field data for drop location 1 at 700-rpm using bulk litter.

Comparison to Field Data	
Coefficient of Determination	-0.4
RMSE (g)	7.0
Relative Deviation	82.2
SDRME	3.7

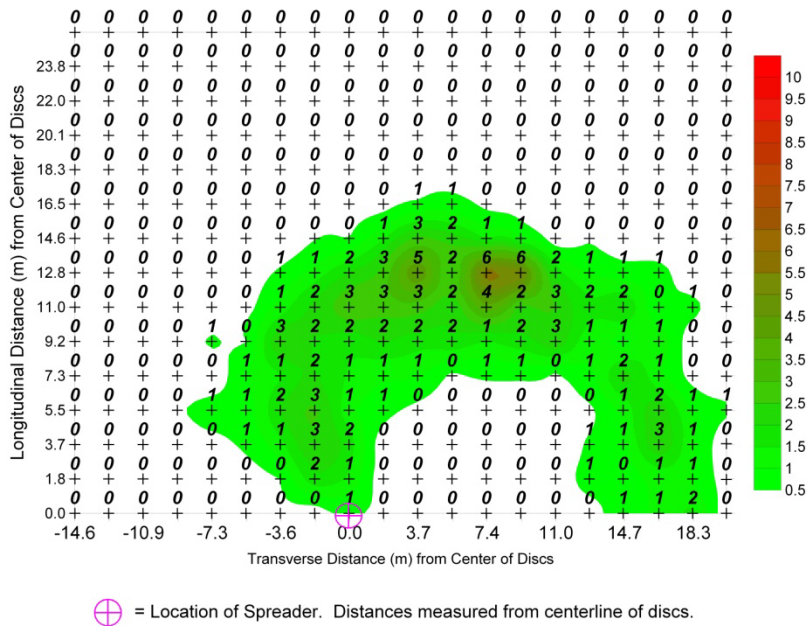

Figure 64. Interpolated surface overlain with simulated mass of bulk litter captured in each virtual collection pan for the drop location 1 (near disc center) with a disc speed of 500-rpm.

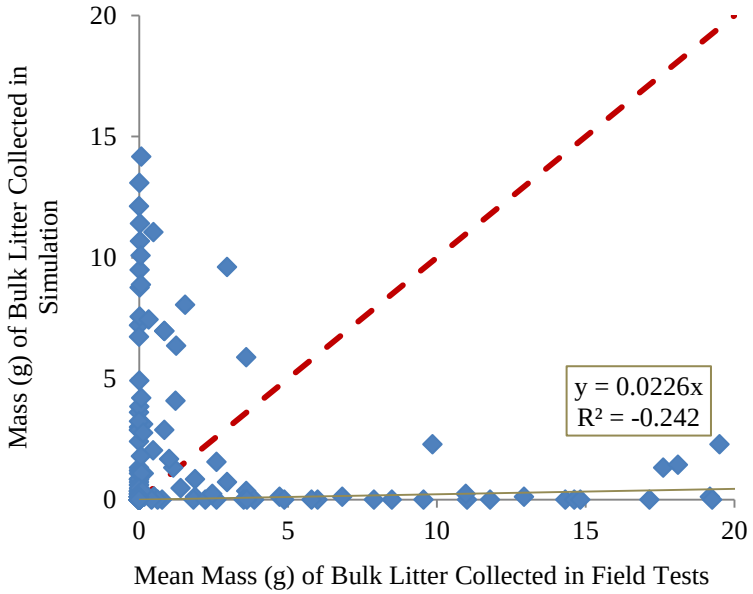

Figure 65. Mass of bulk litter collected within virtual pans vs. actual mass of bulk litter collected during experimental at drop location 1 with disc speed of 500-rpm. Dashed red line represents 1:1 line.

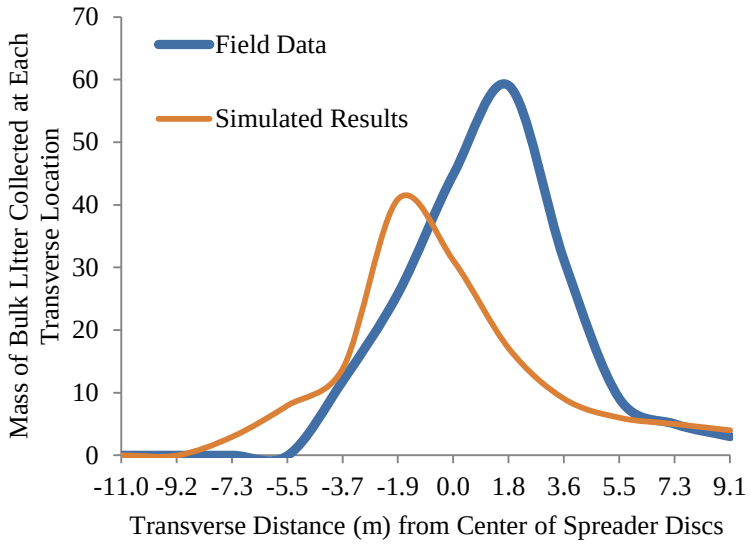

Figure 66. Single-disc transverse spread patterns for the field data and simulated results at drop location 1 with disc speed of 500-rpm using bulk litter.

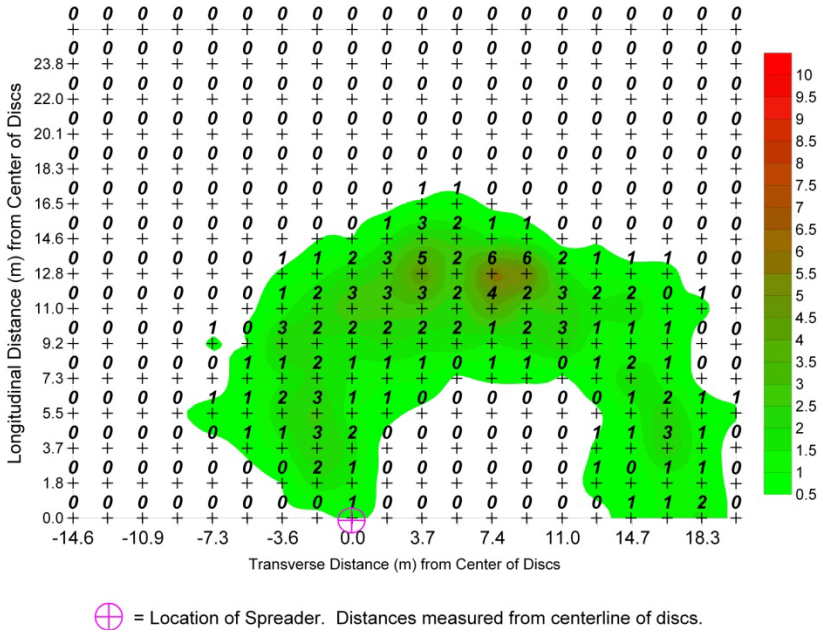

Figure 67. Interpolated surface overlain with simulated mass of bulk litter captured in each virtual collection pan for drop location 1 (near disc center) with a disc speed of 700-rpm.

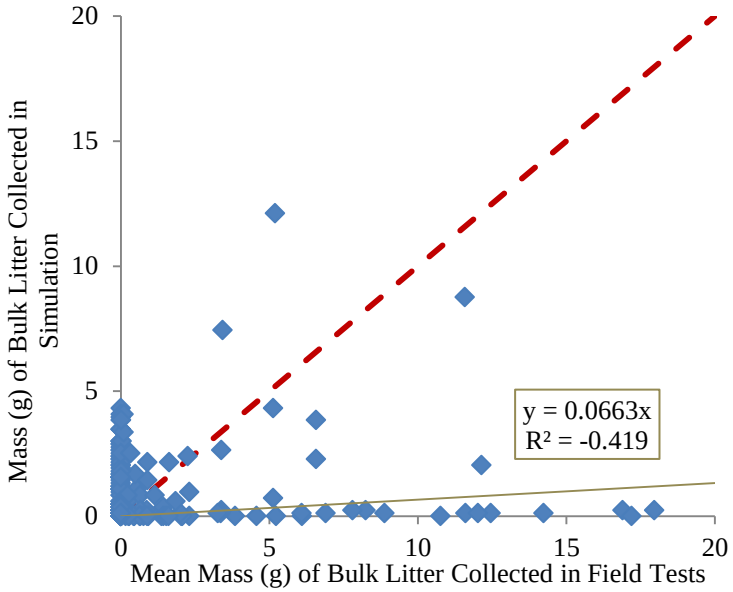

Figure 68. Mass of bulk litter collected within virtual pans vs. actual mass of bulk litter collected during experimental at drop location 1 with disc speed of 700-rpm. Dashed red line represents 1:1 line.

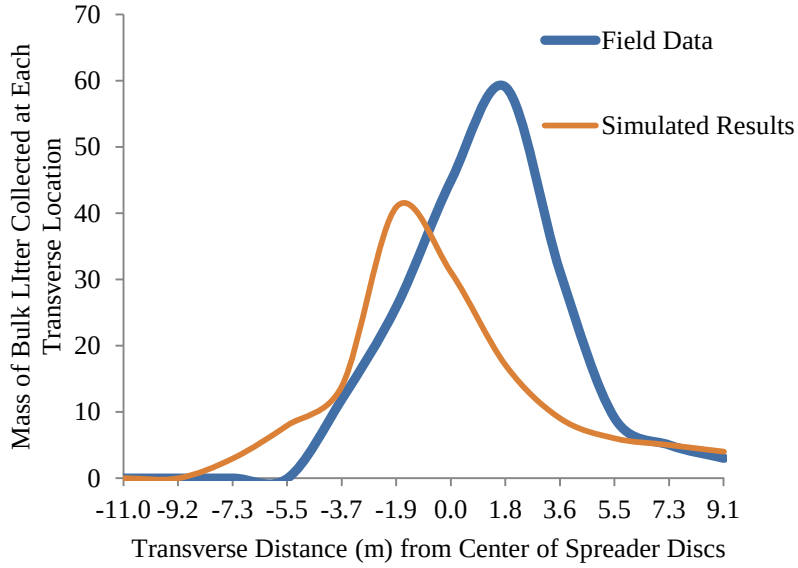

Figure 69. Single-disc transverse spread patterns for the field data and simulated results at drop location 1 with disc speed of 700-rpm using bulk litter.

4.4 Summary

The notion that litter is comprised of a wide range of particle sizes was confirmed after attaining the particle size distribution. Increasing the moisture content of litter resulted in increases in bulk density and particle size. The variability of particle size was quantified through segregating litter into three size classifications. Results from the parameter sensitivity analysis demonstrated that the coefficient of static friction, energy density coefficient, and coefficient of restitution controlled the transverse movement, longitudinal movement, and pattern concentration, respectively. The particle size within the model was limited to 6-mm in diameter for this study. Setting up the DEM model required input parameters to establish particle-to-particle and particle-to-geometry interactions. Initial values attained from the tilt and angle of repose tests were used in establishing a starting point for model calibration. Simulating the tilt and angle of repose tests illustrated the need for calibration of the model from differences in the calculated coefficient of static friction and what the coefficient of static friction was adjusted to in order to replicate the experiments. Calibration of the model to the particle trajectory tests was time consuming with the trial-and-error approach to adjusting input parameters. The simulated spread pattern for plastic BBs showed good correlation to the experimental pattern. The coefficient of determination and RMSE were 0.85 and 2.1, respectively. However, the simulated pattern for bulk litter could not be attained. Validating the model showed that litter conveyance was accurately simulated with percent differences never exceeding 2%. Unfortunately, the model lost its predictability when changing disc speed and drop location for the particle trajectory tests. This limitation was evident for both the BB and litter simulations.

CHAPTER FIVE

CONCLUSIONS

5.1 Conclusions

Setup of a DEM model requires knowledge of the materials being simulated. The input parameters for material properties have to be assumed or measured if not already known. Material property experiments for broiler litter supported the notion that litter was composed of a wide range of particle sizes (dust particles to large chunks). As the MC treatments of the litter increased, the particle size and bulk density increased due to the increase of cohesion between particles. The GSI value decreased most likely due to particles becoming more cohesive as MC increased. Segregation of the litter into size classifications at the 24% MC treatment demonstrated the variability in particle size. The majority of the particle distribution fell within the "medium" size classification which ranged from 0.425-mm to 4.75-mm. Setup of the DEM was completed by importing the spreader geometry and applying dynamics were necessary. Input parameters were established from experimental measurements or assumptions from previous studies.

During the DEM model calibration, a sensitivity analysis on the input parameters of DEM software indicated the "controls" that could be adjusted in order to calibrate or adjust model output. The coefficient of static friction affected the transverse movement of broadcasted particles, the energy density coefficient controlled the longitudinal movement of broadcasted

particles, and the coefficient of restitution impacted the concentration/dispersion of particles within the simulated pattern. Limitations of the model were also discovered during the parameter sensitivity analysis.

The smallest particle size to be defined was 6-mm without causing the model to "freeze up" upon the start of a simulation or the DEM software crashing. As the simulation domain size increased, the time for a simulation to run also increased. Large quantities of small particles also increased simulation time or caused the software to crash. These limitations were most likely due to the computational power (4 processors) and the inability of the model to simulate complex processes that involve particles exhibiting chaotic behavior. Calibration of the model to the plastic BBs yielded comparable results to previous research. The coefficient of determination and RMSE of the calibrated model were 0.85 and 2.1, respectively. Calibration of the DEM model to bulk litter was not attainable (R^2=-0.41, RMSE=6.9) with the "best" simulation using the calculated input values of the bulk litter.

The DEM model validation indicated that the model was capable of accurately simulating litter conveyance. The percent difference between simulated and experimental results never exceeded 2%. When the spinner-disc speed or the drop location of the BBs changed, the model lost its predictive ability. Increasing the disc speed from 400 to 600-rpm resulted in a coefficient of determination and RMSE of 0.28 and 5.8, respectively. Moving from drop location 1 to drop location 2 at 600-rpm resulted in a coefficient of determination and RMSE of 0.60 and 4.8, respectively. Although model calibration was not achieved for the bulk litter, the spatial location and shape of the pattern changed significantly when a change in disc speed was made. Increasing the disc speed from 600 to 700-rpm resulted in a coefficient of determination and RMSE of -0.4 and 7.0, respectively. These results indicated that for a study using different

spreader hardware settings or different materials, a DEM model would have to be calibrated for an individual setup.

5.2 Practical Implications

The results from this research will hopefully provide useful information for future research regarding DEM and spinner-disc spreaders. These results provide more information in characterizing broiler litter over a range of moisture contents. With this knowledge, equipment manufacturers can design equipment to better transport, convey, and distribute litter.

The use of DEM modeling has recently been incorporated into the agriculture industry for equipment and process design. DEM has proved that it provides an accurate means to model material conveyance. Equipment manufacturers could make use of DEM modeling to design mechanical systems in which grains are conveyed, such as in combines. DEM could give engineers more observation into how accurately the material is being conveyed through the various processes. However, when it comes to material distribution, DEM modeling lacks the ability to simulate biological materials where material properties are not constant. As a result, DEM modeling can limit the ability to aid litter spreader manufacturers in designing material distribution systems, at this time.

5.3 Opportunities for Future Research

Based on the results of this research, there exist opportunity to further the understanding of DEM modeling and how it can be used in evaluating spinner-disc spreaders. Since the "straight-forward" approach in modeling the broadcast of material from the spinning discs proved difficult, implementing what EDEM refers to as Applications Programming Interface (API) could prove to aid in this process and improve results. This API allows for the customization of contact physics, particle-field interactions, and particle initialization through C

and C++ programming. Also, user defined custom contact models could better represent particle-to-particle and particle-to-geometry interactions for biological materials. By introducing API to simulating a spinner-disc spreader, there is more opportunity to accurately calibrate the model to the actual material-disc interactions.

Calibration of the DEM model is another area in which future research could provide reduced time for model setup and improved results. The methods presented in this research were tedious and time consuming. A possible solution is to integrate a computer program with the EDEM software in which the input parameters are optimized before the simulation is performed. The calibration process would be performed by the computer program instead of the user. This approach would eliminate the repetitive process of changing input parameters and performing simulations. The integrated computer program would also allow the EDEM software to model biological materials, such as broiler litter, more accurately.

A variable not included in this research that should to be addressed is incorporating the impact of aerodynamics into the modeling process. This feature is an important variable that has an effect on how particles are distributed once they exit the spinning discs. EDEM has recently made progress towards incorporating aerodynamics into its modeling software. The velocity vector of the particle could be defined as it leaves the disc. Using Excel, the landing position could then be estimated. This process would thereby reduce the domain size and incorporate the effects of aerodynamics. Since spread pattern uniformity is essential in applying fertilizer, modeling the spread pattern with the incorporation of aerodynamics should improve the accuracy of the simulated results.

Beyond modeling the interactions more accurately, additional research needs to be conducted on simulating an actual size distribution of particles, changes in particle shape, and

particle ballistics. With a variable material such as broiler litter, a wide range of particle sizes exist and the shape of the particles are not the same within the bulk material. In reality, clumps of litter are broken-up after making contact with the spinning discs. Accurately modeling the ballistic behavior should aid in understanding the interactions that take place between litter and the spinning discs. Modeling the actual size distribution, shapes, and ballistic behavior of particles will add complexity, and therefore simulation time. However, the evaluation of how these factors affect the material flow and distribution needs to be considered in order to better use DEM modeling to understand and evaluate spinner-disc spreaders.

REFERENCES

ASABE Standards. 2009. S341.4: Procedure for Measuring Distribution Uniformity and Calibrating Granular Broadcast Spreaders. St. Joseph, Mich.: ASABE.

ASAE Standards. 2005. D384.2 MAR2005: Manure Production and Characteristics. St. Joseph, Mich.: ASAE.

Brinsfield, R.B., and J.W. Hummel. 1975. Simulation of a New Centrifugal Distributor Design. Trans. ASAE. 18(2): 213-220.

Coetzee, C.J. and S.G. Lombard. 2011. Discrete element method modelling of a centrifugal fertilizer spreader. Biosystems Engineering 109 (4): 308-325.

Campbell, C.M., J.P. Fulton, C.W. Wood, T.P. McDonald, and W.C. Zech. 2010. Utilizing Nutrient over Mass Distribution Patterns for Assessment of Poultry Litter Spreaders. Trans ASABE. 53(3): 659-666.

Cundall, P.A. and O.D.L. Strack. 1979. A discrete numerical model for granular assemblies. Geotechnique. 29(1): 331-336.

Cunningham, F.M. 1963. Performance Characteristics of Bulk Spreaders for Granular Fertilizer. Trans. ASAE. 6(1): 108-114.

Cunningham, F.M. and E.Y.S. Chao. 1967. Design Relationships for Centrifugal Fertilizer Distributors. Trans. ASAE. 10(1): 91-95.

Curry, D., J. Favier, and R.D. LaRoche. 2009. A Systematic Approach to DEM Material model Calibration. Edinburgh EH2 3NH, UK. DEM-Solutions Ltd.

Dintwa E., E. Tijskens, R. Olieslagers, J. De Baerdemaeker, and H. Ramon. 2004. Calibration of a Spinning Disc Spreader Simulation Model for Accurate Site Specific Fertiliser Application. Biosystems Engineering. 88(1): 49-62.

Duhovnik, J., J. Benedicic, and R. Bernik. 2004. Analysis and Design Parameters for Inclined Rotors used for Manure Dispersal on Broadcast Spreaders for Solid Manure. Trans. ASAE. 47(5): 1389-1404.

Edwards, D.R. and T.C. Daniel. 1992. Environmental impacts of On-Farm poultry waste disposal. A review. Bioresource Technology 41(1): 9-33.

ERS-USDA. 2011. Data Sets: US Fertilizer Use and Price. United States Department of Agriculture Economic Research Service. Retrieved March 5, 2012 from http://www.ers.usda.gov/Data/FertilizerUse.

Fasina, O.O. 2006. Flow and Physical Properties of Switchgrass, Peanut Hull, and Poultry Litter. Trans. ASABE. 49(3): 721-728.

Fulton, J.P., S.A. Shearer, S.F. Higgins, M.J. Darr, and T.S. Stombaugh. 2005a. Rate response assessment from various granular VRT applicators. Trans. ASABE. 48(6): 2095-2103.

Fulton, J.P., S.A. Shearer, S.F. Higgins, D.W. Hancock, and T.S. Stombaugh. 2005b. Distribution pattern variability of granular VRT applicators. Trans. ASAE 48(6): 2053-2064.

Glancey, J.L. and R.K. Adams. 1996. Applicator for Sidedressing Row Crops with Solid Wastes. Trans. ASABE. 39(3): 829-835.

Glancey, J.L. and S.C. Hoffman. 1996. Physical Properties of Solid Waste Materials. Applied Engineering in Agriculture. 12(4): 441-446.

Glover, J.W., and J.V. Baird. 1973. Performance of Spinner Type Fertilizer Spreaders. Trans. ASAE 16(1): 48-51.

Gonzalez-Montellano, C. D.F. Llana, J.M. Fuentes, and F. Ayuga. 2011. Deteremination of the mechanical properties of corn grains and olive fruits required in DEM simulations. ASABE Paper No. 1111505. St. Joseph, MI: ASABE.

Grift, T.E. 2000. Spread Pattern Analysis Tool (SPAT): I. Development and Theoretical Examples. Trans. ASAE. 43(6): 1341-1350.

Hammond, C., C. Gould, and W. Adkins. 1994. Calibration of Manure Spreader Including Swath Width. Circular 825. Athens, GA. The University of Georgia Cooperative Extension.

Hawkins, G.W. 1971. The effects of uneven spreading of fertilizers on crop yields. Lime and Fertilizer Conference. Baltimore, MD: Delaware-Maryland Plant Food Association, Inc.

Henshaw, Mike. 2005. Pictorial Guide to Calibrating Poultry Litter Spreaders. Auburn University, AL: Alabama Cooperative Extension System (ACES). Available at: http://home.centurytel.net/ke4rop/litter/. Accessed 31 January 2012.

Hepherd, R. Q. and J. A. Pascal. 1958. The transverse distribution of fertilizer by conventional types of distributor. J. agric. Engng. Res. 3(2): 95.

Hofstee, J.W. 1995. Handling and Spreading of Fertilizers: Part 5, The Spinning Disc Type Fertilizer Spreader. J. agric. Engng. Res. 62: 143-162.

Hofstee, J.W., and W. Huisman. 1990. Handling and Spreading of Fertilizers Part 1: Physical Properties of Fertilizer and Relation to Particle Motion. J. agric. Engng. Res.47: 213-234.

ISO Standards. 1985. ISO 5690-1:1985 Equipment for distributing fertilizers--Test methods--Part 1: Full width fertilizer distributors. Geneva, Switzerland: ISO.

Inns, F.M. and A.R. Reece. 1962. The theory of the centrifugal distributor, II: motion on the disc, off-centre feed. J. agric. Engng. Res. 7(4): 345-353.

Landry, H., C. Lague, and M. Roberge. 2003. Engineering properties of solid and semi-solid livestock manure as related to the modeling of machine-product interactions in handling and land application equipment. ASABE Paper No. 1111505. St. Joseph, MI: ASABE.

Landry, H., C. Lague, and M. Roberge. 2004. Physical and Rheological Properties of Manure Products. Applied Engineering in Agriculture. 20(3): 277-288.

Landry, H., C. Lague, and M. Roberge. 2006a. Discrete Element Modeling of Machine-manure Interactions. Computers and Electronics in Agriculture 52: 90-106.

Landry, H., C. Lague and M. Roberge. 2006b. Discrete Element Representation for Manure Products. Computers and Electronics in Agriculture. 51(2006): 17-34.

Landry, H., F. Thirion, C. Lague, and M. Roberge. 2006c. Numerical Modeling of the Flow of Organic Fertilizers in Land Application Equipment. Computers and Electronics in Agriculture. 51(2006): 35-53.

Mitchell, C.C., J. Blake, and T.W. Tyson. 2006. An Update for Alabama CAWV's: The Scoop on Litter. Alabama Cooperative Extension System.

Mitchell, C.C. and T.W. Tyson. 2001. Calibrating Poultry Litter Spreaders. Alabama Cooperative Extension Service (ACES) Circular ANR-889.

Mitchell, C.C., and J.O. Donald. 1995. The Value and Use of Poultry Manures as Fertilizers. Alabama Cooperative Extension Service (ACES) Circular ANR-244.

Ogburn, C.B. and J.O. Donald. 1990. Calibrating Spreaders for the Application of Animal and Poultry Manure. Alabama Cooperative Extension Service (ACES) Circular 11/90-006.

Olieslagers, B.1997. Fertilizer distribution modelling for centrifugal spreader design. PhD diss. Leuven, Belgium: Katholieke Universiteit, Department of Agricultural and Applied Biological Sciences.

Parish, R.L. 2000. Spreader rate determination from pattern tests compared with rate calibration. Applied Engineering in Agriculture 16(2): 119-120.

Parish, R.L. 2003. Technical Note: Effect of Impeller Angle on Pattern Uniformity. Applied Engineering in Agriculture. 19(5): 531-533.

Parish, R.L., and P.P. Chaney. 1986. Pattern Sensitivity to Location of Fertilizer Drop Point on a Rotary Spreader Impeller. Trans. ASAE 29(2): 374-377, 381.

Pezzi, F. and V. Rondelli. 2002. Evaluation of a Prototype Spreader in the Distribution of Poultry Manure. Applied Engineering in Agriculture. 18(3): 285-291.

Reed, W.B., and E. Wacker. 1970. Determining Distribution Pattern of Dry-Fertilizer Applicators. Trans. ASAE 13(1): 85-89.

Reumers, J., E. Tijskens, and H. Ramon. 2003. Experimental Characterisation of the Cylindrical Distribution Pattern of Centrifugal Fertiliser Spreaders: towards an Alternative for Spreading Hall Measurements. Power and Machinery. 86(4): 431-439.

Ritz, C.W. 2006. The Value of Poultry Litter. Broiler Tip. 2010. Athens, GA: The University of Georgia Cooperative Extension Service.

Sharpley, A.N., S.J. Smith, and W.R. Bain. 1993. Nitrogen and phosphorus fate from long-term poultry litter applications to Oklahoma soils. SSSA J. 57(4): 1131-1137.

Sogaard, H.T. and P. Kierkegaard. 1994. Yield Reduction Resulting from Uneven Fertilizer Distribution. Trans. ASAE. 37(6): 1749-1752.

Srivastava, A.K., C.E. Goering, R.P. Rohrbach, and D.R. Buckmaster. 2006. Engineering Principles of Agricultural Machines, 278-279. 2nd ed. St. Joseph, MI: American Society of Agricultural and Biological Engineers (ASABE).

Tasistro, A.S., D.E. Kissel, and P.B. Bush. 2004. Sampling Broiler Litter: How Many Samples Are Needed? Journal of Applied Poultry Research 13: 163-170.

Thirion F., F. Chabot and D. Andeler. 1998. Determination of physical characteristics of animal manure. Proceedings of RAMIRAN 98 (8th International Conference on Management Strategies for Organic Waste Use in Agriculture) Rennes France, p. 457-469.

Tijskens, B., P. Van Liedekerke, and H. Ramon. 2005. Modelling to aid assessment of fertiliser handling and spreading characteristics. In Proc. 553 of The International Fertiliser Society. London, England.

USDA-NASS. 2011. Alabama Agricultural Statistics. Montgomery, AL: USDA National Agricultural Statistics Service (NASS).

USDA-NRCS. 2001. Phosphorus Index for Alabama: A planning tool to assess and manage P movement. Agronomy Technical Note.

USDA-NRCS. 2011. Conservation Practice Standard: Nutrient Management Code 590. Auburn, AL: Natural Resources Conservation Service (NRCS), AL.

Van Liedekerke, P., J. De Baerdemaeker, and H. Ramon. 2006. Fertilizer Application Control. CIGR Handbook of Agricultural Engineering, 273-278. St. Joseph, MI: American Society of Agricultural and Biological Engineers (ASABE).

Van Liedekerke, P., E. Tijskens, E. Dintwa, J. Anthonis, and H. Ramon. 2006. A discrete element model for simulation of a spinning disc fertilizer spreader I. Single particle simulations. Powder Technology. 170: 71-85.

Van Liedekerke, P., E. Tijskens, and H. Ramon. 2009. Discrete element simulations of the influence of fertiliser physical properties on the spread pattern from spinning disc spreaders. Biosystems Engineering 102(4): 392-405.

Wilhoit, J.H., C.W. Wood, K.H. Yoo, and M.Y. Minkara. 1993. Evaluation of spreader distribution patterns for poultry litter. Applied Engineering in Agriculture. 9: 359-363.

Wilhoit, J. and Q. Ling. 1999. Research Helping Achieve Precision Control and Calibration of Poultry Litter Spreaders. Highlights of Agricultural Research. 46(3).

Wilhoit, J.H., J.S. Bannon, R.R. Duffield, and Q. Ling. 1994. Development and Evaluation of a Drop Applicator for Poultry Litter. Applied Engineering in Agriculture. 10(6): 777-782.

Wood, C.W. 1992. Broiler Litter as Fertilizer: Benefits and Environmental Concerns. p. 304-312. J. P. Blake et al. (ed.) Proc. Nat. Poultry Wastes Manage. Symp. Birmingham, Al. 6-8 Oct. 1992. Auburn Univ. Print. Serv., Auburn, AL.

Wood, C.W. 1998. Agricultural phosphorus and water quality: An overview. In Soil Testing for Phosphorus: Environmental uses and Implication, 5-12. J.T. Sims, ed. Southern Cooperative Series Bulletin No. 389. USDA-CSREES Regional Committee SERA-IEG 17: Minimizing Agricultural Phosphorus Losses for Protection of the Water Resources.

Worley, J.W., P.E. Sumner, and T.M. Bass. 2010. Calibration of Manure Spreaders. Athens, GA: The University of Georgia Cooperative Extension. Available at: http://www.caes.uga.edu/applications/publications/files/pdf/C%20825_2.PDF. Accessed 16 September 2010.

Yildirim, Y. and M. Kara. 2002. Effect of Vane Height on Distribution Uniformity in Rotary Fertilizer Spreaders with Different Flow Rates. Applied Engineering in Agriculture. 19(1): 19-23.

APPENDICES

Appendix A: Chandler Equipment Company C/L Litter and Shavings Spreader

Figure A.1. Chandler Equipment Co. Litter Spreader.

(a) (b)

Figure A.2. (a) Litter spreader rear gate, conveyor chain, flow divider and spinners; (b) Vane used on each spinner-disc.

Manufacturer: Chandler Equipment Company
Dimensions, m: 4.9
Oil capacity, L: 113.6
Tire size: 12.5L x 15
Chain width, cm: 86.4
Spinner diameter, cm: 76.2
Vane height, cm: 7.6
Vane length, cm: 27.9
Max gate height, cm: 35.6
Height of spinner from ground, cm: 74.9

Appendix B: Brand Hydraulics: Electronically Adjustable Proportional Pressure Compensated Flow Control Valve

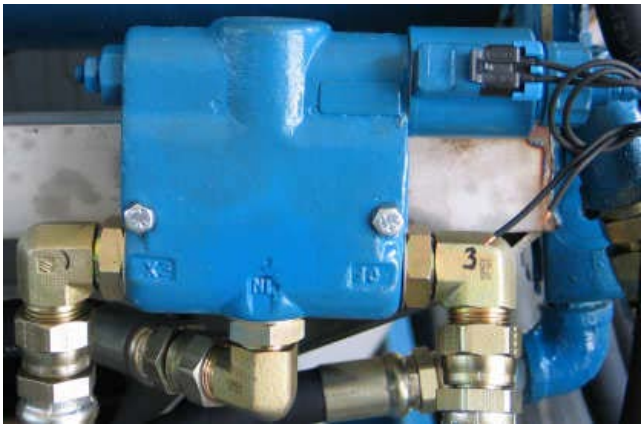

Figure B.1. Brand proportional valve used for spinner and conveyor control.

Manufacturer: Brand Hydraulics
Spinner valve: Operated by pulse width modulation (PWM)
Part #: EFC12-20-12
Flow Rate, LPM: 0 to 75.7
Conveyor valve: Operated by pulse width modulation (PWM)
Part #: EFC12-15-12
Flow Rate, LPM: 0 to 56.8
Coil Voltage, volts: 12
Max pressure, PSI: 3000
Pulse frequency, HZ: 90 to 115

Appendix C: Topcon Precision Ag X20 Console

Figure C.1. X20 console illustrating the main operating screen of the Spreader Control software.

Console:
Processor: 1 GHZ
Memory: 512 Mb
Operating system: Windows XP PRO SP2
Display size: 213-mm (8.4-in.)
Solid state drive: 2 GB
Audio: 1.5 Watt stereo audio amplifier
External line: Input/Output and microphone
Mounting bracket: RAM mount
USB ports: 4 x USB 2.0
Serial RS232 ports: 4
PS2 ports: 2
VGA ports: 1
10/100 Base T Ethernet port: 1

Spreader Control Software:
Version: 1.48
Capabilities: Variable-Rate Application (VRA)
Spinner-Disc Speed Control

Appendix D: Root-cause Analysis Flow Chart

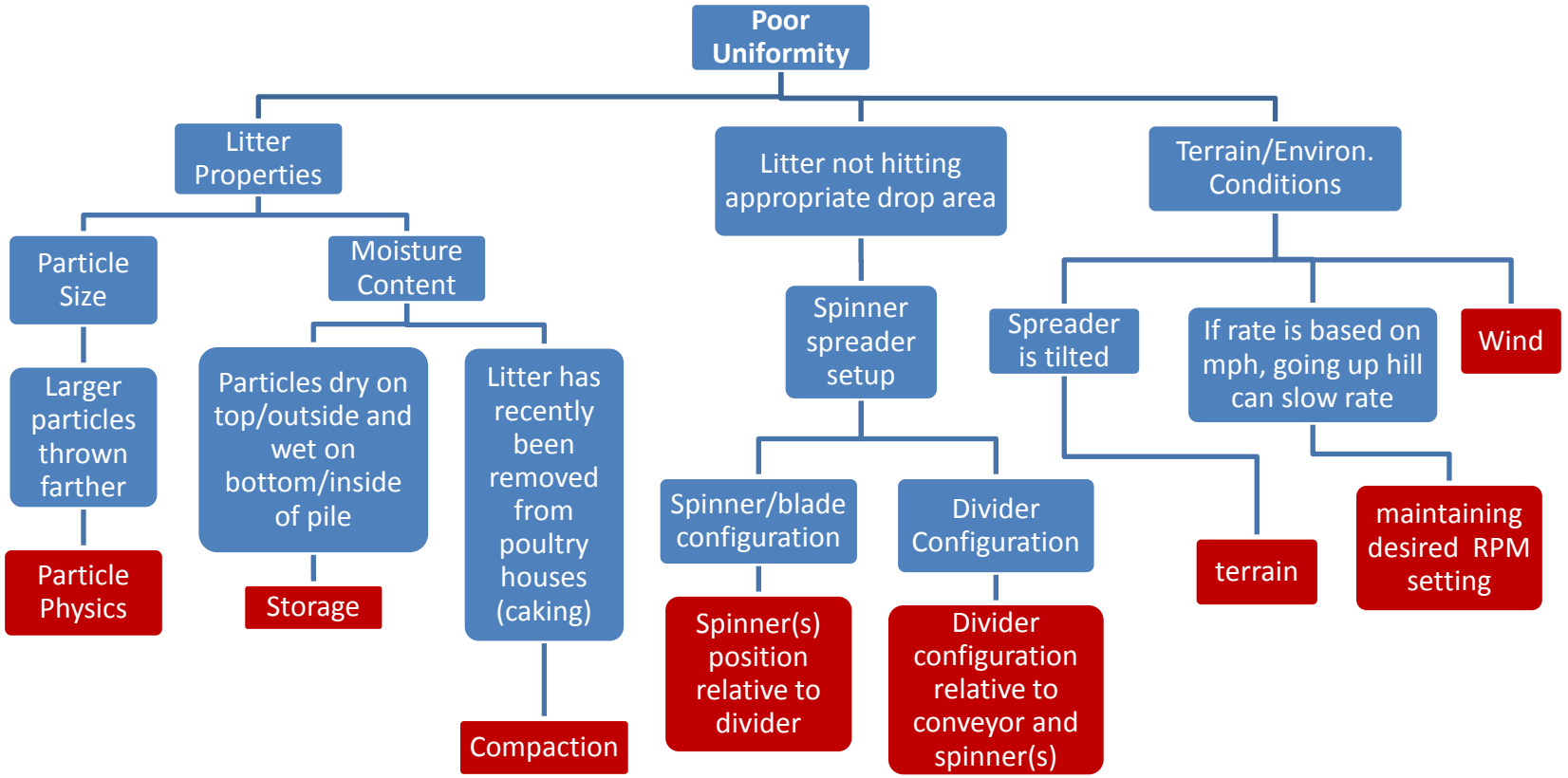

Figure D.1. Root-cause analysis flow chart for poor spread pattern uniformity.

Appendix E: Litter Size Classifications

Figure E.1. Litter size classifications of small, medium, and large at 24% moisture content.

Appendix F: EDEM Parameter and Setup Information

F.1 Material Characteristics (fertilizer, litter, etc.)

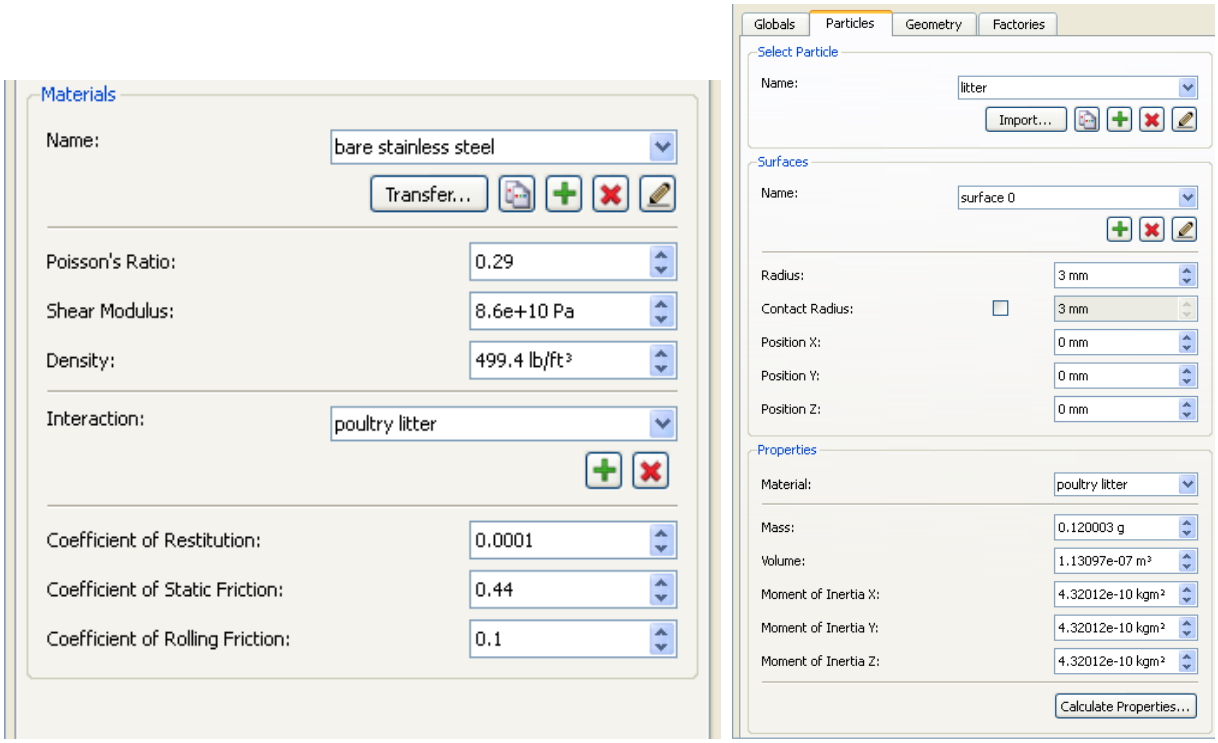

(a) (b)

Figure F.1. EDEM material and interaction menus (a) and EDEM particle information menu (b).

Required by EDEM:

- Required for each material (litter, stainless steel, steel, etc.)
  - Shear modulus
  - Poisson's ratio
  - Particle Density
  - Particle Radius
- Required for each interaction with another material
  - Energy Density Coefficient
  - Coefficient of Static Friction
  - Coefficient of Rolling Friction
  - Coefficient of Restitution

Additional Parameters to Consider:

- Particle Parameters
  - Particle size distribution
  - Particle or material moisture content
  - Particle shape(s)

- Overall Material Parameters
    - Moisture content
    - Cohesion forces
    - Shear ratio
    - Drag Coefficient(s)

Potential Environmental Variables:

- Wind speed and direction
- Humidity
- Temperature

F.2 Variables needed in CAD files

Vane Dimensions

- shape
- length
- pitch

Disc Dimensions

- radius
- cone angle
- horizontal distance between the two discs
- angular speed
- height above ground

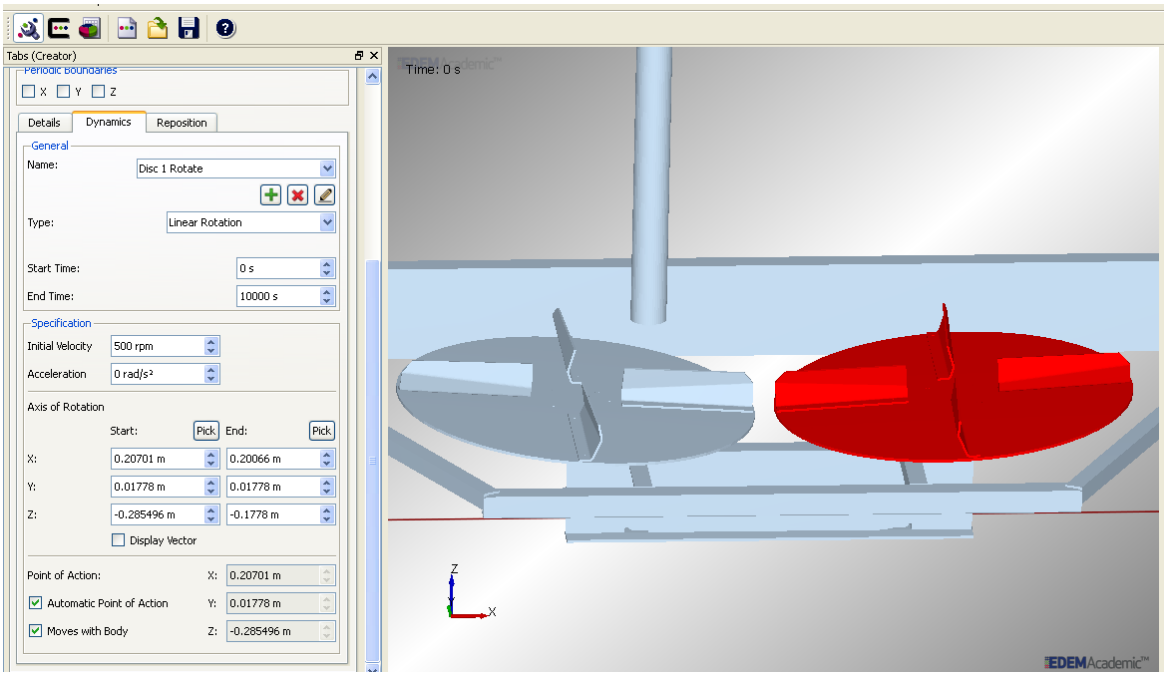

Figure F.2. Geometry dynamics menu within EDEM highlighting the disc (red) in which dynamics are applied.

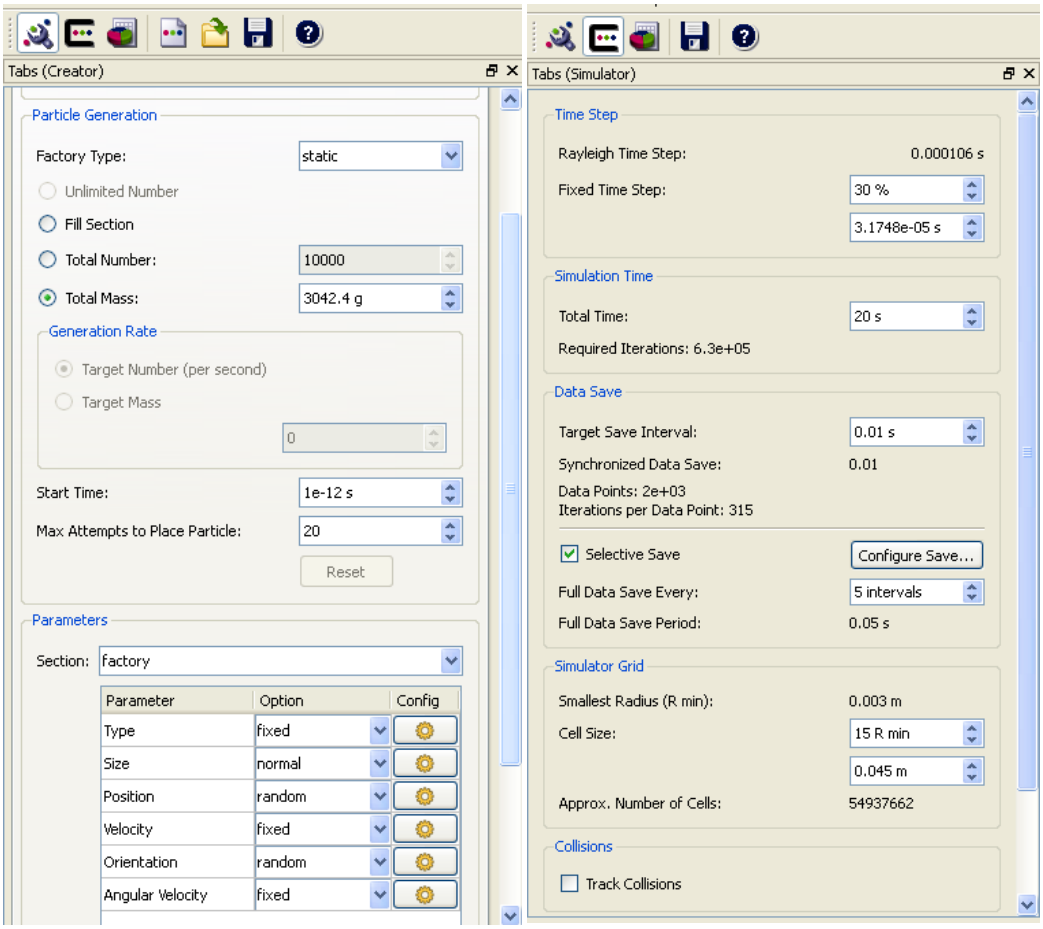

(a) (b)

Figure F.3. Particle factory menu (a) and simulator menu (b) within EDEM.

Appendix G: Examples of EDEM Analysis Capabilities

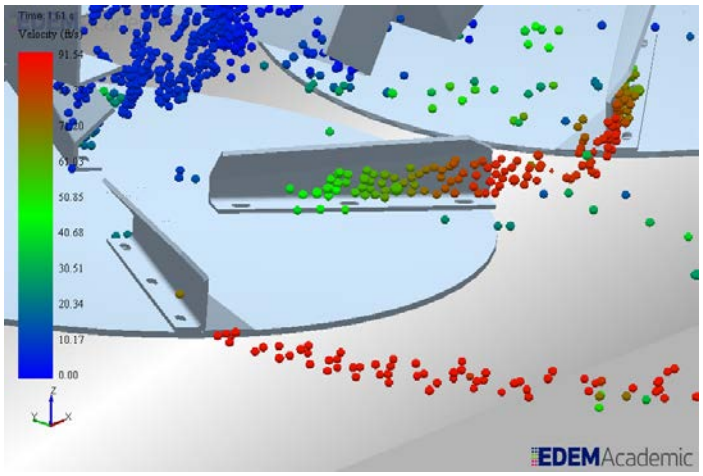

Figure G.1. Particle shading to attain particle velocities (ft/s) at different locations on disc and vane.

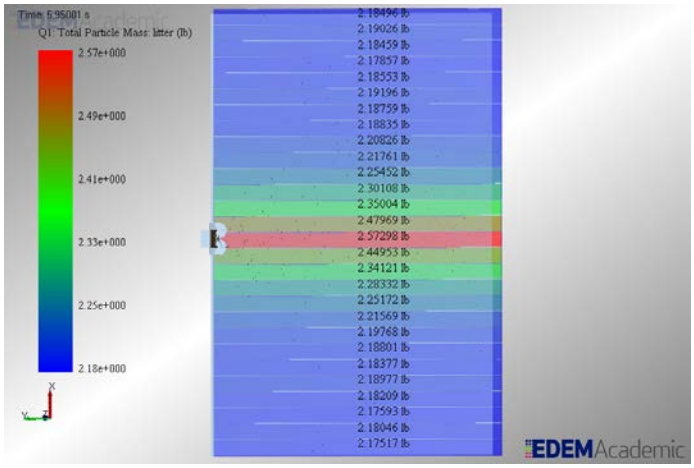

Figure G.2. Grid-binning behind litter spreader representing simulated mass of particles across the swath.

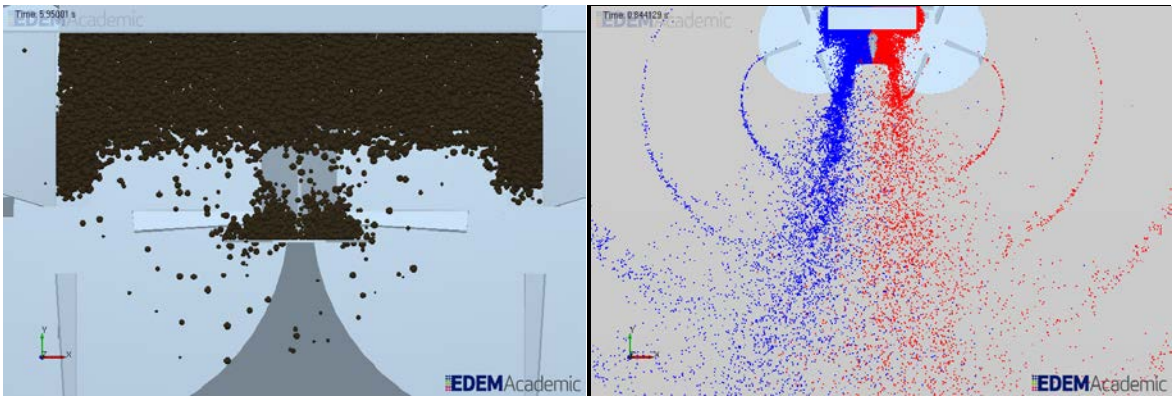

Figure G.3. Identification of particle interactions and disruptions in particle conveyance and distribution. The image on the right depicts displaying particles interacting and being spread by the right (red) and left (blue) spinner-discs and vanes.

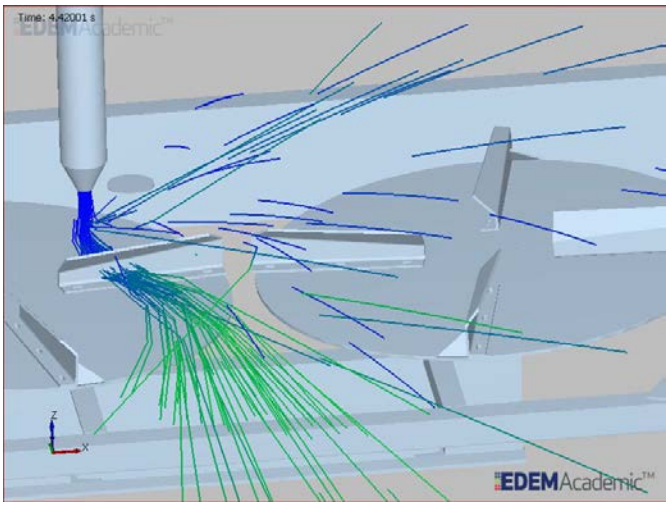

Figure G.4. Ability to display particle trajectories during conveyance and distribution. Some particles bounce off the disc or vane and are not being accelerated by the vanes.

Appendix H: SAS Code

H.1 Three Moisture Content Treatments

```
data litter;
input rep $1. mc;
datalines;
A     18.37
A     17.46
A     18.83
A     19.44
B     23.80
B     22.47
B     23.69
B     23.29
C     31.48
C     30.85
C     29.63
C     29.76
;
Proc print data=litter;run;

Ods html;
proc glm data =litter;
class rep;
model mc = rep;
run;
Ods html close;

data litter1;
input rep $1. mc;
datalines;
A     18.37
A     17.46
A     18.83
A     19.44
B     23.80
B     22.47
B     23.69
B     23.29
;
Proc print data=litter1;run;

Ods html;
proc glm data =litter1;
class rep;
model mc = rep;
run;
Ods html close;

data litter2;
input rep $1. mc;
datalines;
```

```
B     23.80
B     22.47
B     23.69
B     23.29
C     31.48
C     30.85
C     29.63
C     29.76
;
Proc print data=litter2;run;

Ods html;
proc glm data =litter2;
class rep;
model mc = rep;
run;
Ods html close;

data litter3;
input rep $1. mc;
datalines;
A     18.37
A     17.46
A     18.83
A     19.44
C     31.48
C     30.85
C     29.63
C     29.76
;
Proc print data=litter3;run;

Ods html;
proc glm data =litter3;
class rep;
model mc = rep;
run;
Ods html close;
```

H.2 Particle Size Distribution, Bulk Density, and GSI for 3 MC Treatments

```
data litter;
input rep $1. d16 d50 d84 bd gsi;
datalines;
A     0.65  1.85  5.93  327.0 142.96
A     0.70  1.93  6.60  353.0 152.85
A     0.67  1.80  5.98  351.0 147.14
A     0.58  1.44  4.82  349.0 147.53
B     0.77  2.19  6.63  382.0 133.86
B     0.79  2.09  6.91  379.0 146.37
B     0.88  2.61  7.84  381.0 133.49
B     0.84  2.49  7.46  381.0 132.93
C     1.65  3.72  8.29  403.0 89.32
C     1.63  3.90  9.16  406.0 96.49
C     1.84  4.08  9.81  401.0 97.78
```

```
C     1.56  3.27  7.53  406.0 91.32
;
Proc print data=litter;run;

Ods html;
proc glm data =litter;
class rep;
model d16 d50 d84 bd gsi = rep;
run;
Ods html close;

data litter1;
input rep $1. d16 d50 d84 bd gsi;
datalines;
A     0.65  1.85  5.93  327.0 142.96
A     0.70  1.93  6.60  353.0 152.85
A     0.67  1.80  5.98  351.0 147.14
A     0.58  1.44  4.82  349.0 147.53
B     0.77  2.19  6.63  382.0 133.86
B     0.79  2.09  6.91  379.0 146.37
B     0.88  2.61  7.84  381.0 133.49
B     0.84  2.49  7.46  381.0 132.93

;
Proc print data=litter1;run;

Ods html;
proc glm data =litter1;
class rep;
model d16 d50 d84 bd gsi = rep;
run;
Ods html close;

data litter2;
input rep $1. d16 d50 d84 bd gsi;
datalines;
B     0.77  2.19  6.63  382.0 133.86
B     0.79  2.09  6.91  379.0 146.37
B     0.88  2.61  7.84  381.0 133.49
B     0.84  2.49  7.46  381.0 132.93
C     1.65  3.72  8.29  403.0 89.32
C     1.63  3.90  9.16  406.0 96.49
C     1.84  4.08  9.81  401.0 97.78
C     1.56  3.27  7.53  406.0 91.32
;
Proc print data=litter2;run;

data litter3;
input rep $1. d16 d50 d84 bd gsi;
datalines;
A     0.65  1.85  5.93  327.0 142.96
A     0.70  1.93  6.60  353.0 152.85
A     0.67  1.80  5.98  351.0 147.14
A     0.58  1.44  4.82  349.0 147.53
C     1.65  3.72  8.29  403.0 89.32
```

```
C     1.63  3.90  9.16  406.0 96.49
C     1.84  4.08  9.81  401.0 97.78
C     1.56  3.27  7.53  406.0 91.32
;
Proc print data=litter3;run;

Ods html;
proc glm data =litter3;
class rep;
model d16 d50 d84 bd gsi = rep;
run;
Ods html close;

Ods html;
proc glm data =litter2;
class rep;
model d16 d50 d84 bd gsi = rep;
run;
Ods html close;
```

H.3 Size Classifications at 24% MC Treatment

```
data litter;
input rep $1. d16 d50 d84 bd gsi;
datalines;
S     0.68  1.25  2.02  540   53.72
S     0.58  1.13  1.90  520   58.67
S     0.56  1.08  1.80  540   57.30
S     0.58  1.10  1.80  520   55.65
M     0.83  1.97  4.42  350   91.12
M     0.88  2.11  4.53  350   86.69
M     0.77  1.84  4.17  320   92.16
M     0.76  1.83  4.13  340   92.03
L     5.37  9.01  15.83 280   58.06
L     3.98  7.93  16.56 260   79.32
L     2.19  6.82  12.42 270   74.99
L     4.17  7.95  13.49 280   58.64
B     0.77  2.19  6.63  382   133.86
B     0.79  2.09  6.91  379   146.37
B     0.88  2.61  7.84  381   133.49
B     0.84  2.49  7.46  381   132.93
;
Proc print data=litter;run;

Ods html;
proc glm data =litter;
class rep;
model d16 d50 d84 bd gsi = rep;
run;
Ods html close;

data litter2;
input rep $1. d16 d50 d84 bd gsi;
datalines;
S     0.68  1.25  2.02  540   53.72
```

```
S     0.58  1.13  1.90  520   58.67
S     0.56  1.08  1.80  540   57.30
S     0.58  1.10  1.80  520   55.65
M     0.83  1.97  4.42  350   91.12
M     0.88  2.11  4.53  350   86.69
M     0.77  1.84  4.17  320   92.16
M     0.76  1.83  4.13  340   92.03
L     5.37  9.01  15.83 280   58.06
L     3.98  7.93  16.56 260   79.32
L     2.19  6.82  12.42 270   74.99
L     4.17  7.95  13.49 280   58.64
;
Proc print data=litter2;run;

Ods html;
proc glm data =litter2;
class rep;
model d16 d50 d84 bd gsi = rep;
run;
Ods html close;

data litter3;
input rep $1. d16 d50 d84 bd gsi;
datalines;
S     0.68  1.25  2.02  540   53.72
S     0.58  1.13  1.90  520   58.67
S     0.56  1.08  1.80  540   57.30
S     0.58  1.10  1.80  520   55.65
M     0.83  1.97  4.42  350   91.12
M     0.88  2.11  4.53  350   86.69
M     0.77  1.84  4.17  320   92.16
M     0.76  1.83  4.13  340   92.03

;
Proc print data=litter3;run;

Ods html;
proc glm data =litter3;
class rep;
model d16 d50 d84 bd gsi = rep;
run;
Ods html close;

data litter4;
input rep $1. d16 d50 d84 bd gsi;
datalines;
M     0.83  1.97  4.42  350   91.12
M     0.88  2.11  4.53  350   86.69
M     0.77  1.84  4.17  320   92.16
M     0.76  1.83  4.13  340   92.03
L     5.37  9.01  15.83 280   58.06
L     3.98  7.93  16.56 260   79.32
L     2.19  6.82  12.42 270   74.99
L     4.17  7.95  13.49 280   58.64
;
```

```
Proc print data=litter4;run;

Ods html;
proc glm data =litter4;
class rep;
model d16 d50 d84 bd gsi = rep;
run;
Ods html close;

data litter2;
input rep $1. d16 d50 d84 bd gsi;
datalines;
S     0.68  1.25  2.02  540   53.72
S     0.58  1.13  1.90  520   58.67
S     0.56  1.08  1.80  540   57.30
S     0.58  1.10  1.80  520   55.65
L     5.37  9.01  15.83 280   58.06
L     3.98  7.93  16.56 260   79.32
L     2.19  6.82  12.42 270   74.99
L     4.17  7.95  13.49 280   58.64
;
Proc print data=litter2;run;

Ods html;
proc glm data =litter2;
class rep;
model d16 d50 d84 bd gsi = rep;
run;
Ods html close;

data litter;
input rep $1. d16 d50 d84 bd gsi;
datalines;
S     0.68  1.25  2.02  540   53.72
S     0.58  1.13  1.90  520   58.67
S     0.56  1.08  1.80  540   57.30
S     0.58  1.10  1.80  520   55.65
B     0.77  2.19  6.63  382   133.86
B     0.79  2.09  6.91  379   146.37
B     0.88  2.61  7.84  381   133.49
B     0.84  2.49  7.46  381   132.93
;
Proc print data=litter;run;
Ods html;
proc glm data =litter;
class rep;
model d16 d50 d84 bd gsi = rep;
run;
Ods html close;

data litter;
input rep $1. d16 d50 d84 bd gsi;
datalines;
L     5.37  9.01  15.83 280   58.06
L     3.98  7.93  16.56 260   79.32
```

```
L     2.19  6.82  12.42 270   74.99
L     4.17  7.95  13.49 280   58.64
B     0.77  2.19  6.63  382   133.86
B     0.79  2.09  6.91  379   146.37
B     0.88  2.61  7.84  381   133.49
B     0.84  2.49  7.46  381   132.93
;
Proc print data=litter;run;

Ods html;
proc glm data =litter;
class rep;
model d16 d50 d84 bd gsi = rep;
run;
Ods html close;

data litter;
input rep $1. d16 d50 d84 bd gsi;
datalines;
M     0.83  1.97  4.42  350   91.12
M     0.88  2.11  4.53  350   86.69
M     0.77  1.84  4.17  320   92.16
M     0.76  1.83  4.13  340   92.03
B     0.77  2.19  6.63  382   133.86
B     0.79  2.09  6.91  379   146.37
B     0.88  2.61  7.84  381   133.49
B     0.84  2.49  7.46  381   132.93
;
Proc print data=litter;run;

Ods html;
proc glm data =litter;
class rep;
model d16 d50 d84 bd gsi = rep;
run;
Ods html close;
```

H.4 Divider Accuracy Tests at 560-kg/ha Application Rate

```
Data divider;
input rep $1. weight;
datalines;
A 33
A 33
A 29
B 32
B 34
B 31
;
Ods html;
Proc glm data =divider;
class rep;
model weight =rep;
```

```
run;
Ods html close;
```

H.5 Divider Accuracy Tests at 4483-kg/ha Application Rate

```
Data divider1;
input rep $1. weight;
datalines;
A 112
A 110
A 114
B 110
B 116
B 121
;
Ods html;
Proc glm data =divider1;
class rep;
model weight =rep;
run;
Ods html close;
```

H.6 Divider Accuracy Tests at 672- kg/ha Application Rate

```
Data divider3;
input rep $1. weight;
datalines;
A 136
A 121
A 129
B 138
B 114
B 126
;
Ods html;
Proc glm data =divider3;
class rep;
model weight =rep;
run;
Ods html close;
```

Appendix I: Statistical Analysis Results (SAS)

Table I.1. ANOVA results comparing all 3 MC replications against each other.

Source	DF	Sum of Squares	Mean Square	F Value	Pr > F
Model	2	287.07732	143.538658	232.9	<.0001
Error	9	5.546775	0.6163083		
Corrected Total	11	292.62409			

Table I.2. ANOVA results comparing 18% and 24% MC replications.

Source	DF	Sum of Squares	Mean Square	F Value	Pr > F
Model	1	45.840313	45.8403125	86.52	<.0001
Error	6	3.178975	0.52982917		
Corrected Total	7	49.019288			

Table I.3. ANOVA results comparing 24% and 30% MC replications.

Source	DF	Sum of Squares	Mean Square	F Value	Pr > F
Model	1	101.31761	101.317613	175.78	<.0001
Error	6	3.458275	0.5763792		
Corrected Total	7	104.77589			

Table I.4. ANOVA results comparing 18% and 30% MC replications.

Source	DF	Sum of Squares	Mean Square	F Value	Pr > F
Model	1	283.45805	283.45805	381.65	<.0001
Error	6	4.4563	0.7427167		
Corrected Total	7	287.91435			

Table I.5. ANOVA results comparing size distribution for all MC.

Dependent Variable: d16

Source	DF	Sum of Squares	Mean Square	F Value	Pr > F
Model	2	2.3890667	1.19453333	184.72	<.0001
Error	9	0.0582	0.00646667		
Corrected Total	11	2.4472667			

Dependent Variable: d50

Source	DF	Sum of Squares	Mean Square	F Value	Pr > F
Model	2	8.3350167	4.16750833	54.86	<.0001
Error	9	0.683675	0.07596389		
Corrected Total	11	9.0186917			

Dependent Variable: d84

Source	DF	Sum of Squares	Mean Square	F Value	Pr > F
Model	2	16.424517	8.21225833	13.41	0.002
Error	9	5.51195	0.61243889		
Corrected Total	11	21.936467			

Dependent Variable: bd

Source	DF	Sum of Squares	Mean Square	F Value	Pr > F
Model	2	7066.1667	3533.08333	68.71	<.0001
Error	9	462.75	51.416667		
Corrected Total	11	7528.9167			

Dependent Variable: gsi

Source	DF	Sum of Squares	Mean Square	F Value	Pr > F
Model	2	6490.5101	3245.25506	130	<.0001
Error	9	224.66915	24.963239		
Corrected Total	11	6715.1793			

Table I.6. ANOVA results comparing size distribution for 18 and 24 MC.

Dependent Variable: d16

Source	DF	Sum of Squares	Mean Square	F Value	Pr > F
Model	1	0.0578	0.0578	22.82	0.0031
Error	6	0.0152	0.00253333		
Corrected Total	7	0.073			

Dependent Variable: d50

Source	DF	Sum of Squares	Mean Square	F Value	Pr > F
Model	1	0.6962	0.6962	13	0.0113
Error	6	0.3212	0.05353333		
Corrected Total	7	1.0174			

Dependent Variable: d84

Source	DF	Sum of Squares	Mean Square	F Value	Pr > F
Model	1	3.7950125	3.7950125	9	0.024
Error	6	2.531275	0.42187917		
Corrected Total	7	6.3262875			

Dependent Variable: bd

Source	DF	Sum of Squares	Mean Square	F Value	Pr > F
Model	1	2556.125	2556.125	34.48	0.0011
Error	6	444.75	74.125		
Corrected Total	7	3000.875			

Dependent Variable: gsi

Source	DF	Sum of Squares	Mean Square	F Value	Pr > F
Model	1	240.13361	240.133613	8.21	0.0286
Error	6	175.39288	29.2321458		
Corrected Total	7	415.52649			

Table I.7. ANOVA results comparing 24 and 30 MC particle distribution.

Dependent Variable: d16

Source	DF	Sum of Squares	Mean Square	F Value	Pr > F
Model	1	1.445	1.445	172.02	<.0001
Error	6	0.0504	0.0084		
Corrected Total	7	1.4954			

Dependent Variable: d50

Source	DF	Sum of Squares	Mean Square	F Value	Pr > F
Model	1	3.9060125	3.9060125	43.18	0.0006
Error	6	0.542775	0.0904625		
Corrected Total	7	4.4487875			

Dependent Variable: d84

Source	DF	Sum of Squares	Mean Square	F Value	Pr > F
Model	1	4.4253125	4.4253125	6.87	0.0396
Error	6	3.866475	0.6444125		
Corrected Total	7	8.2917875			

Dependent Variable: bd

Source	DF	Sum of Squares	Mean Square	F Value	Pr > F
Model	1	1081.125	1081.125	285.13	<.0001
Error	6	22.75	3.791667		
Corrected Total	7	1103.875			

Dependent Variable: gsi

Source	DF	Sum of Squares	Mean Square	F Value	Pr > F
Model	1	3686.8285	3686.82845	126.14	<.0001
Error	6	175.36215	29.227025		
Corrected Total	7	3862.1906			

Table I.8. ANOVA results comparing 18 and 30 MC particle distribution.

Dependent Variable: d16

Source	DF	Sum of Squares	Mean Square	F Value	Pr > F
Model	1	2.0808	2.0808	245.76	<.0001
Error	6	0.0508	0.00846667		
Corrected Total	7	2.1316			

Dependent Variable: d50

Source	DF	Sum of Squares	Mean Square	F Value	Pr > F
Model	1	7.9003125	7.9003125	94.17	<.0001
Error	6	0.503375	0.08389583		
Corrected Total	7	8.4036875			

Dependent Variable: d84

Source	DF	Sum of Squares	Mean Square	F Value	Pr > F
Model	1	16.41645	16.41645	21.29	0.0036
Error	6	4.62615	0.771025		

Dependent Variable: bd

Source	DF	Sum of Squares	Mean Square	F Value	Pr > F
Model	1	6962	6962	91.21	<.0001
Error	6	458	76.333333		
Corrected Total	7	7420			

Dependent Variable: gsi

Source	DF	Sum of Squares	Mean Square	F Value	Pr > F
Model	1	5808.8031	5808.80311	353.54	<.0001
Error	6	98.583275	16.430546		
Corrected Total	7	5907.3864			

Table I.9. ANOVA results comparing all size classes within 24 MC.

Dependent Variable: d16

Source	DF	Sum of Squares	Mean Square	F Value	Pr > F
Model	3	30.540219	10.1800729	23.55	<.0001
Error	12	5.186875	0.43223958		
Corrected Total	15	35.727094			

Dependent Variable: d50

Source	DF	Sum of Squares	Mean Square	F Value	Pr > F
Model	3	115.36865	38.4562167	174.24	<.0001
Error	12	2.64845	0.2207042		
Corrected Total	15	118.0171			

Dependent Variable: d84

Source	DF	Sum of Squares	Mean Square	F Value	Pr > F
Model	3	363.44662	121.148873	117.55	<.0001
Error	12	12.367575	1.0306313		
Corrected Total	15	375.81419			

Dependent Variable: bd

Source	DF	Sum of Squares	Mean Square	F Value	Pr > F
Model	3	142616.69	47538.8958	445.76	<.0001
Error	12	1279.75	106.6458		
Corrected Total	15	143896.44			

Dependent Variable: gsi

Source	DF	Sum of Squares	Mean Square	F Value	Pr > F
Model	3	15147.127	5049.04235	115.86	<.0001
Error	12	522.94445	43.5787		
Corrected Total	15	15670.072			

Table I.10. ANOVA results comparing small and medium size classes within 24 MC.

Dependent Variable: d16

Source	DF	Sum of Squares	Mean Square	F Value	Pr > F
Model	1	0.0882	0.0882	29.08	0.0017
Error	6	0.0182	0.00303333		
Corrected Total	7	0.1064			

Dependent Variable: d50

Source	DF	Sum of Squares	Mean Square	F Value	Pr > F
Model	1	1.2720125	1.2720125	110.17	<.0001
Error	6	0.069275	0.01154583		
Corrected Total	7	1.3412875			

Dependent Variable: d84

Source	DF	Sum of Squares	Mean Square	F Value	Pr > F
Model	1	11.834113	11.8341125	488.76	<.0001
Error	6	0.145275	0.0242125		
Corrected Total	7	11.979388			

Dependent Variable: bd

Source	DF	Sum of Squares	Mean Square	F Value	Pr > F
Model	1	72200	72200	433.2	<.0001
Error	6	1000	166.66667		
Corrected Total	7	73200			

Dependent Variable: gsi

Source	DF	Sum of Squares	Mean Square	F Value	Pr > F
Model	1	2334.4945	2334.49445	415.79	<.0001
Error	6	33.6879	5.61465		
Corrected Total	7	2368.1824			

Table I.11. ANOVA results comparing small and large size classes within 24 MC.

Dependent Variable: d16

Source	DF	Sum of Squares	Mean Square	F Value	Pr > F
Model	1	22.144513	22.1445125	25.7	0.0023
Error	6	5.170075	0.86167917		
Corrected Total	7	27.314588			

Dependent Variable: d50

Source	DF	Sum of Squares	Mean Square	F Value	Pr > F
Model	1	92.140313	92.1403125	228.8	<.0001
Error	6	2.416275	0.4027125		
Corrected Total	7	94.556588			

Dependent Variable: d84

Source	DF	Sum of Squares	Mean Square	F Value	Pr > F
Model	1	322.32605	322.32605	170.1	<.0001
Error	6	11.3693	1.8948833		
Corrected Total	7	333.69535			

Dependent Variable: bd

Source	DF	Sum of Squares	Mean Square	F Value	Pr > F
Model	1	132612.5	132612.5	1178.8	<.0001
Error	6	675	112.5		
Corrected Total	7	133287.5			

Dependent Variable: gsi

Source	DF	Sum of Squares	Mean Square	F Value	Pr > F
Model	1	260.71861	260.718613	4.15	0.0878
Error	6	376.86158	62.8102625		
Corrected Total	7	637.58019			

Table I.12. ANOVA results comparing medium and large size classes within 24 MC.

Dependent Variable: d16

Source	DF	Sum of Squares	Mean Square	F Value	Pr > F
Model	1	19.437613	19.4376125	22.56	0.0032
Error	6	5.170675	0.86177917		
Corrected Total	7	24.608288			

Dependent Variable: d50

Source	DF	Sum of Squares	Mean Square	F Value	Pr > F
Model	1	71.7602	71.7602	175.69	<.0001
Error	6	2.45075	0.40845833		
Corrected Total	7	74.21095			

Dependent Variable: d84

Source	DF	Sum of Squares	Mean Square	F Value	Pr > F
Model	1	210.63781	210.637813	110.39	<.0001
Error	6	11.448975	1.9081625		
Corrected Total	7	222.08679			

Dependent Variable: bd

Source	DF	Sum of Squares	Mean Square	F Value	Pr > F
Model	1	9112.5	9112.5	62.49	0.0002
Error	6	875	145.833333		
Corrected Total	7	9987.5			

Dependent Variable: gsi

Source	DF	Sum of Squares	Mean Square	F Value	Pr > F
Model	1	1034.8975	1034.89751	16.21	0.0069
Error	6	383.16768	63.861279		
Corrected Total	7	1418.0652			

Table I.13. ANOVA results comparing small and bulk size classes within 24 MC.

Dependent Variable: d16

Source	DF	Sum of Squares	Mean Square	F Value	Pr > F
Model	1	0.0968	0.0968	35.85	0.001
Error	6	0.0162	0.0027		
Corrected Total	7	0.113			

Dependent Variable: d50

Source	DF	Sum of Squares	Mean Square	F Value	Pr > F
Model	1	2.90405	2.90405	88.14	<.0001
Error	6	0.1977	0.03295		
Corrected Total	7	3.10175			

Dependent Variable: d84

Source	DF	Sum of Squares	Mean Square	F Value	Pr > F
Model	1	56.8178	56.8178	371.12	<.0001
Error	6	0.9186	0.1531		
Corrected Total	7	57.7364			

Dependent Variable: bd

Source	DF	Sum of Squares	Mean Square	F Value	Pr > F
Model	1	44551.125	44551.125	660.42	<.0001
Error	6	404.75	67.45833		
Corrected Total	7	44955.875			

Dependent Variable: gsi

Source	DF	Sum of Squares	Mean Square	F Value	Pr > F
Model	1	12905.015	12905.0145	553.96	<.0001
Error	6	139.77677	23.29613		
Corrected Total	7	13044.791			

Table I.14. ANOVA results comparing large and bulk size classes within 24 MC.

Dependent Variable: d16

Source	DF	Sum of Squares	Mean Square	F Value	Pr > F
Model	1	19.313113	19.3131125	22.42	0.0032
Error	6	5.168675	0.86144583		
Corrected Total	7	24.481788			

Dependent Variable: d50

Source	DF	Sum of Squares	Mean Square	F Value	Pr > F
Model	1	62.328613	62.3286125	145	<.0001
Error	6	2.579175	0.4298625		
Corrected Total	7	64.907788			

Dependent Variable: d84

Source	DF	Sum of Squares	Mean Square	F Value	Pr > F
Model	1	108.48645	108.48645	53.26	0.0003
Error	6	12.2223	2.03705		
Corrected Total	7	120.70875			

Dependent Variable: bd

Source	DF	Sum of Squares	Mean Square	F Value	Pr > F
Model	1	23436.125	23436.125	502.65	<.0001
Error	6	279.75	46.625		
Corrected Total	7	23715.875			

Dependent Variable: gsi

Source	DF	Sum of Squares	Mean Square	F Value	Pr > F
Model	1	9497.1762	9497.1762	116.47	<.0001
Error	6	489.25655	81.542758		
Corrected Total	7	9986.4328			

Table I.15. ANOVA results comparing medium and bulk size classes within 24 MC.

Dependent Variable: d16

Source	DF	Sum of Squares	Mean Square	F Value	Pr > F
Model	1	0.0002	0.0002	0.07	0.7982
Error	6	0.0168	0.0028		
Corrected Total	7	0.017			

Dependent Variable: d50

Source	DF	Sum of Squares	Mean Square	F Value	Pr > F
Model	1	0.3321125	0.3321125	8.58	0.0263
Error	6	0.232175	0.03869583		
Corrected Total	7	0.5642875			

Dependent Variable: d84

Source	DF	Sum of Squares	Mean Square	F Value	Pr > F
Model	1	16.791013	16.7910125	100.92	<.0001
Error	6	0.998275	0.16637917		
Corrected Total	7	17.789288			

Dependent Variable: bd

Source	DF	Sum of Squares	Mean Square	F Value	Pr > F
Model	1	3321.125	3321.125	32.95	0.0012
Error	6	604.75	100.791667		
Corrected Total	7	3925.875			

Dependent Variable: gsi

Source	DF	Sum of Squares	Mean Square	F Value	Pr > F
Model	1	4261.9528	4261.95281	175.05	<.0001
Error	6	146.08288	24.347146		
Corrected Total	7	4408.0357			

Table I.16. ANOVA results comparing bins 1 and 2 of experimental tests at 560-kg/ha.

Dependent Variable: weight

Source	DF	Sum of Squares	Mean Square	F Value	Pr > F
Model	1	0.6666667	0.66666667	0.17	0.6981
Error	4	15.333333	3.83333333		
Corrected Total	5	16			

Table I.17. ANOVA results comparing bins 1 and 2 of experimental tests at 4483-kg/ha.

Dependent Variable: weight

Source	DF	Sum of Squares	Mean Square	F Value	Pr > F
Model	1	20.166667	20.1666667	1.17	0.3394
Error	4	68.666667	17.1666667		
Corrected Total	5	88.833333			

Table I.18. ANOVA results comparing bins 1 and 2 of experimental tests at 6725-kg/ha.

Dependent Variable: weight

Source	DF	Sum of Squares	Mean Square	F Value	Pr > F
Model	1	10.666667	10.6666667	0.11	0.7605
Error	4	400.66667	100.166667		
Corrected Total	5	411.33333			

Appendix J: Supporting Model Calibration Data

J.1 Plastic BB Calibration Parameters

	Particle-Geometry Interactions				Particle-Particle Interactions				Statistical Comparison to Field Data			
Test ID	Coeff. Static Friction	Coeff. Rolling Friction	Coeff. of Rest.	Energy Density	Coeff. Static Friction	Coeff. Rolling Friction	Coeff. of Rest.	Energy Density	Correlation Value	R2	(SME)	SDRME
1	0.04	0.04	0.86	2E+05	0.1	0.1	0.81	9E+04	0.70	0.42	0.35	0.68
2	0.04	0.04	0.7	2E+05	0.1	0.1	0.81	9E+04	0.80	0.66	0.39	0.49
3	0.1	0.1	0.86	2E+05	0.1	0.1	0.81	9E+04	0.80	0.57	0.29	0.63
4	0.04	0.04	0.86	2E+05	0.2	0.2	0.81	9E+03	0.40	0.1	0.46	0.83
5	0.04	0.04	0.86	2E+05	0.1	0.1	0.7	9E+04	0.80	0.57	0.37	0.58
6	0.04	0.04	0.7	2E+05	0.1	0.1	0.7	9E+04	0.80	0.41	0.51	0.57
7	0.1	0.1	0.7	2E+05	0.2	0.2	0.7	9E+03	0.70	0.34	0.53	0.61
8	0.1	0.1	0.6	2E+05	0.2	0.2	0.81	9E+03	0.50	0.03	0.63	0.76
9	0.1	0.1	0.86	2E+05	0.1	0.1	0.81	9E+04	0.80	0.68	0.29	0.49
10	0.1	0.1	0.7	2E+05	0.1	0.1	0.81	9E+04	0.86	0.65	0.41	0.43
11	0.1	0.1	0.6	2E+05	0.1	0.1	0.81	9E+04	0.70	0.36	0.53	0.6
12	0.1	0.1	0.8	2E+05	0.1	0.1	0.81	9E+04	0.89	0.78	0.29	0.4
13	0.1	0.1	0.75	2E+05	0.1	0.1	0.81	9E+04	0.80	0.59	0.39	0.5
14	0.1	0.1	0.83	2E+05	0.1	0.1	0.81	9E+04	0.80	0.61	0.28	0.57
15	0.1	0.1	0.77	2E+05	0.1	0.1	0.81	9E+04	0.93	0.84	0.26	0.34
16	0.1	0.1	0.77	2E+05	0.1	0.1	0.81	9E+04	0.89	0.77	0.29	0.39
17	0.1	0.1	0.77	2E+05	0.1	0.1	0.81	9E+04	0.90	0.79	0.28	0.37
18	0.1	0.1	0.78	2E+05	0.1	0.1	0.81	9E+04	0.88	0.73	0.32	0.4
19	0.1	0.1	0.79	2E+05	0.1	0.1	0.81	9E+04	0.72	0.46	0.38	0.62
20	0.08	0.08	0.77	2E+05	0.1	0.1	0.81	9E+04	0.78	0.55	0.38	0.54
21	0.08	0.08	0.75	2E+05	0.1	0.1	0.81	9E+04	0.82	0.63	0.34	0.5
22	0.08	0.08	0.86	2E+05	0.1	0.1	0.81	9E+04	0.81	0.63	0.3	0.52
23	0.1	0.1	0.77	2E+04	0.1	0.1	0.81	9E+04	0.86	0.71	0.3	0.45
24	0.1	0.1	0.77	2E+05	0.1	0.1	0.85	9E+04	0.86	0.7	0.31	0.45
25	0.1	0.1	0.77	0E+00	0.1	0.1	0.9	9E+04	0.84	0.69	0.27	0.48
26	0.1	0.1	0.77	2E+03	0.1	0.1	0.81	9E+04	0.85	0.68	0.32	0.46
27	0.04	0.04	0.7	2E+05	0.1	0.1	0.81	9E+04	0.81	0.56	0.42	0.55
28	0.04	0.04	0.86	2E+05	0.1	0.1	0.87	9E+04	0.80	0.59	0.31	0.56

J.2 Bulk Litter Calibration Parameters

	Particle-Geometry Interactions				Particle-Particle Interactions				Statistical Comparison to Field Data			
Test ID	Coeff. Static Friction	Coeff. Rolling Friction	Coeff. of Rest.	Energy Density	Coeff. Static Friction	Coeff. Rolling Friction	Coeff. of Rest.	Energy Density	Correlation Value	R2	(SME)	SDRME
1	0.44	0.1	0.0001	2.00E+04	0.71	0.1	0.0001	8.00E+03	-0.14	-0.41	1.73	2.67
2	1	1	0.0001	0.00E+00	1	1	0.0001	0.00E+00	-0.06	-0.45	5.07	10.14
3	0	0	0.6	2.00E+07	0	0	0.6	9.00E+04	0.56	0.28	3.89	8.25
4	0	0	0.6	2.00E+07	0	0	0.6	9.00E+04	0.39	0.09	4.59	9.71
5	0	0	0.0001	0.00E+00	0	0	0.0001	0.00E+00	-0.20	-0.46	2.19	3.47
6	0.44	0.44	0.0001	2.00E+04	0.71	0.71	0.0001	8.00E+03	-0.25	-0.53	3.92	7.12
7	0.44	0.1	0.0001	0	0.71	0.1	0.0001	0	-0.15	-0.43	1.72	2.6
8	0	0	0.0001	2E+04	0	0	0.0001	8E+03	-0.20	-0.46	2.21	3.51
9	0.44	0.1	1	2.00E+04	0.71	0.1	1	8.00E+03	0.09	-0.82	2.66	4.38
10	0	0	0.0001	2.00E+04	0.71	0.1	0.0001	8E+03	-0.04	-0.24	8.33	17.39
11	0.44	0.1	0.0001	2.00E+04	0	0	0.0001	8E+03	-0.10	-0.52	2.17	3.45
12	0.75	0.75	0.0001	0.00E+00	0.75	0.75	0.0001	0E+00	-0.10	-0.28	1.85	3.18
13	0.1	0.1	0.77	2E+05	0.1	0.1	0.81	9E+04	-0.15	-0.66	2.58	4.11
14	0.44	0.1	0.0001	-2E+04	0.71	0.1	0.0001	-8E+03	-0.13	-0.37	1.72	2.64
15	1	1	0.0001	0E+00	0	0	0.0001	0E+00	0.06	-0.33	1.92	3.33
16	1	1	0.0001	0E+00	0	0	0.0001	9E+05	-0.04	-0.68	2.25	3.75
17	0.75	0.75	0.0001	0E+00	0.75	0.75	0.0001	0E+00	-0.15	-0.22	2.07	3.81
18	0.5	0.5	0.0001	0E+00	0.5	0.5	0.0001	0E+00	-0.11	-0.31	1.5	2.35
19	0.44	0.44	0.0001	0E+00	0.44	0.44	0.0001	0E+00	-0.12	-0.34	1.64	2.56
20	0.44	0.44	0.1	0E+00	0.44	0.44	0.1	0E+00	-0.12	-0.34	1.64	2.56
21	0.44	0.44	0.2	0E+00	0.44	0.44	0.2	0E+00	-0.12	-0.26	1.34	2.09
22	0.44	0.44	0.3	0E+00	0.44	0.44	0.3	0E+00	-0.11	-0.26	1.38	2.19
23	0.44	0.44	0.4	0E+00	0.44	0.44	0.4	0E+00	-0.10	-0.27	1.38	2.16
24	0.44	0.44	0.5	0E+00	0.44	0.44	0.5	0E+00	-0.06	-0.26	1.38	2.16
25	0.44	0.44	0.6	0E+00	0.44	0.44	0.6	0E+00	-0.09	-0.28	1.43	2.24
26	0.44	0.44	0.7	0E+00	0.44	0.44	0.7	0E+00	-0.09	-0.31	1.43	2.2
27	0.44	0.44	0.8	0E+00	0.44	0.44	0.8	0E+00	-0.10	-0.3	1.44	2.23
28	0.44	0.44	0.9	0E+00	0.44	0.44	0.9	0E+00	-0.09	-0.35	1.55	2.39
29	0.44	0.44	1	0E+00	0.44	0.44	1	0E+00	-0.09	-0.47	1.8	2.79

J.3 Divider Accuracy Test Data

Application Rate: 560-kg/ha

Rep	Time (sec.)	Bin 1 Litter Wt. (lb)	Bin 2 Litter Wt. (lb)	Total Litter Wt. (lb)	% Diff. between Bin 1 and Bin 2
1	20.0	33	32	65	3.0
2	20.0	33	34	67	3.0
3	22.2	29	31	60	6.9

Application Rate: 4483-kg/ha

Rep	Time (sec.)	Bin 1 Litter Wt. (lb)	Bin 2 Litter Wt. (lb)	Total Litter Wt. (lb)	% Diff. between Bin 1 and Bin 2
1	9.7	112	110	222	1.8
2	10.0	110	116	226	5.5
3	9.8	114	121	235	6.1

Application Rate: 6725-kg/ha

Rep	Time (sec.)	Bin 1 Litter Wt. (lb)	Bin 2 Litter Wt. (lb)	Total Litter Wt. (lb)	% Diff. between Bin 1 and Bin 2
1	9.7	158	111	269	29.7
2	10.0	110	117	227	6.4
3	9.8	114	122	236	7.0

Appendix K: Spreadsheet Used to Calculate Energy Density Coefficient

g	9.81				
Particle Material			**Geometry Material**		
Poissons	0.25		Poissons	0.29	
Shear	1.00E+07	Pa	Shear	8.60E+10	Pa
Density	1.79	kg/m3	Density	7999	kg/m3
Youngs	25000000	Pa	Youngs	2.219E+11	Pa
Particle - Particle			**Particle - Geometry**		
NEquiv Youngs	7.5E-08		NEquiv Youngs	3.75E-08	
Equiv Youngs	13333333		Equiv Youngs	26663732	
Particles					
Radius	**0.003**	m			
volume	1.13E-07	m3			
mass	2.02E-07	kg			
Gravity Force	1.99E-06	N			
Equiv Radius	1.68E-03	m			
Overlap	1.95E-08	m	9.75655E-09	m	
Overlap area	4.12E-10		2.06E-10	m2	
	Particle - Particle		**Particle - Geometry**		
Energy Density LOW	5E+03	J/m2	1E+04	J/m2	
Energy Density MEDIUM	8E+03	J/m2	2E+04	J/m2	
Energy Density HIGH	1E+04	J/m2	2E+04	J/m2	

Warning: High Energy Density could cause unphysical results and may require a lower than usual timestep.